

CO₂ capture with liquid crystals: a phase equilibrium study

Proefschrift

ter verkrijging van de graad van doctor

aan de Technische Universiteit Delft,

op gezag van de Rector Magnificus Prof. Ir. K.Ch.A.M. Luyben;

voorzitter van het College voor Promoties,

in het openbaar te verdedigen op

dinsdag, 26 mei, 2015 om 15:00 uur

door

Mariëtte DE GROEN

Ingenieur geboren te Voorburg, Nederland

Dit proefschrift is goedgekeurd door de

promotor: Prof. Dr. Ir. T.J.H. Vlugt

copromotor: Dr. Ir. Th. W. de Loos

Samenstelling promotiecommissie bestaat uit:

Rector magnificus, voorzitter

Prof. Dr. Ir. T.J.H. Vlugt, promotor

Dr. Ir. Th.W. de Loos, copromotor

Prof. Dr. Ir. A.B. de Haan, TNW, TU Delft

Prof. Dr. S.J. Picken, TNW, TU Delft

Prof. Dr. U.K. Deiters, Universität zu Köln

Prof. Dr. E.J. Meijer, Universiteit van Amsterdam

Dr. Ir. B. Breure, Shell



Enabling new technology

This research is supported by the Dutch Technology Foundation STW, applied science division of NWO and the Technology Program of the Ministry of Economic Affairs.

Table of Contents

1. Introduction to CO ₂ capture	1
2. Phase theory of binary mixtures of a liquid crystal and a gas.....	5
3. Phase behaviour of liquid crystals with CO ₂	11
4. Phase behaviour of the system 4'-pentyloxy-4-cyanobiphenyl + CO ₂	23
5. Henry coefficients of selected binary mixtures of a liquid crystal + CO ₂ ...	37
6. Binary and ternary mixtures of liquid crystals with CO ₂	47
7. Phase behaviour of binary mixtures of a liquid crystal and methane.....	67
8. Concluding remarks.....	75
References.....	77
Summary	85
Samenvatting.....	89
Curriculum Vitae.....	93
Published work.....	95
Acknowledgement.....	97
Appendix A. Experimental data of Chapter 3	99
Appendix B. Experimental data of Chapter 4	105
Appendix C. Experimental data of Chapter 5	113
Appendix D. Experimental data of Chapter 6.....	117
Appendix E. Experimental data of Chapter 7	131
Appendix F. Overview of the LCs used	133

1. Introduction to CO₂ capture

In recent years, research on global warming remained an important issue, especially research to prevent the exhaust of greenhouse gases [1-6]. The main goal of several climate initiatives is to lower the atmospheric concentration of greenhouse gases [1,3,7]. As the production capacity of green energy is not developing fast enough to substitute fossil fuels, capturing CO₂ is needed to control the atmospheric CO₂ concentration [7-9]. Several methods for capturing CO₂ are available on the short term, for example post-combustion CO₂ capture with amines, pre-combustion CO₂ capture with solvents like Selexol or Rectisol, or the oxyfuel process [10-16]. However, all capturing methods increase the energy consumption of the fossil fuel power plant. In the case of amine absorption, the energy consumption lowers the production of the complete power plant by 30% to 40% [2,17].

Most commercial processes involve post-combustion CO₂ capture from flue gas. This method is already available since the 1930s, for example for the removal of CO₂ from natural gas [18,19]. The main advantage of post-combustion CO₂ capture is that it can be incorporated easily in existing power plants [17,20]. One of the most used commercial methods is alkanolamine scrubbing [10,19,20]. An aqueous mixture of an alkanolamine is brought into contact with a gaseous stream containing CO₂. The CO₂ binds chemically with the amine component, the CO₂ lean stream is released to the atmosphere. The amine complex is regenerated in another column with steam. The main drawback of this process is that regeneration of the solvent is energetically intensive. Other drawbacks are emissions of alkanolamine, the formation of aerosols and corrosion of the equipment [21-24]. Therefore, an ongoing search is to find solvents needing a lower regeneration temperature [20]. Currently, molecules like diisopropylamine (DIPA) and tertiary amines like methyldiethanolamine (MDEA) are preferentially used because of their lower regeneration temperature [8,24]. Other post-combustion processes which are currently investigated are, amongst others, membrane processes and processes based on the use of phase change ionic liquids, and various types of solid sorbents such as Metal Organic Frameworks (MOFs) or zeolites [24-27].

For new installations pre-combustion capture is considered as a viable option, though no process is found yet with small energy use. Conventional methods are the Selexol and Rectisol processes [28,29]. These processes are based on physical

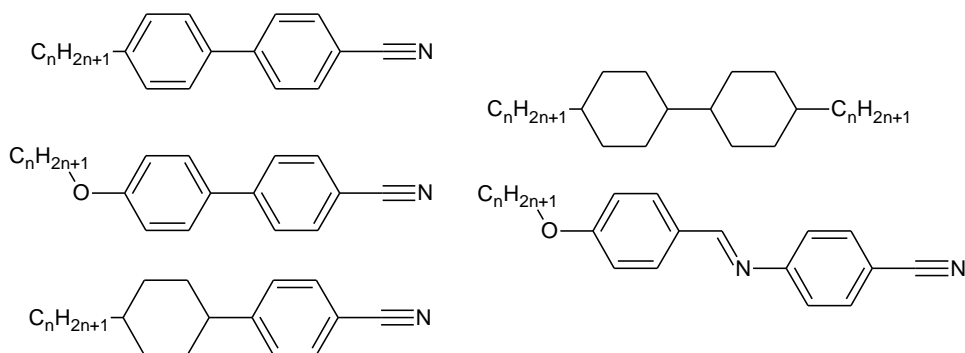


Figure 1.1. Molecular structures of the liquid crystals used in this study.

dissolution of CO₂ using alcohols at elevated pressure [28]. There is an ongoing search for new materials for capturing CO₂ in a more energy efficient way.

Some new materials for pre-combustion CO₂ capture are, amongst others, metal organic frameworks, zeolites and ionic liquids [24,26,28,30]. It is not clear yet which technology will eventually become most promising.

Recently, a process was proposed using liquid crystals for CO₂ capture by Gross and Jansens [31]. The key property of liquid crystals is the structured liquid phase. In case of a nematic phase this is a phase with similar viscosity as the isotropic phase, but the molecules have orientational ordering [32]. The shape of the molecules causes this: liquid crystals have a rigid core, consisting of two or more benzene and/or cyclohexane rings with side tails at the 4- and 4'-positions. Examples of the general structures of the liquid crystals used in this study are shown in Figure 1.1. The solubility of CO₂ is lower in the nematic crystalline phase than in the isotropic disordered phase, because of e.g. a free volume difference [33,34]. If the liquid crystal solvent is saturated in the isotropic phase, and is cooled down at constant pressure until the nematic phase is reached, CO₂ is released from the solvent [31]. This potentially can lead to a lower energy use for capturing CO₂, because the solvent is regenerated by a temperature change of a few degrees Kelvin only [31].

Two parameters are in general important for this process: the solubility of CO₂ in the liquid crystal solvent and the amount of CO₂ released from the solvent in each absorption/desorption cycle as described in the previous paragraph. Very little is known about the solubility of CO₂ in liquid crystals [35,36]. Of these liquid crystals, only the solubility in the liquid crystalline and isotropic phase is studied

with a gravimetric method. The article of Chen describes the solubility of CO₂ and of different gases like N₂ and He in liquid crystals [37]. From this study, it is clear that CO₂ is better soluble than the other gases.

Other types of phase behaviour of liquid crystal + CO₂ systems, like the study of three-phase curves, or the phase transitions from the nematic to the isotropic one-phase areas, are not studied in literature. The only articles on phase behaviour of liquid crystals with solutes published are of T,x -diagrams of mixtures of alkanes [38,39] or organic solutes [40,41] and liquid crystals.

The research discussed in this thesis focuses on the experimental determination of P,T,x -phase diagrams of CO₂ + liquid crystal systems. A short overview of phase theory of these kind of systems is presented in Chapter 2. In Chapter 3 of this thesis binary phase diagrams of a liquid crystal with CO₂ are discussed. Chapter 4 deals with a complete P,T,x -phase diagram of the binary system 5OCB + CO₂. In Chapter 5, phase diagrams of liquid crystals with CO₂ at lower CO₂ concentration and the Henry coefficient of these systems are discussed. Chapter 6 discusses ternary phase diagrams of mixtures of two liquid crystals + CO₂. Finally, Chapter 7 deals with the solubility of methane in various liquid crystals. An overview of the molecular structures of the liquid crystals used is presented in Appendix F. The main conclusion of this thesis is that liquid crystals of the phenyl-cyclohexyl type are most promising for a CO₂ capture process with liquid crystals. Methane is best soluble in apolar liquid crystals. Using binary mixtures of liquid crystals as a solvent leads to better solvent properties for CO₂. However, currently the liquid crystal process is not suitable for commercialization.

2. Phase theory of binary mixtures of a liquid crystal and a gas

Phase theory is the section of thermodynamics describing phase equilibria of one or more substances. These phase equilibria are generally described as functions of pressure P , temperature T and composition x . The main strength of phase theory is the ability to describe a phase diagram in a qualitative way with a minimum of experimental data available [42].

To reach thermodynamic equilibrium, the chemical potentials μ_i of component i should be equal in all the different phases:

$$\mu_i^{\alpha} = \mu_i^{\beta} = \dots = \mu_i^{\pi} \quad (2.1)$$

This equation is valid for n components in π phases. For all the lines and points described in Figure 2.1 this condition holds.

The number of degrees of freedom at equilibrium according to the phase rule of Gibbs is:

$$F = n - \pi + 2 - \phi \quad (2.2)$$

This equation tells us that the number of degrees of freedom F for any equilibrium in the diagram equals to the number of components n plus 2, with the number of phases π and the number of additional relations ϕ subtracted from it. As an example, for a system of two phases, i.e. liquid + vapor, in a binary system, the number of degrees of freedom is 2. When two variables are chosen, the system is completely described. For example, if pressure and temperature are chosen, the composition of the liquid and gas phase are fixed.

2.1. Unary systems

Unary systems have, in general, three different kind of phases: a gas phase G, an isotropic liquid phase I and one or more solid phases denoted with S_i . Liquid crystals have, beside these S, I and G phases one or more liquid crystalline phases. A liquid crystalline phase can be, for example, a nematic phase N or a smectic phase Sm [32]. Smectic phases exist in various types, depending on the type of ordering. In the following, all these liquid crystalline phases are lumped

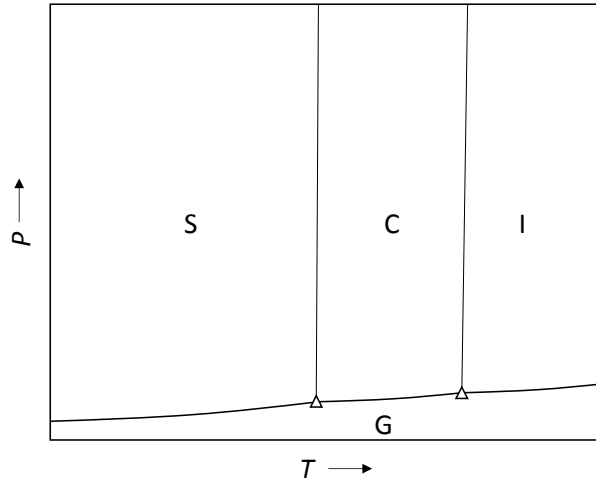


Figure 2.1. Schematic P,T-diagram of a pure liquid crystal. S denotes a solid phase, C the liquid crystalline phase, I the isotropic phase and G the gas phase. Δ denotes the triple points of the liquid crystal.

in one phase, called a condensed phase with symbol C. Figure 2.1 shows a schematic unary phase diagram of such a generalized liquid crystalline substance.

Applying the phase rule of Gibbs to the phase diagram of Figure 2.1, the maximum number of phases being in equilibrium for this one-component system equals 3 ($= 1 + 2$). In this case, the system has zero degrees of freedom. The resulting point in the phase diagram is called a triple point, and it is denoted with a triangle in Figure 2.1. For the unary system shown in Figure 2.1, two triple points are present: the triple point SCG and CIG. At each triple point three two-phase lines intersect, as three different two-phase combinations exist. For example, at the triple point SCG the S + C, the C + G and the S + G phase equilibrium lines intersect. The C + G and the S + G equilibrium pressure correspond to the vaporisation curve of the condensed phase and the sublimation curve, respectively, and is equal to the vapour pressure. The S + C equilibrium corresponds to the phase transition of the solid to the condensed phase. For all these two-phase equilibria the equation of Clausius-Clapeyron is valid [43]:

$$\left(\frac{dP}{dT} \right)_{\text{coex}} = \frac{\Delta H}{T \Delta V} \quad (2.3)$$

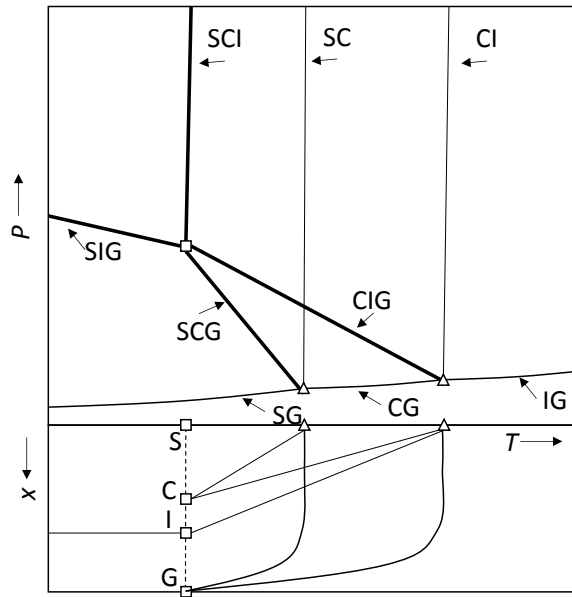


Figure 2.2. Schematic representation of a P,T,x -projection of a liquid crystal with a gas. S is the solid phase, C is the liquid crystalline phase, I is the isotropic phase and G is the gas phase. \triangle is a triple point of the pure LC, \square a quadruple point of the mixture. The thin solid lines correspond to the two-phase equilibria of the unary liquid crystal system. The bold lines correspond to the three-phase equilibria of the binary system. The labels next to the lines represent the corresponding phase equilibria.

Equation (2.3) describes that the slope of the phase equilibrium in the P,T -plane is a relation between the enthalpy change ΔH , the temperature T and the volume change ΔV of the phase transition. An illustration of this formula is the $S + C$ phase equilibrium curve, which has a steep slope and a relative small ΔV compared to the sublimation and the $C + G$ curve. Therefore, as an estimation of the triple point temperature, one can use the S to C phase transition temperature at atmospheric pressure.

2.2. Binary systems

Compared to unary systems, binary systems have an additional degree of freedom. Therefore, a P,T -plane is not sufficient anymore to describe the complete phase behaviour of the system. Mostly, the complete phase behaviour

is shown using a P, T, x -projection. A schematic example of the binary system of a liquid crystal with a gas is shown in Figure 2.2. First, the P, T -projection of such a system will be discussed, followed by the T, x -projection.

The P, T -projection of Figure 2.2 shows the phase equilibria of the pure liquid crystal as shown in Figure 2.1. These are represented with thin lines. The monovariant three-phase equilibria corresponding to the binary mixture are shown as bold lines. The three-phase equilibria shown are the CIG, SCG, SCI and SIG equilibria. As the binary mixture has one degree of freedom left if there are three phases in equilibrium, these three-phase equilibria are represented as a curve in the P, T -diagram. The SCG and the CIG curve end in the corresponding triple point of the pure component. This is easily understandable if one considers the case of an infinitely small amount of gas added to the liquid crystal: the three-phase equilibrium will be hardly influenced and will be close to the triple point. The initial slope of the three-phase equilibrium curve at the triple point SCG can be calculated using Ipat'ev's equation [44]:

$$\frac{dP}{dT} = \frac{H_1 \Delta_{tr} H_{LC}^*}{T_{tr,LC} (H_1 \Delta_{tr} V_{LC}^* - RT_{tr,LC})} \quad (2.4)$$

This equation shows us that the slope of the three-phase curve depends, among others, on the phase transition enthalpy $\Delta_{tr} H_{LC}^*$ of the pure liquid crystal. Therefore, the SCG curve is steeper than the CIG curve in the P, T -diagram. Other factors are the volume change of the phase transition of the pure liquid crystal $\Delta_{tr} V_{LC}^*$, the temperature of the phase transition of the pure liquid crystal $T_{tr,LC}$ and the Henry coefficient H_1 . The two aforementioned three-phase curves, SCG and CIG, intersect in a four-phase point, called a quadruple point. At this point, the four three-phase curves SCG, CIG, SCI and SIG intersect. When the temperature is lower than the temperature of the quadruple point, the nematic phase is not stable anymore. As the number of degrees of freedom at the quadruple point is zero, the four phases have a unique composition and therefore, it is difficult to measure this point. The quadruple point is usually estimated from the intersection of the three-phase curves directly.

With the main elements of the P, T -plane discussed, the T, x -plane will be considered. First, the nature of a three-phase equilibrium at a constant composition is examined. In this case, at a specific temperature and pressure, all the phases are in equilibrium, but the compositions of the different phases are

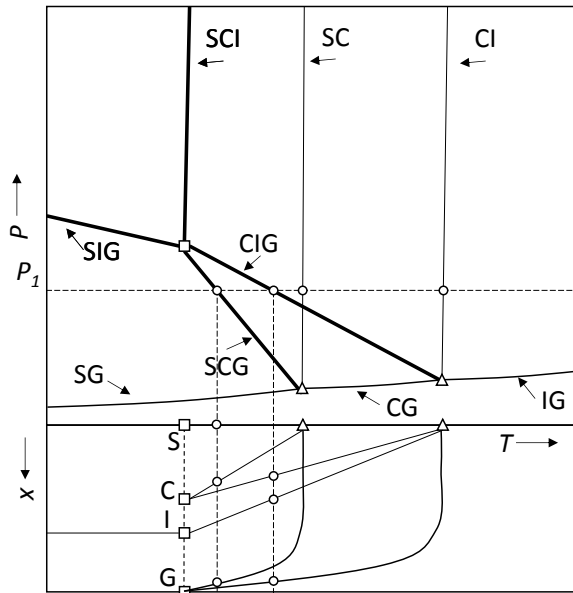


Figure 2.3. P,T,x -projection of a binary system of a liquid crystal with a gas. At (constant) pressure P_1 , the intersections with the three- and two-phase curves are visualized in both the P,T - and the T,x -plane. S is the solid phase, C is the liquid crystalline phase, I is the isotropic phase and G is the gas phase. Δ is the triple point of the pure LC, \square the quadruple point of the mixture.

in principle not equal. Therefore, in the T,x -plane the three-phase equilibrium is represented with three lines, each line describing the composition of one of the phases. For the CIG three-phase equilibrium in a binary system of a liquid crystal and a gas, one can consider the gas-phase as an almost pure gas. In the case of a liquid crystal and a gas, the S phase in the SCG equilibrium can be considered to be pure LC. All the different lines of the three-phase equilibria end in the points of the quadruple point, as the three-phase equilibria in the P,T -plane do.

A T,x -phase diagram for a specific pressure, say P_1 , can be used for designing the CO_2 capture process, as these will show the phase equilibria present and the phase boundaries at the specified process conditions. The procedure of creating a T,x -phase diagram from the P,T,x -projection is shown in Figure 2.3. At pressure P_1 in the P,T -projection, first the SCG curve is crossed. Second, the SC phase transition of the pure component is crossed, and third the CIG curve and the CI

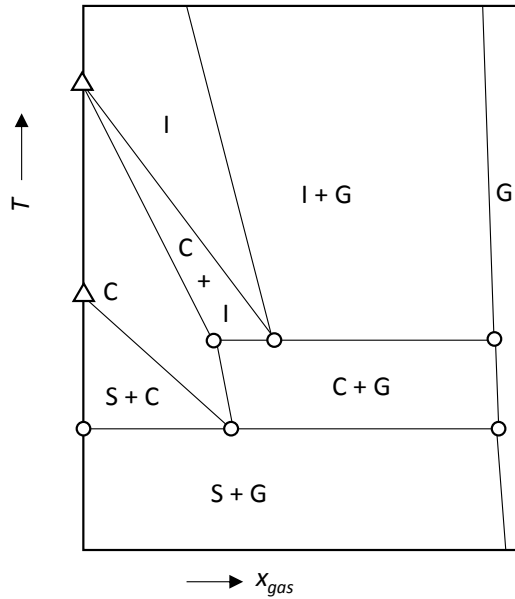


Figure 2.4. T, x -projection of a binary system of a liquid crystal with a gas at (constant) pressure P_1 (see Figure 2.3.) S is the solid phase, C is the liquid crystalline phase, I is the isotropic phase and G is the gas phase. Δ is the triple point of the pure LC. The circles correspond to the intersections with the three-phase equilibria.

phase transition of the pure component. At last, the IG curve of the pure component is crossed. The pure component two-phase equilibria are situated on the T -axes of the T, x -diagram. The compositions of the three-phase equilibria can be found by reading the corresponding curves in the T, x -projection which take part in the equilibrium. The resulting T, x -diagram is shown in Figure 2.4.

3. Phase behaviour of liquid crystals with CO₂

This chapter is based on: M. de Groen, T.J.H. Vlugt, T.W. de Loos, Phase behaviour of liquid crystals with CO₂, Journal of Physical Chemistry B, 116 (2012) 9101-9106

3.1. Introduction

For a CO₂ capture process using liquid crystals, the gas phase can be separated from the liquid phase at a three-phase equilibrium CIG: at this point, a structured phase (C), an isotropic (I) and a gas phase (G) coexist. C denotes a condensed phase: a solid phase, a smectic phase or a nematic phase. In Figure 3.1, the absorption-desorption cycle is shown in a T, x -diagram. The difference in solubility between the structured and isotropic phase determines the amount of CO₂ that can be captured during an absorption-desorption cycle. This depends on the width of the two-phase area C + I. The difference between the initial slopes ($x_{\text{CO}_2} \rightarrow 0$) of the $C \leftrightarrow C + I$ and the $C + I \leftrightarrow I$ curves depends on the phase transition enthalpy and can be calculated using a modified van 't Hoff law [43]:

$$\frac{dx_{\text{CO}_2}^{\text{C}}}{dT} - \frac{dx_{\text{CO}_2}^{\text{I}}}{dT} = \frac{\Delta_{\text{tr}}H}{RT_{\text{tr}}^2} \quad (3.1)$$

Here $\Delta_{\text{tr}}H$ is the phase transition enthalpy, which is positive for the structured to isotropic phase transition of the pure LC, $x_{\text{CO}_2}^{\text{C}}$ and $x_{\text{CO}_2}^{\text{I}}$ are the mole fractions of CO₂ in the structured and isotropic phase, respectively, T is the temperature, T_{tr} is the phase transition temperature and R is the gas constant.

For capturing CO₂, nematic liquid crystals are most interesting because the viscosity of nematic LCs is much lower than that of the smectic LCs. Eq. (3.1) can only be used qualitatively as a measure of the width of the two-phase region for nematic liquid crystals, as published values for $\Delta_{\text{NI}}H$, the phase transition enthalpy for the nematic to isotropic phase, strongly scatter. As an example, in Table 3.1 typical literature values for $\Delta_{\text{NI}}H$ are reported.

Table 3.1. Phase transition temperatures and enthalpies for the pure LCs tested. *S* denotes the solid phase, *Sm* the smectic, *N* the nematic and *I* the isotropic phase.

Molecule	T_{SN} / K	T_{SmN} / K	T_{NI} / K	$\Delta_{NI}H$ / kJ/mol	T_{Sml} / K
5CB	296 [45]		308 [46] 308.35 [47]	0.54 [46] 0.39 [47]	
	296.9 ^c		308.4 ^c		
5OCB	320.5 ^a [46] 325.5 ^b [48] 326.8 ^{b,c}		340.71 [46] 340.55 [47] 341.5 ^c	0.42 [46] 0.20 [47]	
8OCB	326.01 [46] 327.7 ^d	339.80 [46]	352.58 [46] 352.85 [47] 353.2 ^d	0.88 [46] 0.40 [47]	
3,4-BCH					370 ^c
2,3-BCH					341 ^c

^a: Solid phase S_1 , ^b: Solid phase S_2 , ^c: this work, ^d: Provided by Prof. Picken [49].

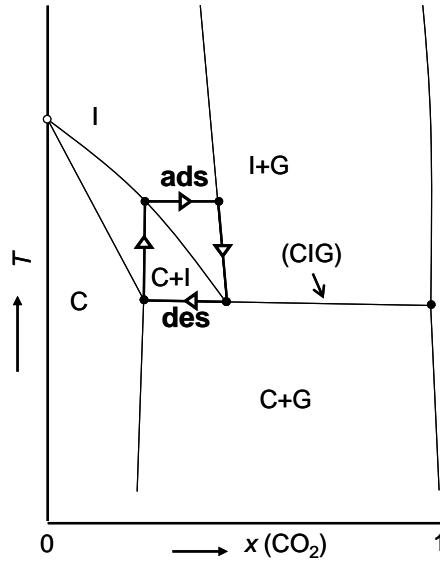


Figure 3.1. T,x -diagram at constant pressure of a liquid crystal with CO_2 . *C* is a structured liquid phase, *I* is the isotropic phase and *G* is the gas phase. The line $\bullet \rightarrow \bullet$ represents the CO_2 adsorption (ads) and desorption (des) cycle as explained in the main text.

Another parameter strongly influencing the applicability of liquid crystals is the solubility of CO₂. A few solubility measurements of CO₂ in liquid crystals are described in literature [35-37,50]. Of the liquid crystals measured, PCH5 has the highest mass based CO₂ solubility, followed by PCH8-CNS and MBBA [37]. A sharp increase in solubility between the isotropic and nematic phase was found [31]. The method used in literature was a gravimetric method. The phase behaviour of liquid crystal + CO₂ systems has not studied before, only the presence of a two-phase region was found [35].

In this chapter, experimental *P,T*-phase diagrams of binary mixtures of CO₂ with different liquid crystals with varying polarity and different alkyl chain length will be discussed at a weight fraction $w_{\text{CO}_2} = 0.05$. These phase diagrams will be used to discuss the influence of molecular structure and polarity on the solubility of CO₂ in liquid crystals.

3.2. Experimental methods

Materials. 4'-pentyloxy-4-cyanobiphenyl, purity 99% mass (5OCB) and 4'-pentyl-4-cyanobiphenyl, purity 99% mass (5CB) were obtained from Alfa Aesar, 4-ethyl-4'-propyl-bicyclohexyl, purity >98% mass (2,3-BCH) and 4-propyl-4'-butyl-bicyclohexyl, purity >98% mass (3,4-BCH) were kindly supplied by Merck, and 4'-octyloxy-4-cyanobiphenyl, purity >98% mass (8OCB) was kindly supplied by Prof. Picken, Delft University of Technology, Delft, The Netherlands. Carbon dioxide was obtained from Linde Gas, with a purity of 4.5. All chemicals were used as received. In Table 3.1 the pure component properties of these liquid crystals are listed.

Setup used. Phase equilibrium measurements were performed according to the synthetic visual method using a Cailletet setup, which is described in detail elsewhere [51]. Up to 365 K, the temperature was controlled with a Lauda RC20 thermostatic water bath within 0.02 K. For liquid crystals with a clearing point higher than 360 K, a silicone oil bath was used, controlled with a Shimaden DSM temperature control unit within 0.02 K. The pressure was measured using a Budenberg or a de Wit pressure balance, both with an uncertainty of 0.005 MPa. The temperature was measured with an ASL F250 Pt100 thermometer with an uncertainty of 0.01 K.

Sample Preparation. 0.1–0.15 g of liquid crystal was weighed in a so-called Cailletet tube. The sample was repeatedly degassed to remove all gaseous

impurities. To prevent evaporation of the liquid crystal, the top of the tube was cooled with liquid nitrogen when vacuum was applied. After completion of the degassing, CO₂ was added as a gas from a calibrated volume using a gas dosing system [51].

Method. The maximum error of isotropic + gas to isotropic ($I + G \leftrightarrow I$), nematic + gas to nematic ($N \leftrightarrow N + G$), and nematic + isotropic + gas (NIG) equilibria, measured at constant temperature, is ± 0.005 MPa. The maximum error of the solid + nematic to nematic ($S + N \leftrightarrow N$), solid + isotropic to isotropic ($S + I \leftrightarrow I$), smectic + nematic to nematic ($Sm + N \leftrightarrow N$), smectic + isotropic to isotropic ($Sm + I \leftrightarrow I$), solid + nematic + gas (SNG), solid + isotropic + gas (SIG), smectic + nematic + gas (SmNG) and smectic + isotropic + gas (SmIG) equilibria measured at constant pressure, is ± 0.03 K. The nematic + isotropic to isotropic ($N + I \leftrightarrow I$) and the nematic to nematic + isotropic ($N \leftrightarrow N + I$) transitions have been measured within an accuracy of 0.01K, unless otherwise stated. In the case of equilibria involving a smectic phase, only transitions in which the smectic phase disappears could be measured, because of the high viscosity of this phase.

3.3. Results

The liquid crystals tested can be divided in three different classes: apolar liquid crystals, polar liquid crystals and weakly polar liquid crystals. An overview of the measured data points is available in Appendix A. The apolar liquid crystals, 2,3-BCH and 3,4-BCH, have a crystal to smectic and at a higher temperature a smectic to isotropic phase transition. Phase equilibria measured for these systems are the three-phase curve SmIG, the bubble-point curve $I + G \leftrightarrow I$ and the curve separating the two-phase region $Sm + I$ and the one-phase area I . The phase diagrams of 2,3-BCH + CO₂ and 3,4-BCH + CO₂, both with a weight fraction of CO₂ of $w_{CO_2} = 0.05$ are provided in Figure 3.2 and 3.3. The addition of CO₂ causes melting point depression: the smectic to isotropic phase transition temperature is shifted to lower temperatures. This is in agreement with Equation (3.1). For comparison, the pure component $Sm \leftrightarrow I$ curve is shown in Figure 3.2 and 3.3 as dashed curve. The $I + G \leftrightarrow I$ curve of 3,4-BCH is found at a higher pressure than the $I + G \leftrightarrow I$ curve of 2,3-BCH.

The pure liquid crystal 8OCB shows a different behaviour: at atmospheric pressure and 326 K, it has a phase transition from solid to smectic, at 340 K from the smectic to the nematic phase and at 353 K from the nematic to the isotropic phase [46]. The phase diagram of this liquid crystal with CO₂ at $w_{CO_2} = 0.05$, is

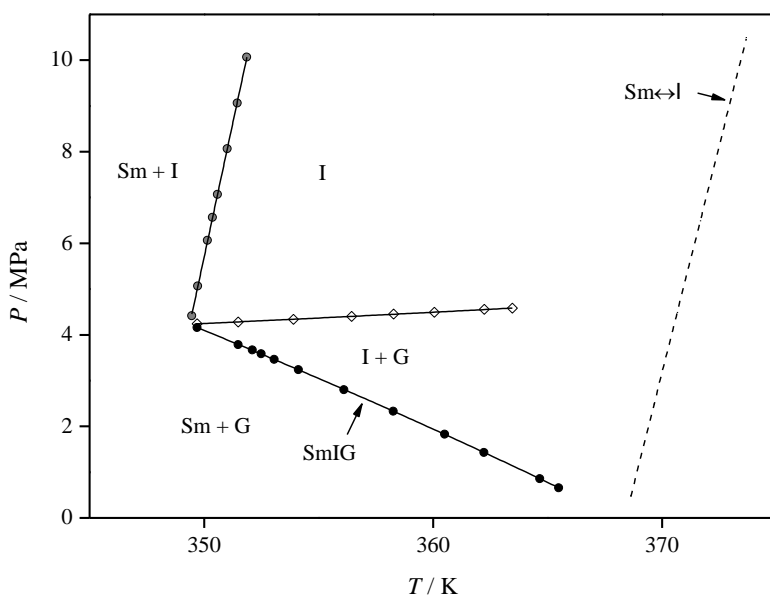


Figure 3.2. P,T -diagram of 4-propyl-4'-butyl bicyclohexyl + CO_2 , $w_{\text{CO}_2} = 0.05$. Description of symbols used: ● $\text{Sm} + \text{I} \leftrightarrow \text{I}$, ◇ $\text{I} + \text{G} \leftrightarrow \text{I}$, ● $\text{Sm} + \text{I} + \text{G}$. The dashed curve is the $\text{Sm} \leftrightarrow \text{I}$ phase transition of the pure LC.

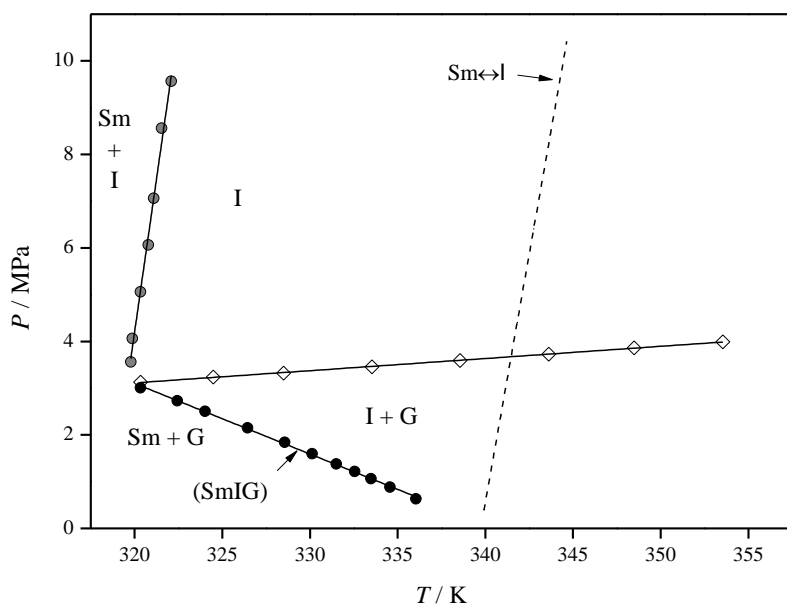


Figure 3.3. P,T -diagram of 4-ethyl-4'-propyl bicyclohexyl + CO_2 , $w_{\text{CO}_2} = 0.05$. Description of symbols used: ● $\text{Sm} + \text{I} \leftrightarrow \text{I}$, ◇ $\text{I} + \text{G} \leftrightarrow \text{I}$, ● $\text{Sm} + \text{I} + \text{G}$. The three-phase curve has notation between parentheses (...). The dashed curve is the $\text{Sm} \leftrightarrow \text{I}$ phase transition of the pure LC.

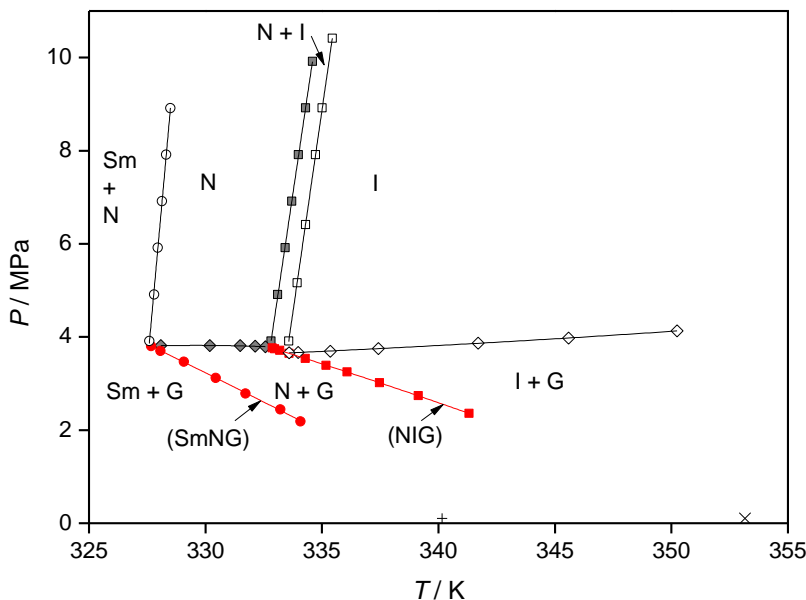


Figure 3.4. P,T -diagram of 4'-octyloxy-4-cyanobiphenyl + CO_2 , $w_{\text{CO}_2} = 0.05$. Description of symbols used: \circ $\text{Sm} + \text{N} \leftrightarrow \text{N}$, \blacksquare $\text{N} \leftrightarrow \text{N} + \text{I}$, \square $\text{N} + \text{I} \leftrightarrow \text{I}$, \blacklozenge $\text{N} + \text{G} \leftrightarrow \text{N}$, \diamond $\text{I} + \text{G} \leftrightarrow \text{I}$, \bullet $\text{Sm} + \text{N} + \text{G}$, \blacksquare $\text{N} + \text{I} + \text{G}$, $+$ $\text{Sm} \leftrightarrow \text{N}$ for the pure LC at 1 bar, \times $\text{N} \leftrightarrow \text{I}$ for the pure LC at 1 bar. Three-phase curves have notations between parentheses (...).

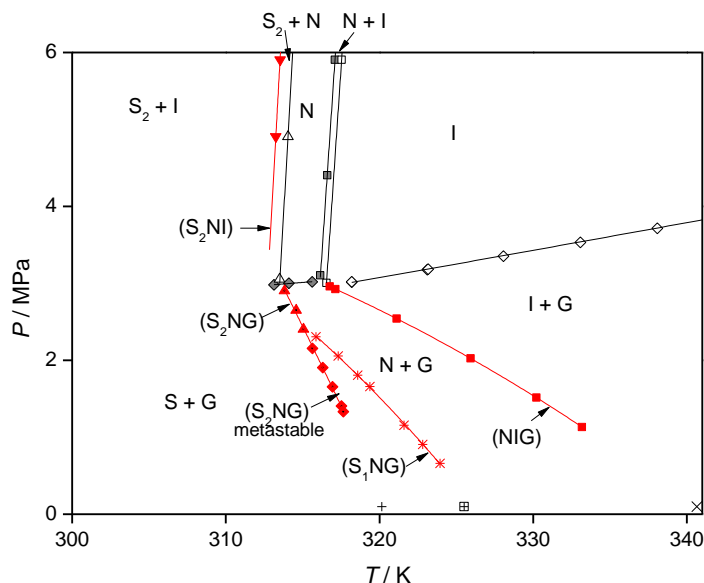


Figure 3.5. Part of P,T -diagram of 4'-pentyloxy-4-cyanobiphenyl + CO_2 , $w_{\text{CO}_2} = 0.05$. Description of symbols used: ∇ $\text{S}_2 + \text{N} + \text{I}$, \triangle $\text{S}_2 + \text{N} \leftrightarrow \text{N}$, \blacksquare $\text{N} \leftrightarrow \text{N} + \text{I}$, \square $\text{N} + \text{I} \leftrightarrow \text{I}$, \blacklozenge $\text{N} + \text{G} \leftrightarrow \text{N}$, \diamond $\text{I} + \text{G} \leftrightarrow \text{I}$, \blacktriangle $\text{S}_2 + \text{N} + \text{G}$, \blacklozenge metastable $\text{S}_2 + \text{N} + \text{G}$, \times $\text{S}_1 + \text{N} + \text{G}$, \blacksquare $\text{N} + \text{I} + \text{G}$, $+$ $\text{S}_2 \leftrightarrow \text{N}$ for the pure LC at 1 bar, \boxplus $\text{S}_1 \leftrightarrow \text{N}$ for the pure LC at 1 bar, \times $\text{N} \leftrightarrow \text{I}$ for the pure LC at 1 bar. Three-phase curves have notations between parentheses (...).

presented in Figure 3.4. Bubble-points were measured for both the nematic and the isotropic phase. Compared to the endpoint of the bubble-point curve of the nematic phase, the bubble-point curve of the isotropic phase starts at a lower pressure, indicating a solubility difference. The temperature of the smectic to nematic and the nematic to isotropic phase transition is shifted to lower temperatures and due to the binary nature of the system the phase transition became a trajectory instead of a sharp transition. The width of the two-phase area $N + I$ is 0.8 K and the isotropic phase starts to form at 332.8 K at 3.9 MPa.

Two three-phase curves were measured for this system: the $SmNG$ curve and the NIG curve. The $SmNG$ curve is measured from the intersection of the bubble-point curve and the $Sm + N \leftrightarrow N$ phase transition line and the NIG curve starts at the intersection of the bubble-point curve and the $N \leftrightarrow N + I$ phase transition line.

The phase diagram of the binary system 5OCB + CO_2 at $w_{CO_2} = 0.05$ is shown in Figure 3.5. For 5OCB, two solid phases were found, S_1 and S_2 . Pure 5OCB has an atmospheric $N \leftrightarrow I$ transition at 341 K, a $S_1 \leftrightarrow N$ transition at 324 K and a metastable $S_2 \leftrightarrow N$ transition at 317 K according to the results in Chapter 4. Figure 3.5 shows the phase behaviour of the aforementioned binary system. When CO_2 is added to the liquid crystal, the S_2 phase becomes more stable than the S_1 phase. Therefore, a quadruple point S_1S_2NG was found at 314.9 K, 2.49 MPa. At this point, four three-phase curves should intersect: the S_1NG , S_2NG , S_1S_2N and S_1S_2G curve. The last two mentioned three-phase curves could not be detected with the used experimental method as it would require the detection of solid-solid transitions. At temperatures lower than this quadruple point, S_2 is most stable and the three-phase equilibrium line S_2NG is found. However, as the $S_1 \leftrightarrow S_2$ phase transition does not occur instantaneous, part of this line is measured in the metastable region. As the melting point depression for the nematic phase is larger than for the solid phase, an intersection of the S_2NI and the S_2NG line is found at 312.8 K, 3.32 MPa. This intersection is the quadruple point S_2NIG , where the three-phase equilibrium curves S_2NG , NIG , S_2NI and S_2IG intersect. At temperatures lower than the quadruple point, the nematic phase becomes metastable. The boundary between the $S_2 + I$ and $S_2 + N$ two-phase regions is the S_2NI three-phase line. At temperatures below this quadruple point the nematic phase is not stable anymore.

Pure 5CB has a crystal \leftrightarrow nematic and a nematic \leftrightarrow isotropic phase transition. The phase diagram of this liquid crystal with CO_2 is shown in Figure 3.6. The weight fraction of CO_2 is $w_{CO_2} = 0.05$. As the nematic region of the pure

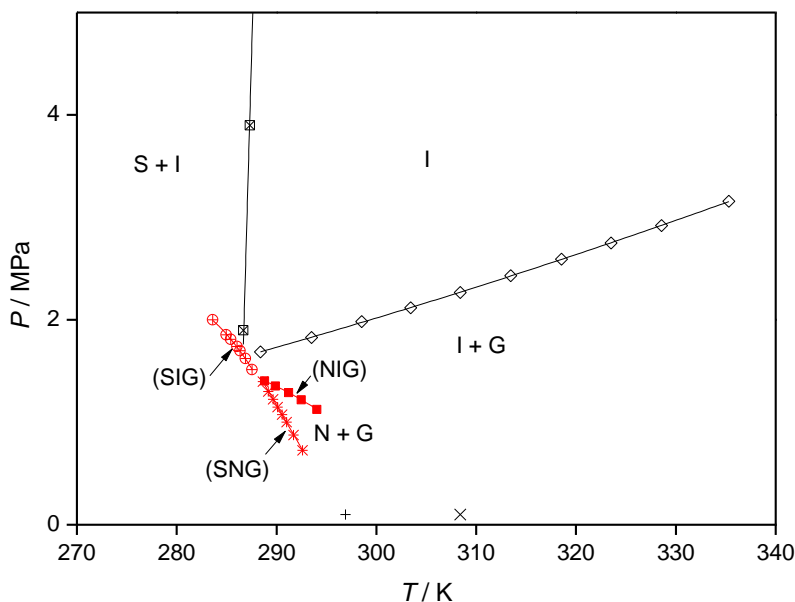


Figure 3.6. Part of P,T -diagram of 4'-pentyl-4-cyanobiphenyl + CO_2 , $w_{\text{CO}_2} = 0.05$. Description of symbols used: \boxtimes $S + I \leftrightarrow I$, \oplus $S + I + G$, \diamond $I + G \leftrightarrow I$, \times $S + N + G$, \blacksquare $N + I + G$, $+$ $S \leftrightarrow N$ for the pure LC at 1 bar, \times $N \leftrightarrow I$ for the pure LC at 1 bar. Three-phase curves have notations between parentheses (...).

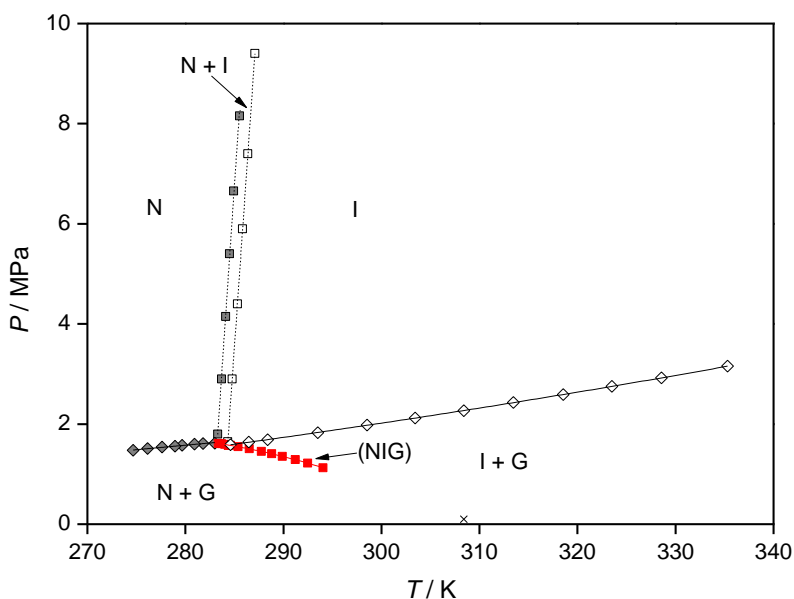


Figure 3.7. Metastable part of the P,T -diagram of 4'-pentyl-4-cyanobiphenyl + CO_2 , $w_{\text{CO}_2} = 0.05$. Description of symbols used: \blacksquare $N \leftrightarrow N + I$, \square $N + I \leftrightarrow I$, \blacklozenge $N + G \leftrightarrow N$, \diamond $I + G \leftrightarrow I$, \blacksquare $N + I + G$, \times $N \leftrightarrow I$ phase transition for the pure LC at 1 bar. The three-phase curve has notation between parentheses (...).

component is smaller than that of the other liquid crystals tested, the quadruple point SNIG is found at a lower pressure than the $I + G \leftrightarrow I$ curve, and a stable $N + I \leftrightarrow I$ curve could not be measured. At the quadruple point, which is found around 288 K, 1.4 MPa, the three-phase curves NIG, SNG, SIG intersect. The fourth three-phase curve intersecting at this point would be the SNI phase transition, but this could not be measured at this concentration. When the solid is not crystallizing, the metastable part of the phase diagram is found, with the nematic to isotropic phase transition. The metastable part of the diagram is shown in Figure 3.7.

3.4. Discussion

The solubility of CO_2 is influenced by the polarity of the liquid crystal. As illustrated in Figure 3.8, the apolar liquid crystals have the lowest mass based solubility and 5CB the highest solubility. The solubility of CO_2 in the case of 5CB is higher than in the case of 5OCB, but in literature ether groups are considered to increase the solubility of CO_2 [52]. A possible explanation for this behaviour is a distorted quadrupolar moment of the benzene ring, leading to decreased affinity for CO_2 . Benzene rings have a quadrupolar moment, and ab initio computations have shown that CO_2 forms transient heterodimers with benzene [53]. However, as the system is dense, the interaction between CO_2 and the benzene ring will also depend on for example the packing of the molecules and solvent-solvent interactions.

Henry coefficients can be used to rank the CO_2 capacity of the solvents. The Henry coefficient can be calculated using:

$$[H_1 / \text{MPa}] = \lim_{x_{\text{CO}_2} \rightarrow 0} \frac{[f_{\text{CO}_2} / \text{MPa}]}{x_{\text{CO}_2}} \quad (3.2)$$

In equation (3.2), f_{CO_2} is the fugacity of CO_2 at the experimentally determined bubble point pressure, x_{CO_2} is the mole fraction of the sample and H is the Henry coefficient. Assuming that the gas phase is pure CO_2 and the isotropic phase is an ideal mixture, the Henry coefficient, H_1 , of CO_2 in the isotropic phase can be estimated using

$$H_1 = \frac{f_{\text{CO}_2}}{x_{\text{CO}_2}} \quad (3.3)$$

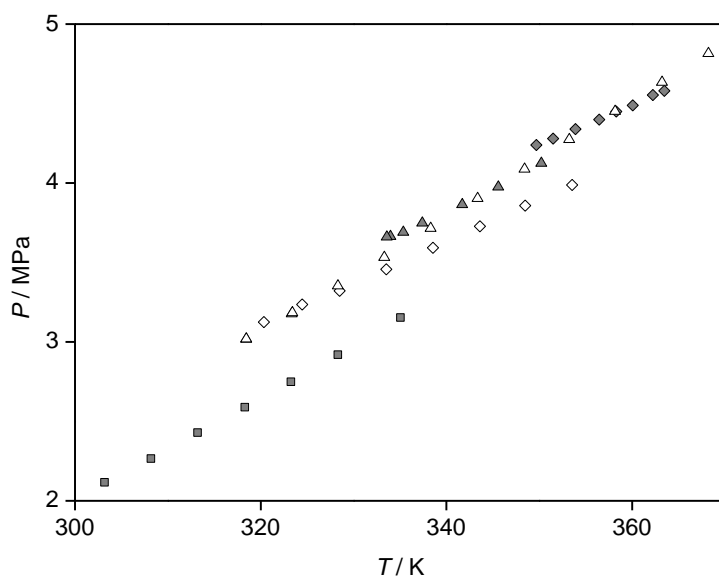


Figure 3.8. Bubble-point curves of various liquid crystals with $w_{\text{CO}_2} = 0.05$.

◆ 4-propyl-4'-butyl bicyclohexyl, ◇ 4-ethyl-4'-propyl bicyclohexyl,
 ▲ 4'-octyloxy-4-cyanobiphenyl, △ 4'-pentyloxy-4-cyanobiphenyl,
 ■ 4'-pentyl-4-cyanobiphenyl.

Table 3.2. Estimated Henry coefficients (H_1) for CO_2 in LCs at $T = 350 \text{ K}$.

LC molecule	H_1 / MPa	
	Mole based	Mass based
5CB	14.4	66.3
5OCB	15.3	73.5
8OCB	13.6	73.0
PB	15.5	74.2
EP	15.9	70.1

Experimental bubble-point data from the experiments was used to calculate the Henry coefficients at 350 K using an equation of state for calculating the fugacity coefficient of CO₂, see Table 3.2 [54]. In this table it is shown that increasing the length of the hydrocarbon chain of the LC leads to a higher mole based solubility: 3,4-BCH and 8OCB have a lower mole based Henry coefficient than 2,3-BCH and 5OCB, respectively. For ionic liquids with different chain lengths the same trend is observed [52].

3.5. Conclusion

P,T-phase diagrams have been determined for five binary systems of a liquid crystal + CO₂, at $w_{\text{CO}_2} = 0.05$. Of the liquid crystals investigated, 5CB has the highest solubility of CO₂. The apolar liquid crystals tested, 3,4-BCH and 2,3-BCH, have the lowest solubility of CO₂. These liquid crystals are not suitable for CO₂ capture, because of the high viscosity of the smectic phase. 5OCB and 8OCB have a lower solubility of CO₂ than 5CB, probably caused by a distortion of the quadrupole moment of the benzene ring. The molar solubility of CO₂ was found to be higher for molecules with a longer hydrocarbon tail. The liquid crystals tested in this chapter are not promising enough for a CO₂ capture process because of the low CO₂ solubility.

4. Phase behaviour of the system 4'-pentyloxy-4-cyanobiphenyl + CO₂

This chapter is based on: M. de Groen, H. Matsuda, T.J.H. Vlugt, T.W. de Loos, Phase behaviour of the system 4'-pentyloxy-4-cyanobiphenyl + CO₂, Journal of Chemical Thermodynamics, 59 (2013) 20-27.

4.1. Introduction

To design a process for CO₂ capture with liquid crystals, the P,T,x -phase diagram of a liquid crystal with CO₂ should be known to be able to select the proper process conditions. Such a study has not been executed before.

In this chapter, the results of a detailed experimental investigation on the phase behaviour of the system 4'-pentyloxy-4-cyanobiphenyl (5OCB) (1) + CO₂ (2) are presented at varying CO₂ concentrations, whereas in the previous chapter only the isopleth at a concentration of $w_{\text{CO}_2} = 0.05$ was studied. Based on the experimentally determined P,T -diagrams (isopleths at constant w_{CO_2} concentration) a proposal is made for a P,T -projection of the binary system. The isopleths were studied up to a CO₂ mole fraction of 0.72, at a temperature range of 280 – 360 K, and at pressures up to 12 MPa. For the isotropic phase, the molar Henry coefficient was calculated at 341 K to be 13.7 MPa based on the f,x -diagram up to $x_2 = 0.327$. This chapter is organized as follows. In section 4.2, the experimental method will be described, in section 4.3 the measured isopleths and in section 4.4 the discussion of these isopleths with a proposal for a P,T -projection.

4.2. Experimental methods

Materials. 4'-pentyloxy-4-cyanobiphenyl, 99 mass % (5OCB) was obtained from Alfa Aesar and used as received. Carbon dioxide was obtained from Linde Gas, with a purity of 4.5. An overview of the materials used is presented in Table 4.1.

Phase equilibrium measurements. Phase equilibria were visually measured according to the synthetic method using a Cailletet apparatus, as described in

Table 4.1. Overview of chemicals used in this chapter.

Chemical name	Source	Purity	Purification
CO ₂	Linde Gas	Volume fraction 0.99995	Used as received
4'-pentyloxy-4-cyanobiphenyl (5OCB)	Alfa Aesar	Mass fraction (GC) 0.999	Used as received

Chapter 3. Phase equilibria involving the disappearance of a solid phase were measured by changing the temperature while keeping the pressure constant, with an accuracy of 0.05 K unless stated otherwise. The phase boundaries between the two-phase regions nematic + isotropic and the homogeneous one-phase regions nematic or isotropic were measured at constant pressure with an accuracy of 0.01 K. The other phase equilibria were measured by varying the pressure while the temperature was kept constant, with an accuracy of 0.005 MPa, unless stated otherwise.

4.3. Results

P,T-phase diagrams of pure 5OCB and of 5OCB + CO₂ mixtures [(1- x_{CO_2}) 5OCB + x_{CO_2} CO₂] for mole fractions x_{CO_2} = 0.057, 0.159, 0.241, 0.329, 0.400, 0.497 and 0.720 have been measured. The experimental results are presented in Figures 4.1-4.8. The tables with the measured data are presented in Appendix B. In the binary system, next to two solid modifications of 5OCB (*S*₁ and *S*₂) also two isotropic liquid phases (*I*₁ and *I*₂) were found.

The pressure dependence of the solid (*S*₁) to nematic (*N*) and of the nematic (*N*) to isotropic (*I*₂) phase transition of pure 5OCB is shown in Figure 4.1. According to DSC measurements in literature, 5OCB has a nematic to isotropic liquid transition at 340.6 K and two different solid to nematic phase transitions at 320.5 and 325.5 K [46,48,55] at atmospheric pressure. The extrapolated data of the phase transitions to a pressure of 0.1 MPa, gave a solid to nematic phase transition at 326.8 K and a nematic to isotropic phase transition at 341.5 K, which corresponds well with the results in literature [46,48,55], the maximum deviation is 1.3 K. In literature, also a transition of another solid modification (*S*₂)

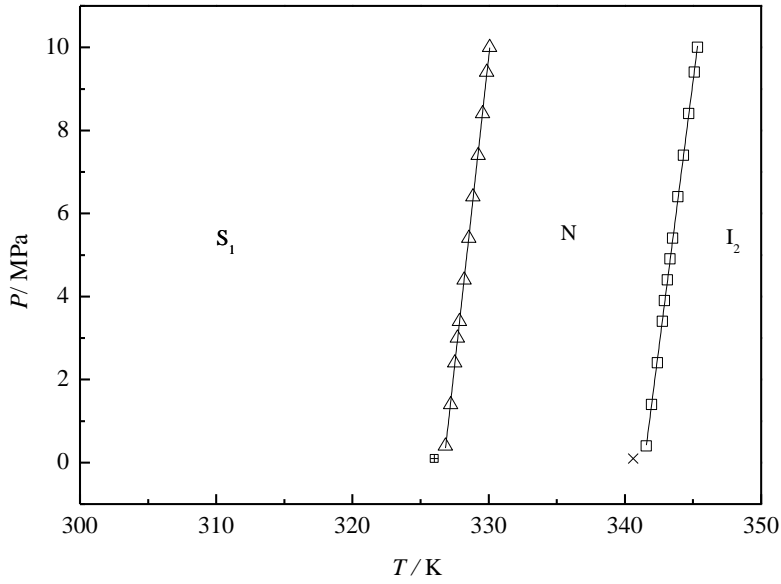


Figure 4.1. P,T -diagram of pure 5OCB. S_1 denotes the solid phase, N the nematic phase and I_2 the isotropic phase. Description of the used symbols: $\triangle S_1 \leftrightarrow N$, $\square N \leftrightarrow I_2$, $\boxplus S_1 \leftrightarrow N$ literature value at 0.1 MPa, $\times N \leftrightarrow I$ literature value at 0.1 MPa [55].

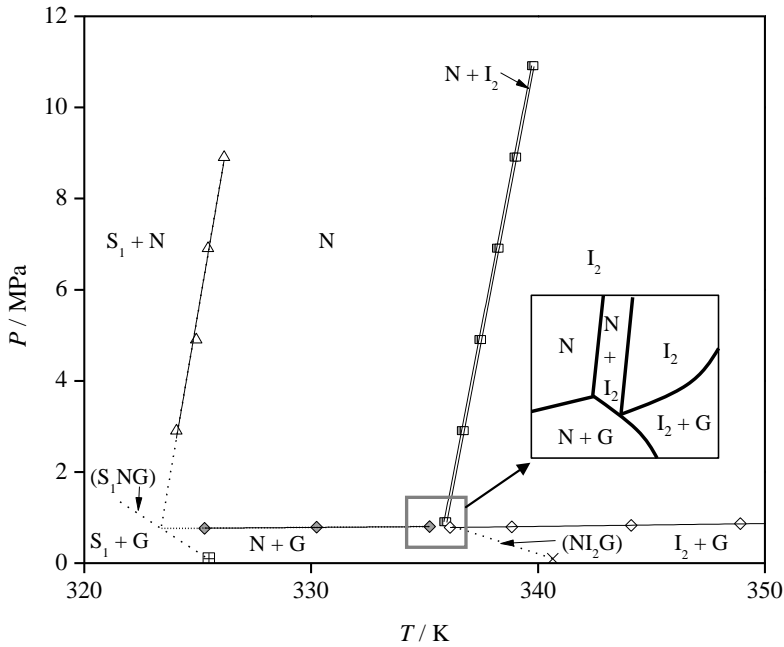


Figure 4.2. P,T -diagram of the system 5OCB + CO_2 for $x_{\text{CO}_2} = 0.057$. Description of the used symbols: $\triangle S_2 + N \leftrightarrow N$, $\blacksquare N \leftrightarrow N + I_2$, $\square N + I_2 \leftrightarrow I_2$, $\blacklozenge N + G \leftrightarrow N$, $\diamond I_2 + G \leftrightarrow I_2$, $\boxplus S_1 \leftrightarrow N$ for the pure LC at 0.1 MPa, $\times N \leftrightarrow I$ for pure 5OCB at 0.1 MPa. Notations between parentheses (...) denote three-phase curves. Dotted lines are added as a guide to the eye.

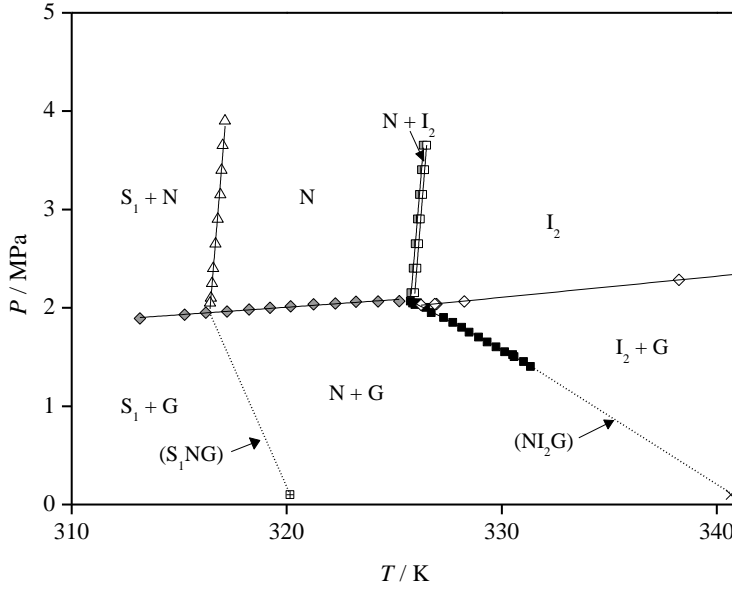


Figure 4.3. P,T -diagram of the system 5OCB + CO₂ for $x_{\text{CO}_2} = 0.159$. Description of the used symbols: \blacksquare $N \leftrightarrow N + I_2$, \square $N + I_2 \leftrightarrow I_2$, \blacklozenge $N + G \leftrightarrow N$, \diamond $I_2 + G \leftrightarrow I_2$, \blacksquare $N + I_2 + G$, \triangle $S_1 + N \leftrightarrow N$, \boxplus $S_1 \leftrightarrow N$ for pure 5OCB at 0.1 MPa, \times $N \leftrightarrow I_2$ for pure 5OCB at 0.1 MPa. Notations between parentheses (...) denote three-phase curves. Dotted lines are added as a guide to the eye.

to nematic is reported [55]. However, this transition was not found in this study for pure 5OCB.

The phase diagram of 5OCB + CO₂ at $x_{\text{CO}_2} = 0.057$, shown in Figure 4.2, shows behaviour which is to be expected for a binary mixture of a liquid crystal with CO₂. For this composition, the bubble-points of the nematic phase ($N + G \leftrightarrow N$) and of the isotropic liquid phase ($I_2 + G \leftrightarrow I_2$) were measured. The two-phase region $N + I_2$ is very narrow, the width is only 0.13 K. This two-phase region separates the homogeneous one-phase region N found at lower temperature from the one-phase region I_2 at higher temperature. At low pressure this two-phase region is separated from the two-phase region $N + G$ by the NI_2G three-phase curve (see inset in Figure 4.2). The pressure difference of the points of intersection of the $N + I_2 \leftrightarrow N$ curve and the $N + G \leftrightarrow N$ and that of the $N + I_2 \leftrightarrow I_2$ curve and the $I_2 + G \leftrightarrow I_2$ curve is only 0.02 MPa. In Figure 4.1 also points

of the $S_1 + N \leftrightarrow N$ phase boundary are plotted. The three-phase lines S_1NG and Nl_2G , are indicated with dotted lines in the Figure 4.2.

The system of $5OCB + CO_2$ for $x_{CO_2} = 0.159$ shows the same type of diagram as the phase diagram of $x_{CO_2} = 0.057$, see Figure 4.3. Compared to the system $5OCB + CO_2$ for $x_{CO_2} = 0.057$, apart from the three-phase curve Nl_2G the same phase equilibria were measured. The three-phase curve Nl_2G will end at the pure component's triple point Nl_2G . As the $N \leftrightarrow l_2$ curve of pure $5OCB$ is very steep, it can be assumed that this triple point practically coincides with the phase transition $N \leftrightarrow l_2$ of pure $5OCB$ at atmospheric pressure. At this higher concentration the $N + l_2$ two-phase region has become slightly wider and the phase boundaries of the two-phase region, $N + l_2 \leftrightarrow l_2$ and $S_1 + N \leftrightarrow N$, were found at lower temperatures than the same phase equilibria of the system with $x_{CO_2} = 0.057$. However, the temperature difference between the boundaries of the homogeneous nematic phase, $S_1 + N \leftrightarrow N$ and $N \leftrightarrow N + l_2$, has become smaller because the slope dP/dT is higher for the S_1NG curve than for the Nl_2G curve.

The phase diagram of the system $5OCB + CO_2$ for $x_{CO_2} = 0.241$, shown in Figure 4.4, has been reported in Chapter 3. At this concentration, two different solid modifications were found, S_1 and S_2 . Two three-phase equilibria of solid $5OCB$, the nematic phase and the gas phase were found: S_2NG and S_1NG . Part of the S_2NG line was measured in the metastable region. These two three-phase curves intersect in a quadruple point S_1S_2NG . The coordinates of this quadruple point were determined by intersecting the two extrapolated three-phase curves and found to be $T = (315.2 \pm 0.1)$ K and $P = (2.43 \pm 0.01)$ MPa. The other two three-phase curves intersecting at this quadruple point should be S_1S_2N and S_1S_2G , but these phase equilibria could not be measured, as this would require the detection of a $S_1 \leftrightarrow S_2$ phase transition. This type of phase transition cannot be determined visually. The other quadruple point found in this system, S_2Nl_2G , calculated from the experiments at $T = (313.0 \pm 0.1)$ K, $P = (3.24 \pm 0.01)$ MPa, is the point where the nematic to isotropic and the solid to nematic phase transition lines coincide: a S_2Nl_2 phase transition line is measured. Other three-phase curves intersecting at this point should be the S_2NG , S_2l_2G and Nl_2G curve. A higher CO_2 mole fraction is required to measure the intersection of the last two three-phase curves. When the three-phase curves S_1NG , S_2NG and Nl_2G are extrapolated to higher temperature, the binary three-phase curves correctly end in the pure component triple points, the metastable S_2NG triple point, the S_1NG and Nl_2G triple point, respectively, with a maximum error of 0.5 K, assuming

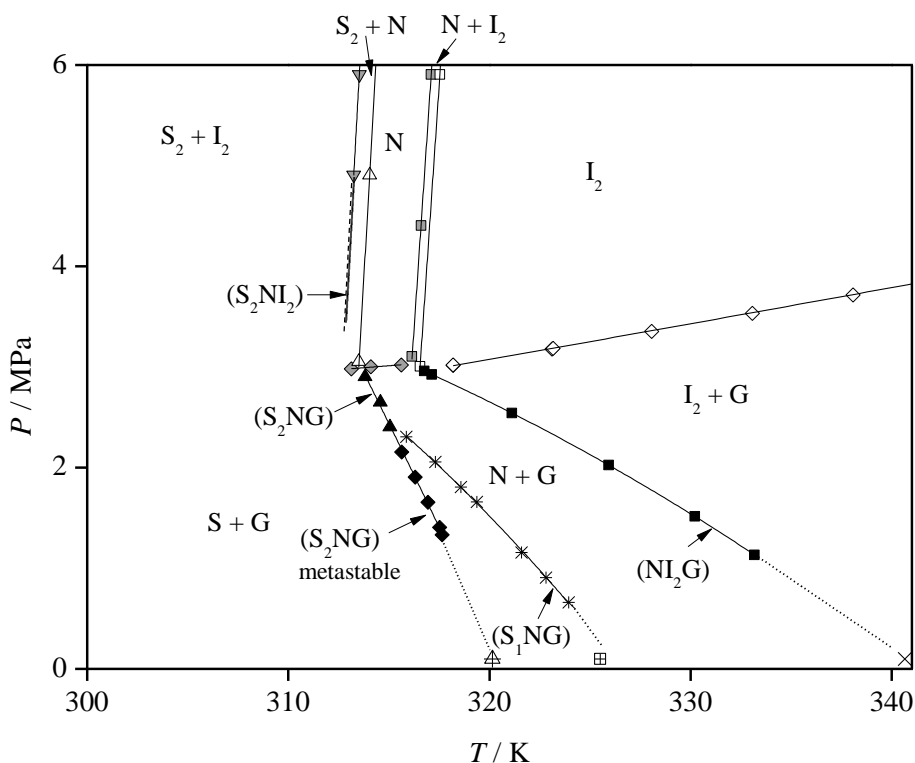


Figure 4.4. Part of P, T -diagram of the system $5OCB + CO_2$ for $x_{CO_2} = 0.241$, reproduced from [56]. Description of the used symbols: ∇ $S_2 + N + I_2$, \triangle $S_2 + N \leftrightarrow N$, \blacksquare $N \leftrightarrow N + I_2$, \square $N + I_2 \leftrightarrow I_2$, \blacklozenge $N + G \leftrightarrow N$, \diamond $I_2 + G \leftrightarrow I_2$, \blacktriangle $S_2 + N + G$, \blacklozenge metastable $S_2 + N + G$, \ast $S_1 + N + G$, \blacksquare $N + I_2 + G$, \triangleleft $S_2 \leftrightarrow N$ for pure 5OCB at 0.1 MPa, \boxplus $S_1 \leftrightarrow N$ for pure 5OCB at 0.1 MPa, \times $N \leftrightarrow I$ for pure 5OCB at 0.1 MPa. Notations between parentheses (...) denote three-phase curves. Dotted lines are added as a guide to the eye.

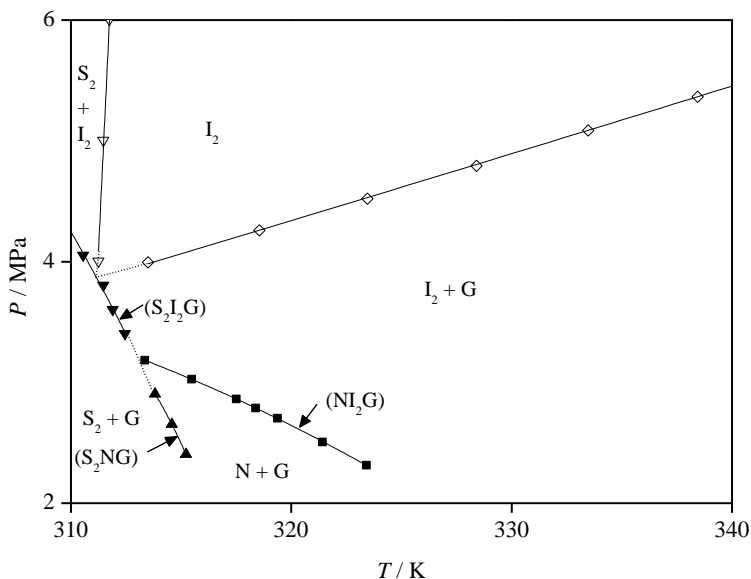


Figure 4.5. Part of the P,T -diagram of the system $5\text{OCB} + \text{CO}_2$ for $x_{\text{CO}_2} = 0.329$. Only the stable phase equilibria are shown. Description of the used symbols: ∇ $S_2 + I_2 \leftrightarrow I_2$, \diamond $I_2 + G \leftrightarrow I_2$, \blacktriangledown $S_2 + I_2 + G$, \blacktriangle $S_2 + N + G$, \blacksquare $N + I_2 + G$. Notations between parentheses (...) denote three-phase curves. Dotted lines are added as a guide to the eye.

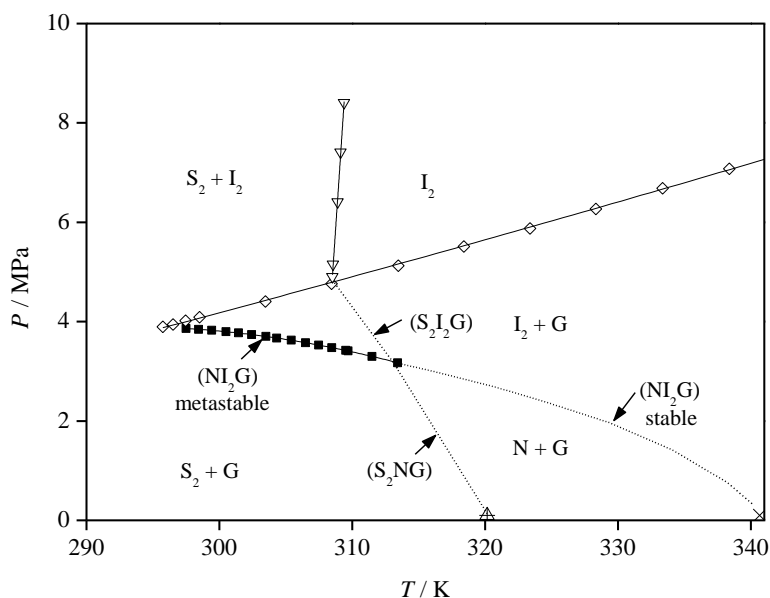
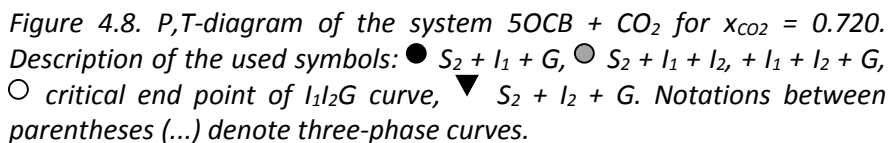
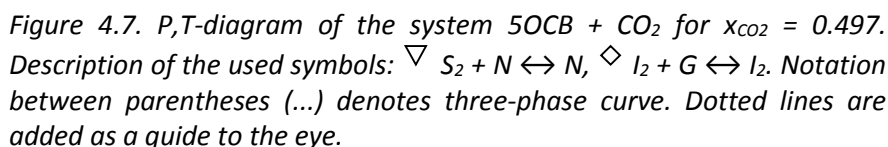


Figure 4.6. P,T -diagram of the system $5\text{OCB} + \text{CO}_2$ for $x_{\text{CO}_2} = 0.400$. Description of the used symbols: ∇ $S_2 + I_2 \leftrightarrow I_2$, \diamond $I_2 + G \leftrightarrow I_2$, \blacksquare metastable $N + I_2 + G$, \blacktriangle $S_2 \leftrightarrow N$ for pure 5OCB at 0.1 MPa , \times $N \leftrightarrow I$ for pure 5OCB at 0.1 MPa . Notations between parentheses (...) denote three-phase curves. Dotted lines are added as a guide to the eye.



again that the transition temperature at atmospheric pressure is equal to the triple-point temperature.

The P, T -diagram of the system 5OCB + CO₂ for $x_{\text{CO}_2} = 0.329$ is presented in Figure 4.5. At this concentration, the quadruple point S_2Nl_2G is at lower pressure than the bubble-point curve $l + G \leftrightarrow l$. Three of the four three-phase curves ending at this quadruple point, S_2l_2G , S_2NG and Nl_2G could be measured up to this quadruple point. The phase boundaries of the $N + l_2$ two-phase region, $N + l_2 \leftrightarrow l_2$ and the $N \leftrightarrow N + l_2$ could still be measured, but both are metastable. The width of the $N + l_2$ two phase region is still increasing with increasing CO₂ concentration. The calculated quadruple point S_2Nl_2G was found at $T = (313.0 \pm 0.1)$ K, $P = (3.21 \pm 0.01)$ MPa. At $x_{\text{CO}_2} = 0.400$ and $x_{\text{CO}_2} = 0.497$, shown in Figure 4.6 and Figure 4.7, the phase diagram has the same structure as the phase diagram for $x_{\text{CO}_2} = 0.329$, but the metastable nematic to isotropic phase transitions could not be measured because the mixture crystallized before this phase equilibrium could be detected. In these figures the non-measured three-phase curves are added as dashed curves.

The phase diagram of $x_{\text{CO}_2} = 0.720$ with 5OCB, presented in Figure 4.8, shows liquid-liquid demixing. The three-phase curve liquid-liquid gas ends at high temperature in a critical end point $l_2 + (l_1 = G)$ at $T = (304.4 \pm 0.1)$ K and $P = (7.41 \pm 0.01)$ MPa, and at lower temperature in a quadruple point $S_1l_1l_2G$ calculated from the experiments at $T = (301.6 \pm 0.1)$ K, $P = (6.97 \pm 0.03)$ MPa. At this point the $S_2l_1l_2$, S_2l_1G , the S_2l_2G and the l_1l_2G three-phase curves intersect. The S_2l_1G and the l_1l_2G curves almost coincide with the vapour pressure curve of pure CO₂, the temperature of the critical end point of the 5OCB + CO₂ system is slightly higher than the critical temperature of pure CO₂ [54].

4.4. Discussion

A f, x -diagram at constant temperature was used to calculate the Henry coefficient of CO₂ in the isotropic phase from the $l_2 + G \leftrightarrow l_2$ bubble-point curves. The Henry coefficient can be calculated using Equation (3.2). The fugacity was calculated using the equation of state for pure carbon dioxide of Span and Wagner [54], assuming that the gas phase consists of pure CO₂. A second order polynomial was used for fitting the bubble-points at 341 K up to $x_{\text{CO}_2} = 0.329$. Figure 4.9 shows the resulting figure. Up to $x_{\text{CO}_2} = 0.329$ the experimental points can be described using a linear function, the maximum deviation found was

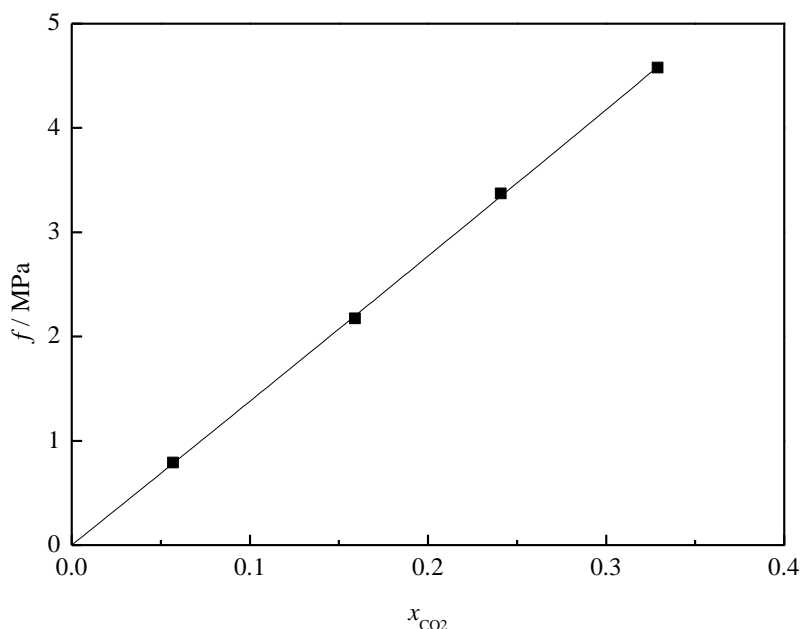


Figure 4.9. f, x -diagram of the system 5OCB + CO₂ up to $x_{\text{CO}_2} = 0.329$ for the isotropic phase. The line is a fitted second order polynomial. f is the fugacity of gaseous pure CO₂ at bubble-point conditions, calculated using the equation of state of Span and Wagner [54].

0.04 MPa. The Henry coefficient determined at 341 K by calculating the derivative of this linear function at $x_{\text{CO}_2} = 0$ was found to be 14.0 MPa.

In literature, three pure component phase transitions of 5OCB are reported: a $S_2 \leftrightarrow N$ phase transition at $T = 320$ K, a $S_1 \leftrightarrow N$ phase transition at $T = 326$ K and a $N \leftrightarrow I_2$ phase transition at 340.6 K [55]. No solid-solid transition has been reported in literature. A reason could be that these phase transitions can have a low phase transition enthalpy; these are not always detectable with DSC or a similar method.

The $S_2 \leftrightarrow N$ phase transition was only found when liquid 5OCB is quickly cooled to 253 K, yielding S_2 crystals. Upon heating these crystals the S_2N transition is found [57]. In our experiments we were only able to measure the S_1N phase transition with the Cailletet equipment. From the quadruple point S_1S_2NG found in the system 5OCB + CO₂ at $x_{\text{CO}_2} = 0.241$ one can conclude that a S_1S_2N and a S_1S_2G three-phase curve should be present in the system. Since CO₂ does not

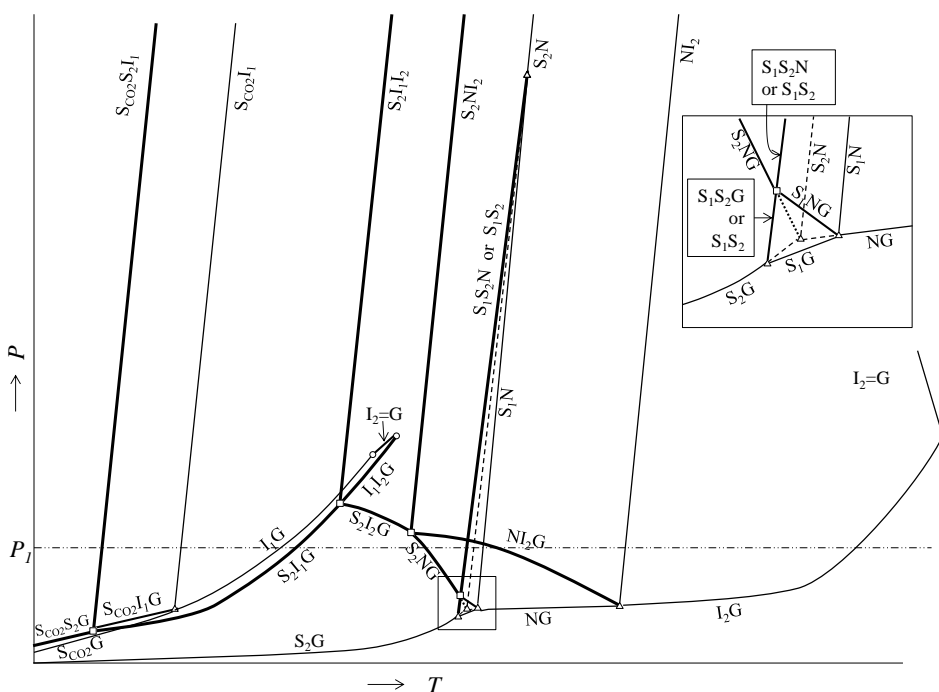


Figure 4.10. P,T -projection of 5OCB + CO_2 . Thin lines correspond to equilibria of the unary system CO_2 or 5OCB, bold lines to equilibria of the binary system 5OCB + CO_2 , dashed lines to metastable phase equilibria. The horizontal dash-dotted line corresponds to the isobar at pressure P_1 (see Figure 4.11). In this system, liquid-liquid demixing is found near the vapour pressure curve of CO_2 , where I_1 is the CO_2 -rich isotropic phase and I_2 the 5OCB-rich isotropic phase. For 5OCB, two solid phases were found: S_1 and S_2 , in the inset the phase behaviour of the two substances is shown. Other phases present are solid CO_2 (S_{CO_2}), the nematic phase N , and the gas phase G .

dissolve in the solid phase, the temperature of the S_2S_1 phase transition will not be influenced by the presence of CO_2 . This implies that the pure component $S_2 \leftrightarrow S_1$ phase transition coincides with the binary three-phase curves S_1S_2N and S_1S_2G .

Combining the information obtained from the experimental isopleths of Figures 4.1 to 4.8 a schematic P,T -projection of the binary system 5OCB + CO_2 can be constructed. This is shown in Figure 4.10. For pure 5OCB the two-phase curves

Table 4.2. Interpolated quadruple points for the system 5OCB + CO₂. S₁ and S₂ denote the solid phases of 5OCB, N denotes the nematic phase, I₂ the 5OCB-rich isotropic phase, I₁ the CO₂ rich isotropic phase and G the gas phase.

x_{CO_2}	T / K	P / MPa
Quadruple point: S ₁ S ₂ NG		
$x_{\text{CO}_2} = 0.241$	315.2 ± 0.1	2.43 ± 0.01
Quadruple point: S ₂ NI ₂ G		
$x_{\text{CO}_2} = 0.241$	313.0 ± 0.1	3.24 ± 0.01
$x_{\text{CO}_2} = 0.329$	313.0 ± 0.1	3.20 ± 0.01
Using all available data of S ₂ I ₂ G, S ₂ NG, SNI and NI ₂ G three-phase curves	313.02-313.15	3.21-3.24
Quadruple point: S ₂ I ₁ I ₂ G		
$x_{\text{CO}_2} = 0.720$	301.6 ± 0.1	6.97 ± 0.03

S₁S₂G, S₁S₂N, S₁NG, S₂NG and NI₂G. The triple point S₂NG is metastable: it is only found if S₁ is not formed. The part of the phase diagram of pure 5OCB including the 4 triple points S₁S₂G, S₁S₂N, S₁NG and S₂NG resembles the well-known phase diagram of sulphur [42,58]. The rhombic phase of sulphur should be replaced by S₂, the monoclinic phase by S₁ and the liquid sulphur phase by N. In the inset in Figure 4.10 it is clearly visible that the two solids are enantiotropic. For the system 5OCB + CO₂ the aforementioned quadruple points S₁S₂NG (see inset), S₂NI₂G and S₂I₁I₂G are found, with their corresponding three-phase lines. An overview of the P, T coordinates of these quadruple points is presented in Table 4.2. To complete the phase diagram, at low temperatures the triple point of CO₂ a quadruple point S_{CO₂}S₂I₁G should be present with the three-phase curves S_{CO₂}S₂G, S_{CO₂}I₂G, S₂I₁G and S_{CO₂}S₂I₁. As S_{CO₂} will also undergo melting point depression, this quadruple point should be lower in temperature than the triple point S_{CO₂}I₁G.

In Figure 4.11, a schematic T, x -diagram at pressure $P_1 = 3.0 \text{ MPa}$ (see Figure 4.10) is shown. Near the NI₂G phase equilibrium CO₂ could be separated by cooling the

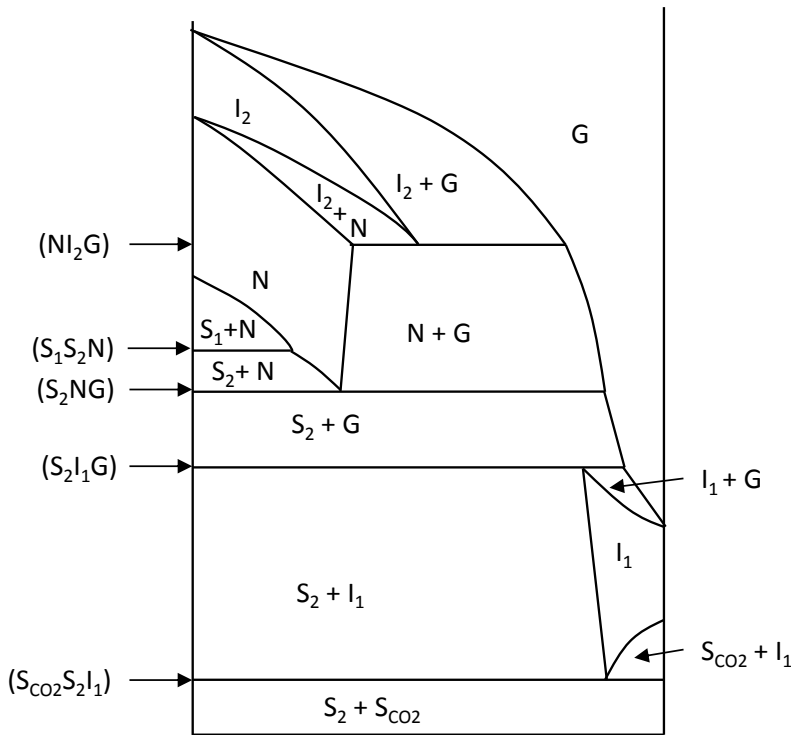


Figure 4.11. Schematic T,x -diagram at constant pressure $P_1 = 3.0$ MPa (see Figure 4.10). S_1 and S_2 denote the solid phases of 5OCB, S_{CO_2} the solid phase of CO_2 , N the nematic phase, I_1 the CO_2 -rich isotropic phase, I_2 the 5OCB-rich isotropic phase and G the gas phase. The three-phase equilibria are shown between parentheses (...). At the three-phase equilibrium NI_2G , CO_2 can be captured: the mixture is cooled down from the isotropic phase and splits in a gas phase and a nematic phase. The mole fraction of CO_2 in the nematic phase is lower than in the gas phase.

mixture only a few degrees, leading to a phase transition from the isotropic to the nematic phase. As the solubility of CO_2 is larger in the isotropic phase than in the nematic phase, at constant pressure a gas phase consisting mainly of CO_2 will be formed. The maximum difference in weight fraction of CO_2 between the isotropic and nematic phase is obtained when the pressure of the quadruple point S_2NI_2G is chosen as the operating pressure, for in this case the S_2NG and the NI_2G three-phase curves coincide in the T,x -diagram. This maximum is only

$w_{\text{CO}_2} = 0.001$ for 5OCB. Therefore, we feel that 5OCB is not suited for CO_2 capture: the difference between the isotropic and the nematic phase is too small to capture CO_2 effectively.

4.5. Conclusion

The binary system 4'-pentyloxy-4-cyanobiphenyl + CO_2 shows liquid-liquid demixing. It is found that 5OCB has two different solid phases, S_1 and S_2 . CO_2 can be captured at the NI_2G three-phase equilibrium, but for this molecule the difference in weight fraction of CO_2 between the isotropic and nematic phase is only $w_{\text{CO}_2} = 0.001$.

5. Henry coefficients of selected binary mixtures of a liquid crystal + CO₂

This chapter is based on: M. de Groen, B.C. Ramaker, T.J.H. Vlugt, T.W. de Loos, Phase behaviour of liquid crystal + CO₂ mixtures, Journal of Chemical and Engineering Data, 59 (2014) 1667-1672.

5.1. Introduction

To study the feasibility of a CO₂ capture process using liquid crystals as a solvent, the solubility of CO₂ in liquid crystals is of particular importance. In Chapter 3 we found that weakly polar molecules like 4'-pentyl-4-cyanobiphenyl have the highest CO₂ solubility. To have a fair basis of comparison, one can use the Henry coefficient as a quantitative measure of gas solubility. To obtain the Henry coefficient with sufficient accuracy, solubility measurements at a low CO₂ concentration should be performed. According to the detailed study of the phase diagram of 4'-pentyloxy-4-cyanobiphenyl with CO₂ up to a mole fraction of $x_{\text{CO}_2} = 0.7$, as described in Chapter 4, a concentration of $x_{\text{CO}_2} \leq 0.1$ should be in the Henry regime. This chapter focuses on the solubility of CO₂ in liquid crystals with different polarity at a low concentration of CO₂, around $x_{\text{CO}_2} = 0.06$ mol/mol. The liquid crystals studied in this work are 4-ethyl-4'-propyl bicyclohexyl and 4-propyl-4'-butyl bicyclohexyl, two apolar liquid crystals with a smectic phase, and 4'-heptyloxy-4-cyanobiphenyl, 4,4'-hexyloxy benzyldiene aminobenzonitrile and 4'-pentyl-4-cyanobiphenyl, liquid crystals with a nematic phase and polar groups. The influence of oxygen groups, size of the molecule and of the cyanogroup is studied. Based on the experimental results we conclude that apolar molecules have a lower solubility than polar molecules. Furthermore, adding a polar group between two benzene rings significantly lowers the solubility of CO₂.

5.2. Experimental methods

Materials used. An overview of the chemicals used is provided in Table 5.1. 4-ethyl-4'-propyl bicyclohexyl and 4-propyl-4'-butyl bicyclohexyl, purity $\geq 98\%$ mass were kindly supplied by Merck KGaA. 4'-heptyloxy-4-cyanobiphenyl, purity 99.9% mass (GC) was obtained from Alfa Aesar, 4'-pentyl-4-cyanobiphenyl,

Table 5.1. Overview of chemicals used in this chapter.

Chemical name	Source	Purity	Purification
4-ethyl-4'-propyl bicyclohexyl	Merck	≥ 98% mass	Used as received
4-propyl-4'-butyl bicyclohexyl	Merck	≥ 98% mass	Used as received
4'-heptyloxy-4-cyanobiphenyl	Alfa Aesar	99.9% mass	Used as received
4'-pentyl-4-cyanobiphenyl	Alfa Aesar	99% mass	Used as received
4,4'-hexyloxy benzylidene aminobenzonitrile	Frinton Laboratories	98% mass	Used as received
CO ₂	Linde Gas	Volume fraction 0.99995	Used as received

purity 99% mass was obtained from Alfa Aesar, 4,4'-hexyloxy benzylidene aminobenzonitrile, purity 98% mass was obtained from Frinton Laboratories. Dry carbon dioxide, purity 4.5, was obtained from Linde Gas. All chemicals were used without further purification.

The nature of the impurities of the liquid crystals is unknown. However it is likely that the impurities are very similar compounds as the ones studied in this manuscript and the impact of the impurities on the phase behaviour will be very small. DSC measurements of the solid-nematic transitions of the pure liquid crystals agree within 1.5 K with literature values [59], which is fairly good agreement.

Phase Equilibrium Measurements. Phase equilibrium measurements were performed according to the synthetic visual method using a Cailletet setup, as described in Chapter 3. Phase equilibria measured were the bubble points of the nematic and isotropic phase, determined at constant temperature with an uncertainty of 0.005 MPa. The monovariant three-phase curves nematic + isotropic + gas (NIG) and smectic + isotropic + gas (SmIG) were also determined

at constant temperature with an uncertainty of 0.005 MPa. Furthermore, the two-phase transitions of the nematic + isotropic to isotropic state, the nematic + isotropic to nematic state, the smectic + isotropic to isotropic state and the solid + nematic to nematic state were measured by changing the temperature at constant pressure with an uncertainty of 0.02 K, except for the solid + nematic to nematic equilibrium which was measured with an uncertainty of 0.1 K. Because of high viscosities, bubble points of the smectic phase and phase transitions starting from a homogeneous smectic phase could not be measured.

5.3. Results and discussion

Since the proposed separation process is based on the difference in solubility of CO₂ between the anisotropic and isotropic phase transition [31], measurements were focused on equilibria involving the isotropic, nematic and smectic phase. The tabulated data is presented in Appendix C.

The two apolar liquid crystals, 4-ethyl-4'-propyl bicyclohexyl and 4-propyl-4'-butyl bicyclohexyl, have only a smectic phase. For the pure substances, the smectic to isotropic phase transition at $P = 0.1$ MPa is found at $T = 341$ K and 370 K, respectively. For these liquid crystals the phase transitions smectic + isotropic to isotropic, the bubble-point curve isotropic + gas (G) to isotropic and the three-phase curve SmIG were measured. The results are presented in Figures 5.1 and 5.2. The extrapolation of the three-phase curves to zero pressure intersects with the temperature axis at $T = 340$ K for 4-ethyl-4'-propyl bicyclohexyl and at $T = 369$ K for 4-propyl-4'-butyl bicyclohexyl. This point of intersection should coincide with the corresponding triple point of the liquid crystal, which can be approximated by the pure component phase transition temperature at atmospheric pressure.

4,4'-Hexyloxy benzylidene aminobenzonitrile has a solid to nematic phase transition at 330 K and a nematic to isotropic phase transition at 375 K at 0.1 MPa [59]. Binary data of 4,4'-hexyloxy benzylidene aminobenzonitrile with CO₂ have not been published in literature before. The mole fraction of CO₂ in the mixture was $x_{\text{CO}_2} = 0.066$. Phase equilibria measured for this mixture were the two-phase to homogeneous phase transitions solid + nematic to nematic, nematic + isotropic to nematic and nematic + isotropic to isotropic. Furthermore, the bubble points of the nematic + gas to nematic and isotropic + gas to isotropic state were measured. The extrapolation of the three-phase curve nematic +

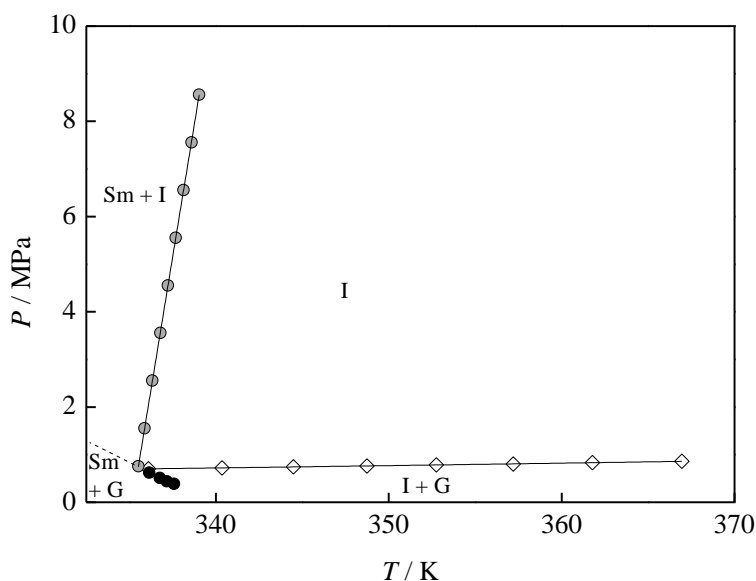


Figure 5.1. P,T -diagram of 4-ethyl-4'-propyl bicyclohexyl + CO_2 , $x_{\text{CO}_2} = 0.052$. Description of symbols used: \bullet $\text{Sm} + \text{I} \leftrightarrow \text{I}$, \diamond $\text{I} + \text{G} \leftrightarrow \text{I}$, \bullet $\text{Sm} + \text{I} + \text{G}$. The dashed curve is an extrapolation of the three-phase curve $\text{Sm} + \text{I} + \text{G}$ to lower temperatures. The lines are added as a guide to the eye.

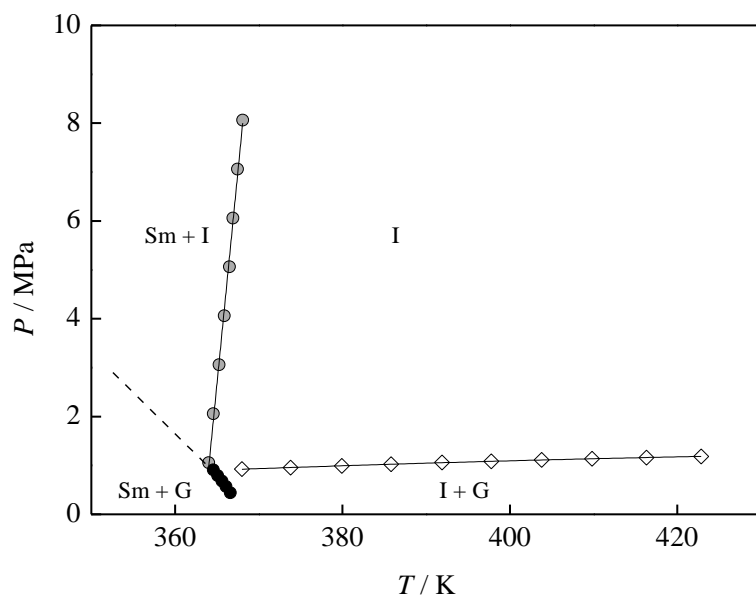


Figure 5.2. P,T -diagram of 4-propyl-4'-butylbicyclohexyl + CO_2 , $x_{\text{CO}_2} = 0.057$. Description of symbols used: \bullet $\text{Sm} + \text{I} \leftrightarrow \text{I}$, \diamond $\text{I} + \text{G} \leftrightarrow \text{I}$, \bullet $\text{Sm} + \text{I} + \text{G}$. The dashed curve is an extrapolation of the three-phase curve $\text{Sm} + \text{I} + \text{G}$ to lower temperatures. The lines are added as a guide to the eye.

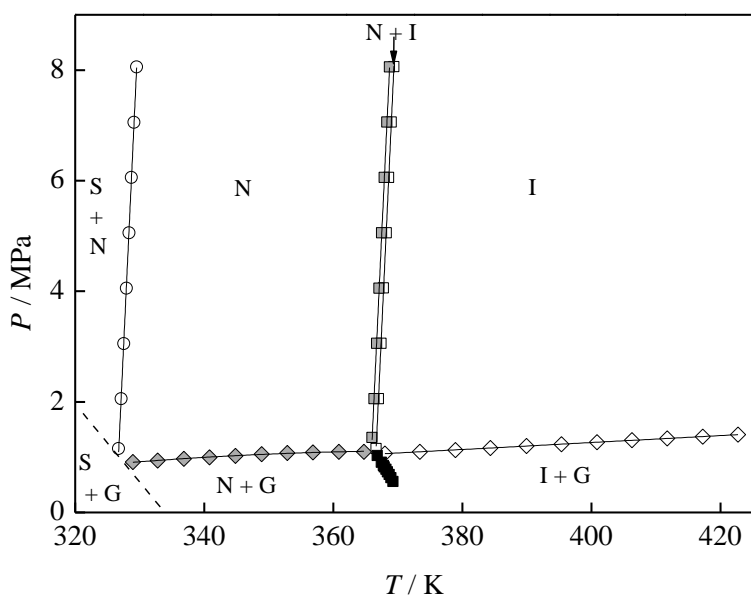


Figure 5.3. P,T -diagram of 4,4'-hexyloxy benzylidene aminobenzonitrile + CO_2 , $x_{\text{CO}_2} = 0.066$. Description of symbols used: \circ $S + N \leftrightarrow N$, \blacksquare $N \leftrightarrow N + I$, \square $N + I \leftrightarrow I$, \blacklozenge $N + G \leftrightarrow N$, \diamond $I + G \leftrightarrow I$, \blacksquare $N + I + G$. The dashed line is the expected three-phase curve $S + N + G$. The lines are added as a guide to the eye.

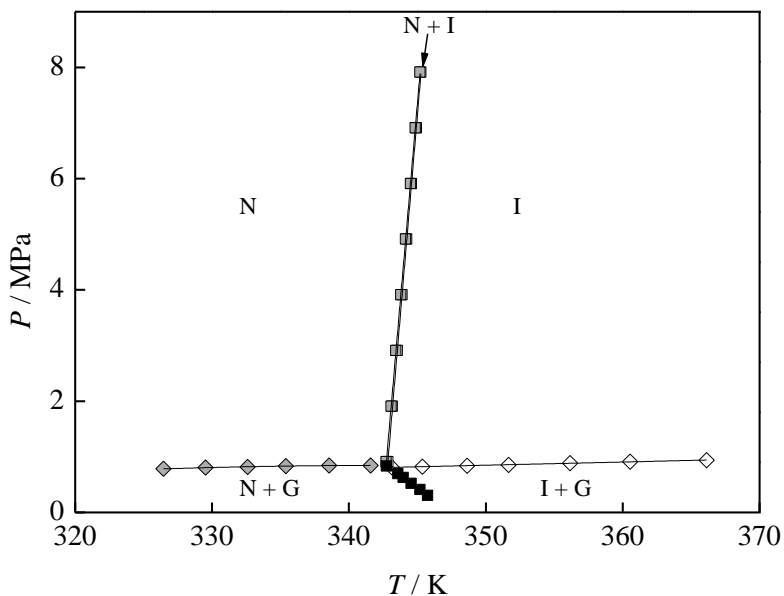


Figure 5.4. P,T -diagram of 4'-heptyloxy-4-cyanobiphenyl + CO_2 , $x_{\text{CO}_2} = 0.063$. Description of symbols used: \blacksquare $N \leftrightarrow N + I$, \square $N + I \leftrightarrow I$, \blacklozenge $N + G \leftrightarrow N$, \diamond $I + G \leftrightarrow I$, \blacksquare $N + I + G$. The lines are added as a guide to the eye.

isotropic + gas (NIG) to $P = 0$ MPa gave $T = 372$ K. The width of the N + I two-phase area was 0.5 K. The results are presented in Figure 5.3.

4'-Heptyloxy-4-cyanobiphenyl has a solid to nematic phase transition at 327 K and a nematic to isotropic phase transition at 348 K at 0.1 MPa [32]. The mole fraction of CO₂ in the mixture was $x_{\text{CO}_2} = 0.063$. Phase transitions measured for this mixture are the nematic + isotropic to nematic phase transition, nematic + isotropic to isotropic phase transition, the bubble-point curves isotropic + gas to isotropic and nematic + gas to nematic and the three-phase curve nematic + isotropic + gas. The results are presented in Figure 5.4. 4'-Pentyl-4-cyanobiphenyl has a solid to nematic phase transition at 297 K and a nematic to isotropic phase transition at 308 K at 0.1 MPa, as shown in Chapter 3. The same phase equilibria as for 4'-heptyloxy-4-cyanobiphenyl were measured. The composition of the mixture was $x_{\text{CO}_2} = 0.055$. The results of the measurements are presented in Figure 5.5.

For binary mixtures, three-phase equilibria are monovariant and independent of concentration and can be used to examine the consistency of different isopleths. In Figure 5.6, the three-phase equilibria are shown for the measurements of this chapter and of previously published data in Chapter 3. The three-phase equilibria of 4-ethyl-4'-propyl bicyclohexyl, 4-propyl-4'-butyl bicyclohexyl and 4'-pentyl-4-cyanobiphenyl are in agreement with the data of Chapter 3, which are at higher CO₂ mole fractions for these components, and are in line with the pure component smectic to isotropic transitions or nematic to isotropic transition, respectively.

If the Henry coefficients are estimated from the measured I + G to I equilibria for all tested liquid crystals, one can compare the solubility of CO₂ in the liquid crystals measured. The Henry coefficients are calculated using:

$$\phi_i P = x_i H_i \quad (5.1)$$

ϕ_i is the fugacity coefficient of pure CO₂ at bubble-point conditions, calculated from the equation of state of pure CO₂ [54,60], P is the bubble-point pressure, x_i is the mole fraction of CO₂ in the liquid phase which is equal to the overall composition of CO₂ at bubble-point conditions. It is assumed that the gas phase is pure CO₂, and that the liquid phase is behaving ideal (*i.e.*, the activity coefficient equals unity). The results in Figure 5.7 show that at low temperature 4'-pentyl-4-cyanobiphenyl has the lowest Henry coefficient of CO₂ and therefore the highest solubility. As the I + G to I equilibrium line is less steep for 4'-heptyloxy-4-cyanobiphenyl, around 340 K and at higher temperature

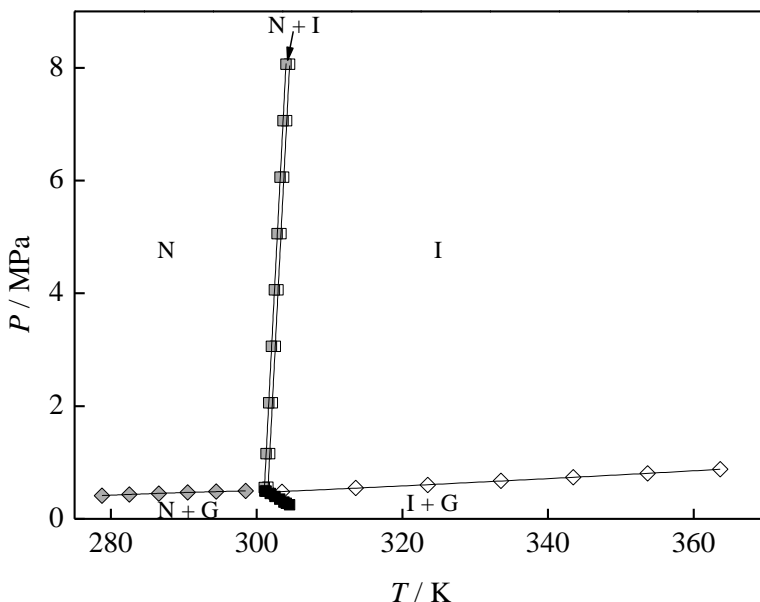


Figure 5.5. P,T -diagram of 4'-pentyl-4-cyanobiphenyl + CO_2 , $x_{\text{CO}_2} = 0.055$. Description of symbols used: \blacksquare $N \leftrightarrow N + I$, \square $N + I \leftrightarrow I$, \blacklozenge $N + G \leftrightarrow N$, \diamond $I + G \leftrightarrow I$, \blacksquare $N + I + G$. The lines are added as a guide to the eye.

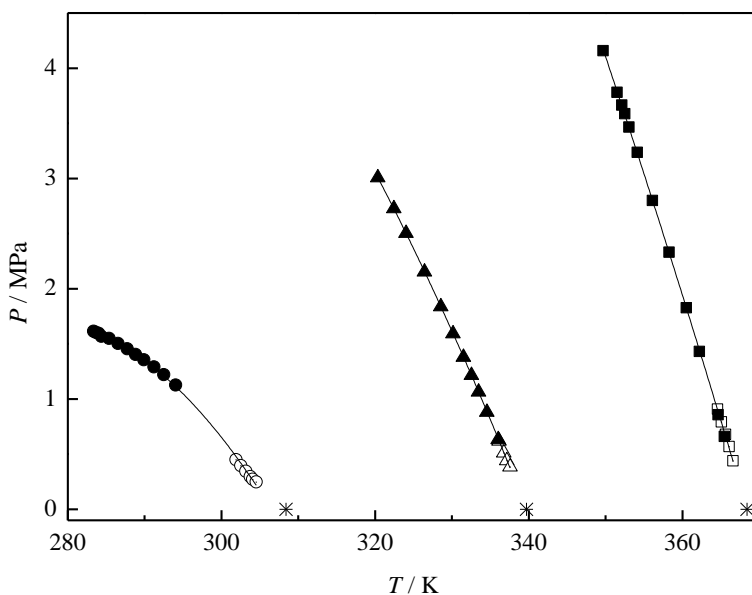


Figure 5.6. P,T -diagram with comparison of three-phase curves of 4-pentyl-4'-cyanobiphenyl ($N + I + G$, \circ), 4-ethyl-4'-propyl bicyclohexyl ($\text{Sm} + I + G$, \triangle), 4-propyl-4'-butyl bicyclohexyl ($\text{Sm} + I + G$, \square) and the pure component triple points estimated from the pure component phase transitions $\text{Sm} + I \leftrightarrow I$ and $N + I \leftrightarrow I$, respectively, at $P = 0$ (*). Filled symbols: data published for $w_{\text{CO}_2} = 0.05$ (see Chapter 3), open symbols: this work. The lines are fitted second order polynomials and are added as a guide to the eye.

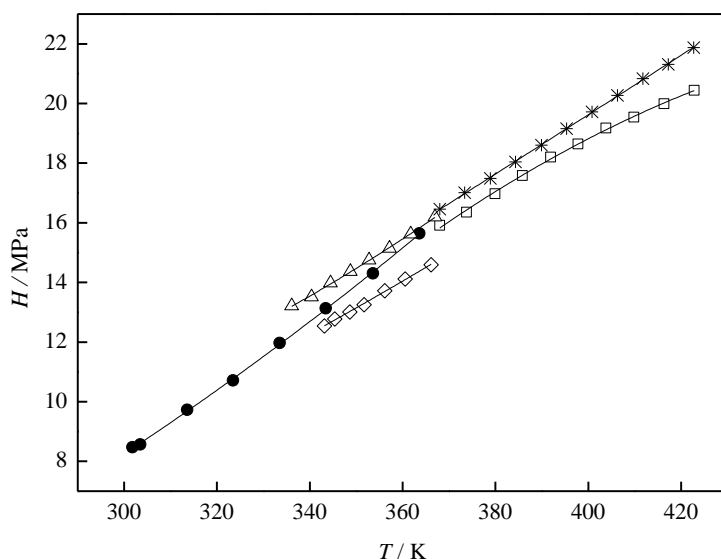


Figure 5.7. Molar Henry coefficients as function of temperature for the solubility of CO_2 in 4-ethyl-4'-propyl bicyclohexyl (Δ), 4-propyl-4'-butyl bicyclohexyl (\square), 4,4'-hexyloxy benzylidene aminobenzonitrile ($*$), 4'-heptyloxy-4-cyanobiphenyl (\diamond) and 4'-pentyl-4-cyanobiphenyl (\bullet). The lines are fitted second order polynomials and are added as a guide to the eye.

4'-heptyloxy-4-cyanobiphenyl has the lowest Henry coefficient of the liquid crystals tested in this chapter. Overall, 4,4'-hexyloxy benzylidene aminobenzonitrile has the highest Henry coefficient. An increasing alkyl chain number leads to a lower Henry coefficient according to the results of 4-ethyl-4'-propyl bicyclohexyl and 4-propyl-4'-butyl bicyclohexyl. It can be concluded that molecules with moderate polarity such as 4'-pentyl-4-cyanobiphenyl and 4'-heptyloxy-4-cyanobiphenyl have lower Henry coefficients than the apolar cyclohexyl and the strong polar 4,4'-hexyloxy benzylidene aminobenzonitrile. It seems that a polar group between the two benzene rings has a negative influence on the solubility of CO_2 in these kinds of solvents. The feasibility of the use of liquid crystals for CO_2 capture is difficult to judge at this stage as research on this topic is in the start-up phase. Before any conclusion can be drawn more information on for example kinetics and process design should be available.

5.4. Conclusion

Phase diagrams of binary mixtures of five different liquid crystals with CO₂ were measured. The solubility of CO₂ of three of these LCs was in good agreement with previously published data. Of all liquid crystals tested, 4'-pentyl-4-cyanobiphenyl and 4'-heptyloxy-4-cyanobiphenyl have the highest solubility, and 4,4'-hexyloxy benzylidene aminobenzonitrile the lowest. A longer alkyl side chain seems to lower the solubility of CO₂. Polar groups may lower the solubility of CO₂, especially if this polar group is between two benzene rings.

6. Binary and ternary mixtures of liquid crystals with CO₂

This chapter is based on M. de Groen, T.J.H. Vlugt, T.W. de Loos, Binary and ternary mixtures of liquid crystals with CO₂, submitted to AIChE journal.

6.1. Introduction

In the previous chapters, phase diagrams of binary mixtures of liquid crystals and CO₂ were studied. Two parameters are of utmost importance for a CO₂ capture process using liquid crystals: the CO₂ solubility and the CO₂ solubility difference (Δx) between the nematic and the isotropic phases. In the previous chapters we outlined the influence of different molecular groups of liquid crystals on the solubility of CO₂. The liquid crystals with the highest CO₂ solubility are 4'-pentyl-4-cyanobiphenyl or 4'-pentyloxy-4-cyanobiphenyl, molecules which can be described as weakly polar molecules. The apolar and polar molecules investigated have a lower CO₂ solubility. The CO₂ solubility difference between the nematic and isotropic phase depends on the free volume change and the enthalpy change of the N \leftrightarrow I phase transition [33]. This can be determined when the complete phase diagram is measured. This is performed previously for the system 5OCB + CO₂ in Chapter 4.

None of the liquid crystals tested so far has suitable properties for CO₂ capture. Of most liquid crystals, the temperature range of the existence of the nematic phase is too small, or the temperature of the N \leftrightarrow I phase change is too low, leading to an infeasible process. To create a liquid crystal solvent with optimal properties, a mixture of two or more liquid crystals can be considered. A classification of all possible phase diagrams of a mixture of two liquid crystals is provided by Pestov *et al.* [61]. It shows that if two nematic liquid crystals are mixed, the nematic phase is in most cases a homogeneous solution and the same holds for the isotropic phase. Furthermore, the phase behaviour of a mixture of two liquid crystals shows a nematic solid behaviour analogous to an eutectic system. By carefully choosing the liquid crystals, one can create a solvent with a significant lower solid to nematic phase transition temperature and therefore a larger Δx .

Table 6.1. Chemicals used in this chapter.

Chemical name	Abbreviation	Source	Purity	Purification
4'-propylcyclohexyl-4-benzonitrile	PCH3	Merck	≥ 98% mass	Used as received
4'-heptylcyclohexyl-4-benzonitrile	PCH7	Merck	≥ 98% mass	Used as received
4'-pentyloxy-4-cyanobiphenyl	5OCB	Alfa Aesar	99% mass	Used as received
4'-heptyloxy-4-cyanobiphenyl	7OCB	Alfa Aesar	99.9% mass	Used as received
Carbon dioxide	CO ₂	Linde Gas	Volume fraction 0.99995	Used as received

To investigate the influence of replacing the pure liquid crystal with a mixture of two liquid crystals, the ternary mixture 4'-heptyloxy-4-cyanobiphenyl (7OCB) + 4'-pentyloxy-4-cyanobiphenyl (5OCB) + CO₂ is measured at constant 7OCB/5OCB composition of $x_{5OCB}/x_{7OCB} \approx 1.78$ with different mole fractions of CO₂, namely $x_{CO_2} = 0.062, 0.138, 0.248, 0.337$. Also, the phase behaviour of the ternary system of 4'-propylcyclohexyl-4-benzonitrile (PCH3) + 4'-heptylcyclohexyl-4-benzonitrile (PCH7) + CO₂ with the ratio of PCH3 and PCH7 fixed at $x_{PCH7}/x_{PCH3} = 3.00$, at CO₂ concentrations $x_{CO_2} = 0.138, 0.244$ and 0.332 , was studied. The main conclusion of this work is that the mixture of PCH3 + PCH7 is most promising for CO₂ capture, as this mixture has the highest CO₂ solubility and the largest Δx .

6.2. Experimental methods

An overview of the materials used in this chapter is presented in Table 6.1. The liquid crystals used were 4'-pentyloxy-4-cyanobiphenyl and 4'-heptyloxy-4-cyanobiphenyl, purity 99% mass, obtained from Sigma-Aldrich, and 4'-propylcyclohexyl-4-benzonitrile and 4'-heptylcyclohexyl-4-benzonitrile, purity 98% mass, provided by Merck KGaA. CO₂, purity 4.5, was obtained from Linde Gas.

The measurements were performed using a Cailletet setup, which is of the synthetic, visual type. A description can be found in Chapter 3. Phase equilibria measured with an accuracy of 0.005 MPa and 0.02 K were the two-phase equilibria $I + G \leftrightarrow I$, $N + G \leftrightarrow N$, $N + I \leftrightarrow N$, $N + I \leftrightarrow I$, and the three-phase equilibria $N + I + G$, $N + I + G \leftrightarrow N + I$, $N + I + G \leftrightarrow I + G$, $N + I + G \leftrightarrow N + G$. Phase equilibria involving the solid (S) phase were the two-phase equilibria $S + I \leftrightarrow I$, $S + N \leftrightarrow N$ and the three-phase equilibria $S + N + G$ and $S + I + G$, all measured with an accuracy of 0.005 MPa and 0.05 K.

6.3. Results

To investigate the phase behaviour of the ternary mixtures of two liquid crystals with CO_2 , first of all the unary and binary phase diagrams of the substances used should be known. Therefore, the unary and binary phase diagrams will be discussed prior to the description of the ternary phase diagrams. First, the results for the ternary system $5\text{OCB} + 7\text{OCB} + \text{CO}_2$ will be presented followed by the system of $\text{PCH3} + \text{PCH7} + \text{CO}_2$. The tabulated experimental data is available in Appendix D.

The P, T -diagram of pure 7OCB, shown in Figure 6.1, was measured in the Cailletet-setup for comparison with literature data. The $S \leftrightarrow N$ and $N \leftrightarrow I$ phase transitions were measured. The $S \leftrightarrow N$ phase transition at atmospheric pressure was found at a temperature 2 K higher than the literature value, the $N \leftrightarrow I$ phase transition was 1 K lower [32].

The results of the mixture of $7\text{OCB} + \text{CO}_2$, $x_{\text{CO}_2} = 0.260$, are shown in Figure 6.2. Phase transitions measured for this mixture were the two-phase equilibria $I \leftrightarrow I + G$, $N \leftrightarrow N + G$, $N \leftrightarrow N + I$, $I \leftrightarrow N + I$, and the three-phase equilibria $N + I + G$ which is located between the two-phase regions $N + G$ and $I + G$. The extrapolation of this line should end in the triple point $N + I + G$ of the pure LC. The coordinates of this triple point of 7OCB are 347 K at 0.1 MPa, estimated from the pure component phase transition. The $S + N \leftrightarrow N$ phase equilibrium of the mixture of 7OCB with CO_2 , $x_{\text{CO}_2} = 0.260$, was estimated to be at $T = 322$ K at $P = 5.0$ MPa.

The experimental results of the binary mixture of $5\text{OCB} + 7\text{OCB}$ at $x_{5\text{OCB}}/x_{7\text{OCB}} = 1.79$ are shown in Figure 6.3. The equilibria measured were the $N \leftrightarrow N + I$ and $I \leftrightarrow N + I$ two-phase equilibria. The $S \leftrightarrow S + N \leftrightarrow N$ phase transition was difficult to detect visually. A slow increase of the temperature at a constant pressure of

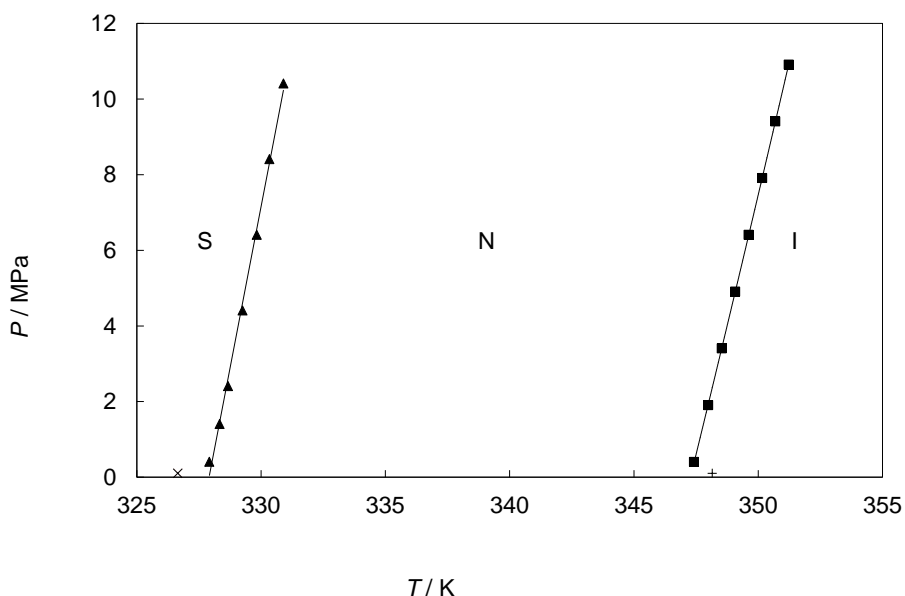


Figure 6.1. P,T -diagram of pure 4'-heptyloxy-4-cyanobiphenyl. S denotes the solid phase, N the nematic phase and I the isotropic phase. \blacktriangle $S \leftrightarrow N$; \blacksquare $N \leftrightarrow I$; \times $S \leftrightarrow N$ phase transition at $P = 0.1$ MPa [32]; $+$ $N \leftrightarrow I$ phase transition at $P = 0.1$ MPa [32]. The lines are linear fits of the data points.

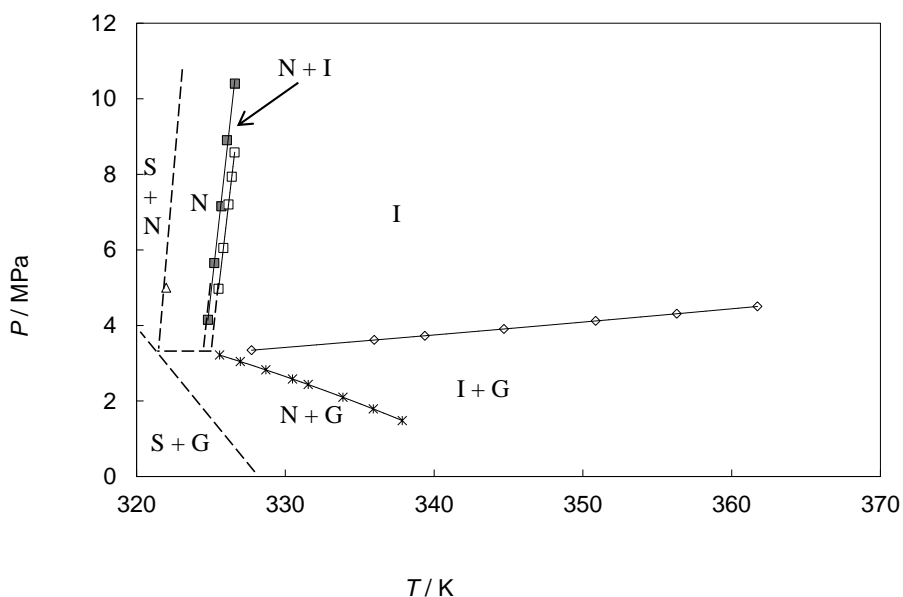


Figure 6.2. P,T -diagram of the binary mixture 4,4'-heptyloxy cyanobiphenyl + CO_2 at $x_{\text{CO}_2} = 0.260$. S denotes the solid phase, N the nematic phase, I the isotropic phase and G the gas phase. \triangle $S + N \leftrightarrow N$; \blacksquare $N + I \leftrightarrow N$; \square $N + I \leftrightarrow I$; $*$ $N + I + G$; \diamond $I + G \leftrightarrow I$. The dashed lines are added as a guide to the eye, the solid lines are polynomial fits through the data points.

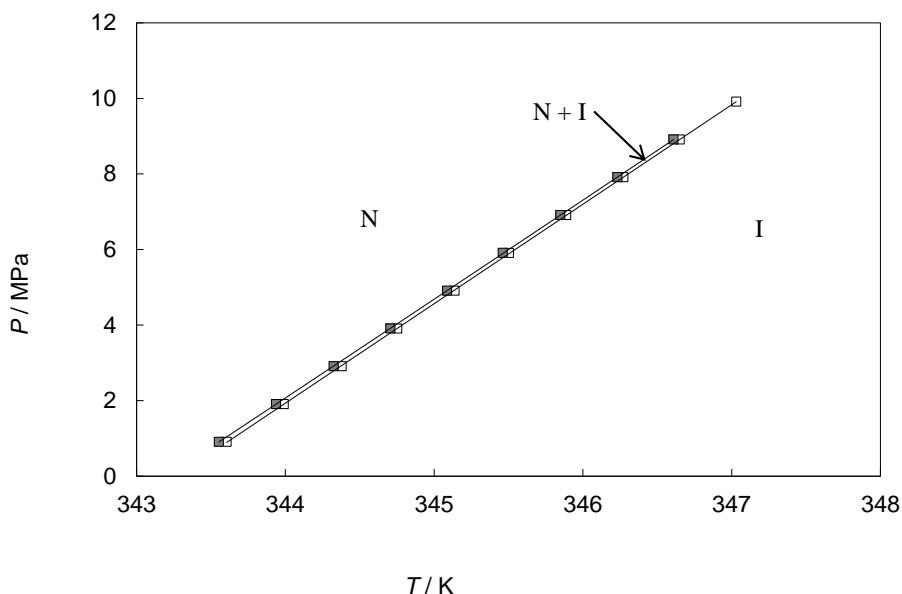


Figure 6.3. P,T -diagram of the binary mixture 4'-heptyloxy-4-cyanobiphenyl + 4'-pentyloxy-4-cyanobiphenyl, $x_{50CB}/x_{70CB} = 1.79$. N denotes the nematic phase, I the isotropic phase. ■ $N \leftrightarrow N + I$; □ $N + I \leftrightarrow I$. The solid lines are linear fits through the data points.

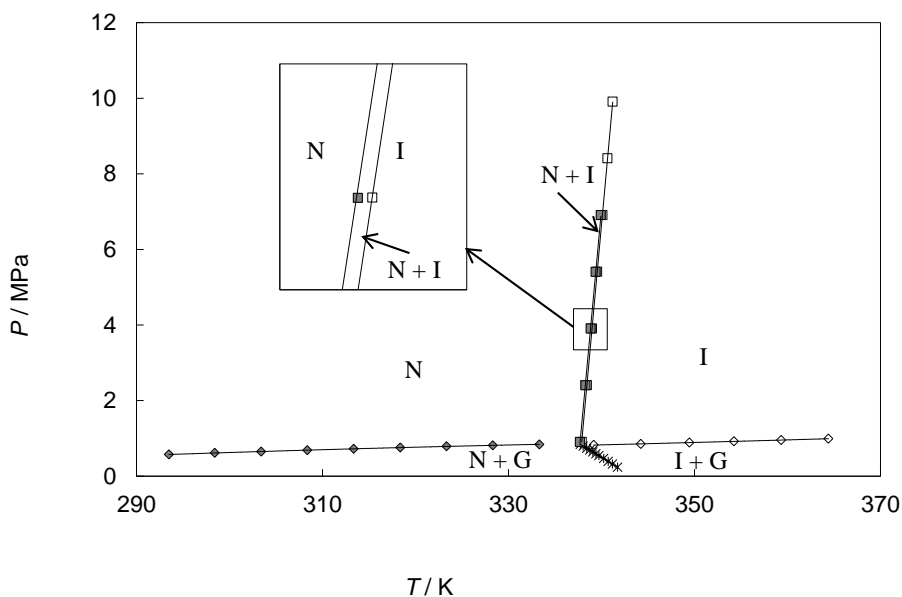


Figure 6.4. P,T -diagram of the ternary mixture 4'-heptyloxy-4-cyanobiphenyl + 4'-pentyloxy-4-cyanobiphenyl + CO_2 , $x_{50CB}/x_{70CB} = 1.77$, $x_{CO_2} = 0.062$. N denotes the nematic phase, I the isotropic phase and G the gas phase. ■ $N + I \leftrightarrow N$; □ $N + I \leftrightarrow I$; * $I + G \leftrightarrow N + I + G$; ◆ $N + G \leftrightarrow N$; ◇ $I + G \leftrightarrow I$. The solid lines are fits through the data points. The inset shows the two-phase area $N + I$.

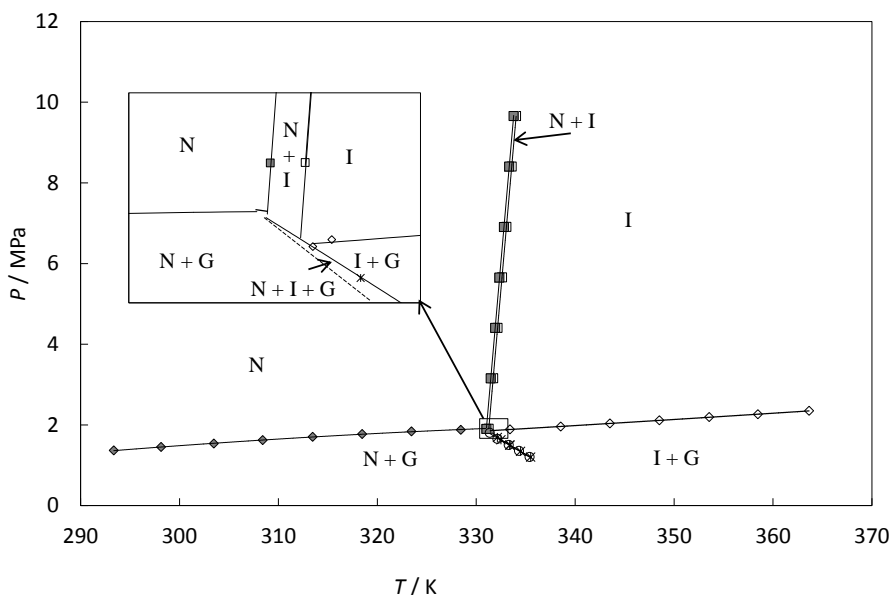


Figure 6.5. P,T -diagram of the ternary mixture 4'-heptyloxy-4-cyanobiphenyl + 4'-pentyloxy-4-cyanobiphenyl + CO_2 , $x_{5\text{OCB}}/x_{7\text{OCB}} = 1.77$, $x_{\text{CO}_2} = 0.131$. N denotes the nematic phase, I the isotropic phase and G the gas phase. ■ $N + I \leftrightarrow N$; □ $N + I \leftrightarrow I$; * $I + G \leftrightarrow N + I + G$; ◆ $N + G \leftrightarrow N$; ◇ $I + G \leftrightarrow I$. The dashed line is added as a guide to the eye, the solid lines are fits through the data points. The inset shows an enlargement of the point of intersection.

$P = 0.91$ MPa showed that the phase transition temperature was between $T = 300.6$ and 300.8 K. The temperature range (ΔT) of the two-phase area $N + I$ is very small, $\Delta T = 0.05$ K.

When CO_2 is added to the binary mixture of 5OCB + 7OCB, the temperature range of the $N + I$ two-phase area becomes larger. The temperature range for $x_{\text{CO}_2} = 0.062$ is $\Delta T = 0.15$ K. Equilibria measured were $N + G \leftrightarrow N$, $I + G \leftrightarrow I$, $N + I \leftrightarrow I$, $N \leftrightarrow I + N$, and the three-phase equilibria $N + I + G \leftrightarrow I + G$. The result of this system is shown in Figure 6.4, the inset shows an enlargement of the $N + I \leftrightarrow I$ two-phase area. The system can be described as a pseudo-binary system composed of CO_2 and a mixture of 7OCB + 5OCB with a fixed composition, namely $x_{5\text{OCB}}/x_{7\text{OCB}} = 1.77$. In this case the extrapolation of the three-phase equilibria of the ternary mixture to $P = 0.1$ MPa should yield approximately the

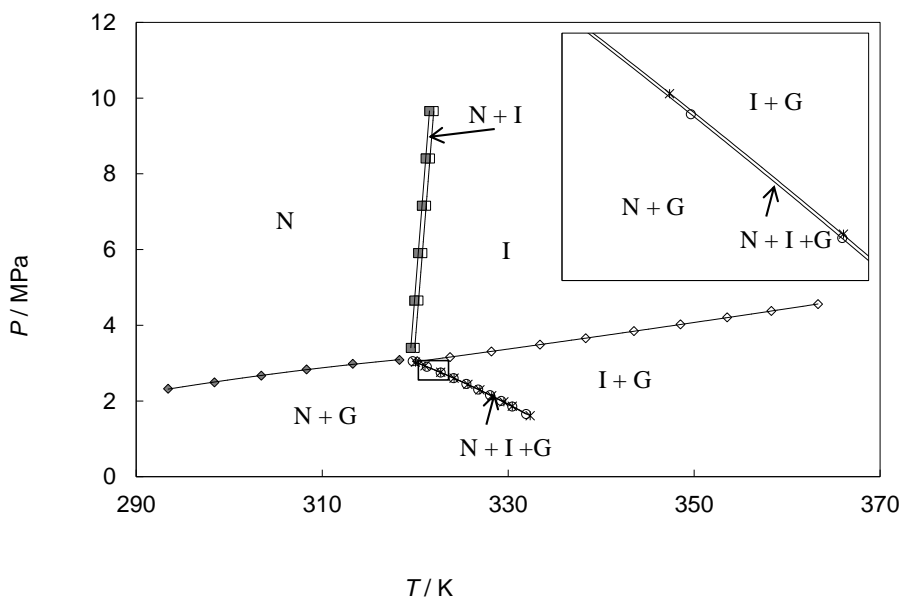


Figure 6.6. P,T -diagram of the ternary mixture 4'-heptyloxy-4-cyanobiphenyl + 4'-pentyloxy-4-cyanobiphenyl + CO_2 , $x_{50\text{CB}}/x_{70\text{CB}} = 1.76$, $x_{\text{CO}_2} = 0.248$. N denotes the nematic phase, I the isotropic phase and G the gas phase. \blacksquare $N + I \leftrightarrow N$; \square $N + I \leftrightarrow I$; $*$ $I + G \leftrightarrow N + I + G$; \circ $N + G \leftrightarrow N + I + G$; \blacklozenge $N + G \leftrightarrow N$; \blacklozenge $I + G \leftrightarrow I$. The solid lines are polynomial fits through the data points.

same point as is obtained by extrapolating the $N + I \leftrightarrow I$ phase transition of the binary mixture of the two liquid crystals to $P = 0.1$ MPa.

In Figures 6.5, 6.6 and 6.7, the effect of adding a larger amount of CO_2 to the binary mixture of 5OCB and 7OCB is clearly visible. In Figure 6.5, $x_{\text{CO}_2} = 0.131$, in Figure 6.6, $x_{\text{CO}_2} = 0.248$ and in Figure 6.7 $x_{\text{CO}_2} = 0.337$. The $N + I$ two-phase area becomes wider and shifts to lower temperature. The three-phase area $N + I + G$ is made visible in Figure 6.6; its width is approximately 0.005 MPa, which is close to the experimental error. Though this is a very small difference, the $N + I + G \leftrightarrow N + G$ phase transition was measured at a lower pressure than the $N + I + G \leftrightarrow I + G$ three-phase equilibrium, independent of the measurement method. Other phase transitions measured for these mixtures were $I + G \leftrightarrow I$ and $N + G \leftrightarrow N$.

The other system investigated was the system $\text{PCH3} + \text{PCH7} + \text{CO}_2$. The pure component phase equilibria of the liquid crystals at $P = 0.1$ MPa are published in

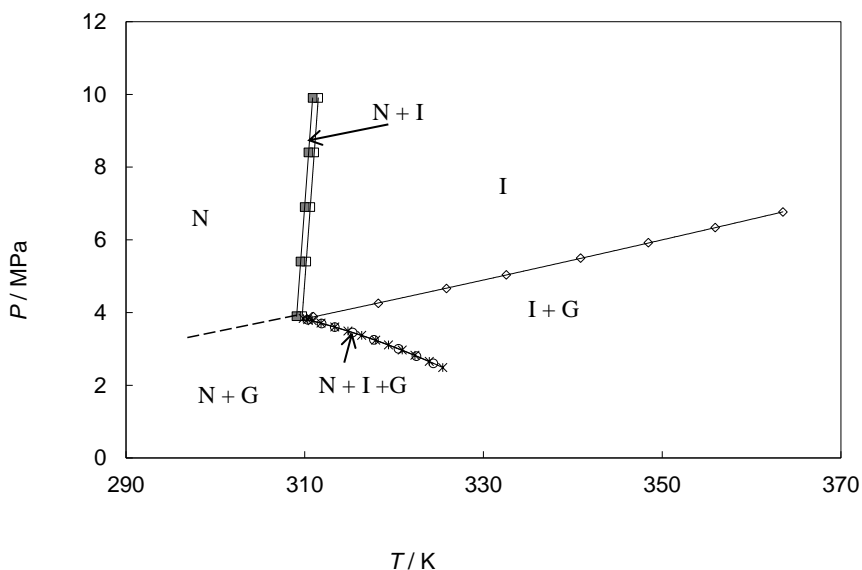


Figure 6.7. P,T -diagram of the ternary mixture 4'-heptyloxy-4-cyanobiphenyl + 4'-pentyloxy-4-cyanobiphenyl + CO_2 , $x_{50\text{CB}}/x_{70\text{CB}} = 1.77$, $x_{\text{CO}_2} = 0.337$. N denotes the nematic phase, I the isotropic phase and G the gas phase. \blacksquare $N+I \leftrightarrow N$; \square $N+I \leftrightarrow I$; $*$ $I+G \leftrightarrow N+I+G$; \circ $N+G \leftrightarrow N+I+G$; \blacklozenge $N+G \leftrightarrow N$; \diamond $I+G \leftrightarrow I$. The dashed line is added as a guide to the eye, the solid lines are polynomial fits through the data points.

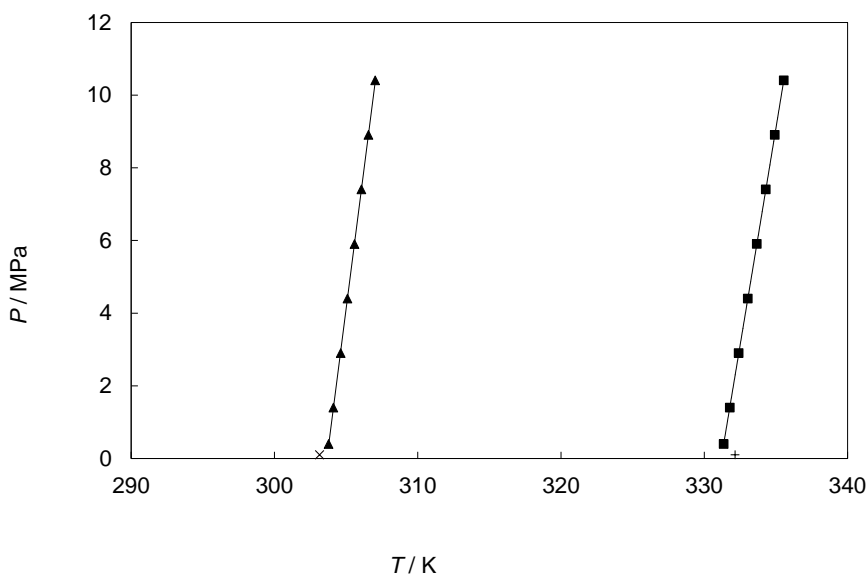


Figure 6.8. P,T -diagram of pure 4'-heptylcyclohexyl-4-benzonitrile. S denotes the solid phase, N the nematic phase and I the isotropic phase. \blacktriangle $S \leftrightarrow N$; \blacksquare $N \leftrightarrow I$; \times $S \leftrightarrow N$ phase transition at $P = 0.1$ MPa [32]; $+$ $N \leftrightarrow I$ phase transition at $P = 0.1$ MPa [32]. The lines are linear fits of the data points.

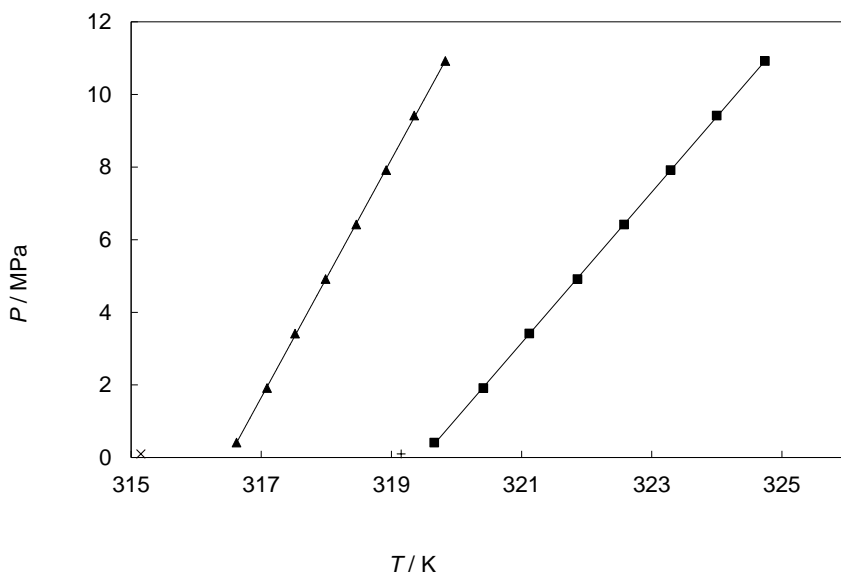


Figure 6.9. P,T -diagram of pure 4'-propylcyclohexyl-4-benzonitrile. S denotes the solid phase, N the nematic phase and I the isotropic phase. \blacktriangle $S \leftrightarrow N$; \blacksquare $N \leftrightarrow I$; \times $S \leftrightarrow N$ phase transition at $P = 0.1$ MPa [32]; $+$ $N \leftrightarrow I$ phase transition at $P = 0.1$ MPa [32]. The lines are linear fits of the data points.

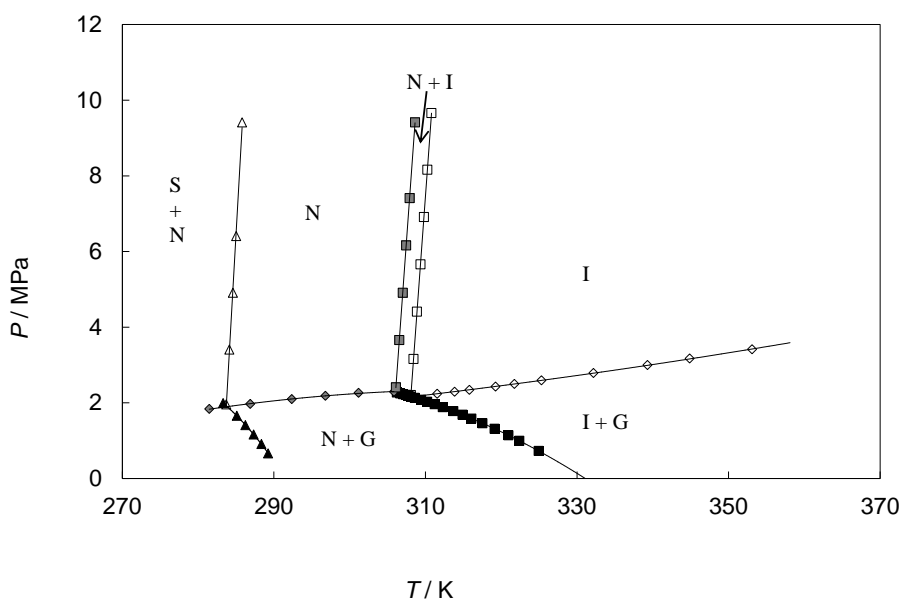


Figure 6.10. P,T -diagram of the binary mixture 4'-heptylcyclohexyl-4-benzonitrile + CO_2 at $x_{\text{CO}_2} = 0.213$. S denotes the solid phase, N the nematic phase, I the isotropic phase and G the gas phase. \triangle $S + N \leftrightarrow N$; \blacktriangle $S + N + G$; \blacksquare $N + I \leftrightarrow N$; \square $N + I \leftrightarrow I$; $*$ $N + I + G$; \diamond $I + G \leftrightarrow I$. The solid lines are first and second order polynomial fits through the data points.

literature [32]. For comparison the pure component phase equilibria have been measured and are shown in Figure 6.8 and 6.9 together with the literature data.

Pure PCH3 has a $S \leftrightarrow N$ and a $N \leftrightarrow I$ phase transition at $T = 316.5$ and 319.5 K, respectively [32]. Pure PCH7 has a phase transition from $S \leftrightarrow N$ and from $N \leftrightarrow I$ at $T = 306$ and 332 K, respectively [32]. PCH3 has a smaller temperature range of the nematic phase than PCH7.

The binary phase diagram of PCH7 + CO₂ at $x_{\text{CO}_2} = 0.213$ is shown in Figure 6.10. Phase equilibria measured were the $S + N \leftrightarrow N$, $N \leftrightarrow I + N$, $I \leftrightarrow N$ and $I, N + G \leftrightarrow N$, $I + G \leftrightarrow I$, and the three-phase equilibria $S + N + G$ and $N + I + G$. For this liquid crystal the three-phase curve $S + N + G$ does not end in the pure components' triple point. This is an indication that another solid phase has crystallized. Unless the phase diagram is fully known, we cannot judge if this solid phase is stable at this conditions. Compared to the binary systems 5OCB + CO₂ of Chapter 4 and 7OCB + CO₂ (this chapter), this liquid crystal has a broader $N + I$ two-phase area.

The binary phase diagram of PCH3 + CO₂ at $x_{\text{CO}_2} = 0.050$, which is quite close to the quadruple point composition, is shown in Figure 6.11. At pressures lower than the $I + G \leftrightarrow I$ phase equilibria the two three-phase curves $S + I + G$ and $N + I + G$ intersect with each other. The third three-phase equilibrium, $S + N + I$, is partly measured and should intersect with these two lines as well, but as the concentration of CO₂ is slightly higher than the CO₂ concentration at the quadruple point, this curve is intersected by the two-phase equilibrium $S + I \leftrightarrow I$. The $N + I \leftrightarrow I$ and the $N \leftrightarrow N + I$ two-phase equilibria as well as the $N + I + G$ are only stable at the right side of the $S + N + I$ three-phase curve. At the left side they can only be measured if the solid phase is not crystallizing. The $N + G \leftrightarrow N$ equilibria are also metastable. The $S + N \leftrightarrow N$ phase equilibrium should intersect with the intersection of the $N + I \leftrightarrow N$ and the three-phase curve $S + N + I$, but this was not measured.

The binary P, T -phase diagram of PCH3 + CO₂ at $x_{\text{CO}_2} = 0.214$ is shown in Figure 6.12. Only equilibria involving the solid phase, the isotropic phase and the G phase are stable, because the concentration is higher than the quadruple point concentration. The equilibria measured for this substance are $I + G \leftrightarrow I$, $S + I \leftrightarrow I$ and $S + I + G$. To create a mixture with a larger nematic temperature range, ternary mixtures of PCH3, PCH7 and CO₂ are considered at a composition $x_{\text{PCH7}}/x_{\text{PCH3}} = 3.00$ with a varying amount of CO₂. In Figure 6.13, the binary phase diagram of PCH3 and PCH7 is shown at the aforementioned composition. Phase

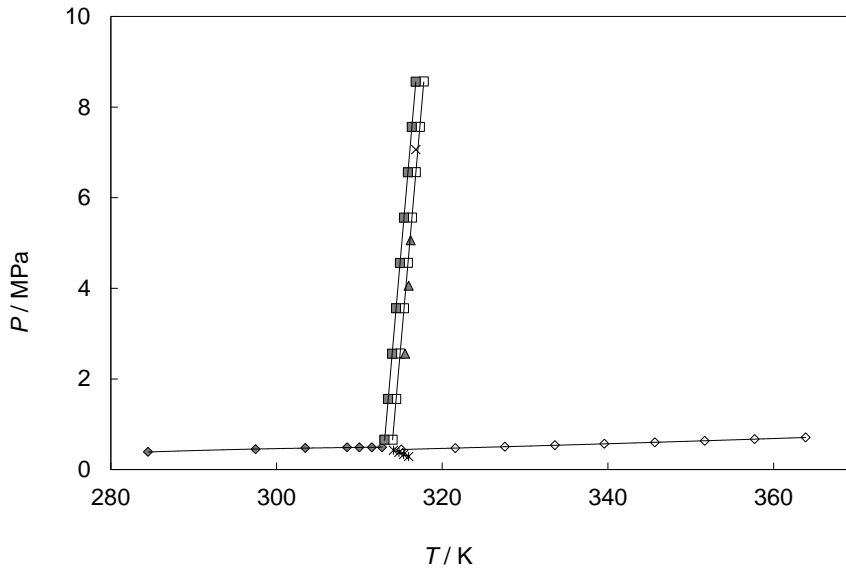


Figure 6.11. P,T -diagram of the binary mixture 4'-propylcyclohexyl-4-benzonitrile + CO_2 at $x_{\text{CO}_2} = 0.050$. S denotes the solid phase, N the nematic phase, I the isotropic phase and G the gas phase. $\blacktriangle S + I \leftrightarrow I$; $\blacksquare N + I \leftrightarrow I$; $\square N + I \leftrightarrow I$; $\times S + N + I$; $*$ $N + I + G$; $\diamond I + G \leftrightarrow I$. The solid lines are first and second order polynomial fits through the data points.

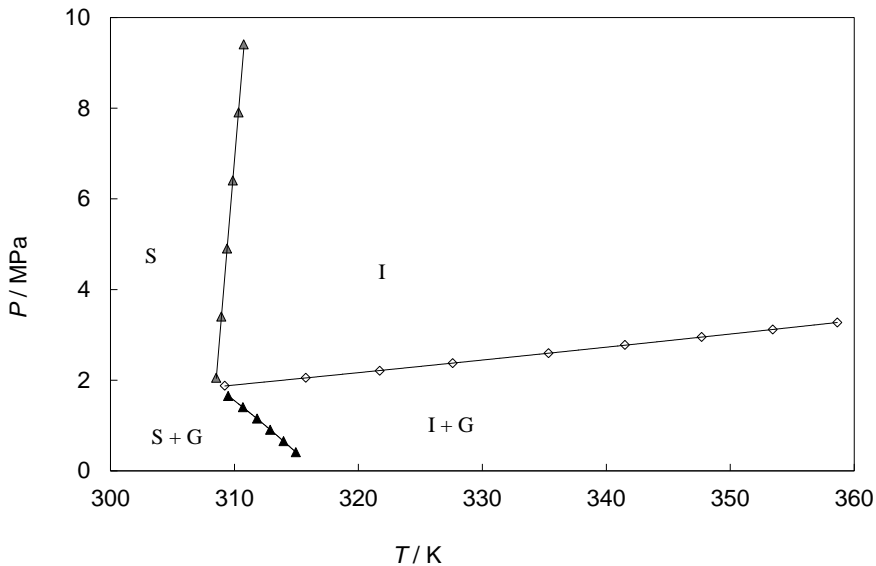


Figure 6.12. P,T -diagram of the binary mixture 4'-propylcyclohexyl-4-benzonitrile + CO_2 at $x_{\text{CO}_2} = 0.214$. S denotes the solid phase, N the nematic phase, I the isotropic phase and G the gas phase. $\blacktriangle S + I \leftrightarrow I$; $\diamond I + G \leftrightarrow I$; $\blacktriangle S + I + G$. The solid lines are first or second order polynomial fits through the data points.

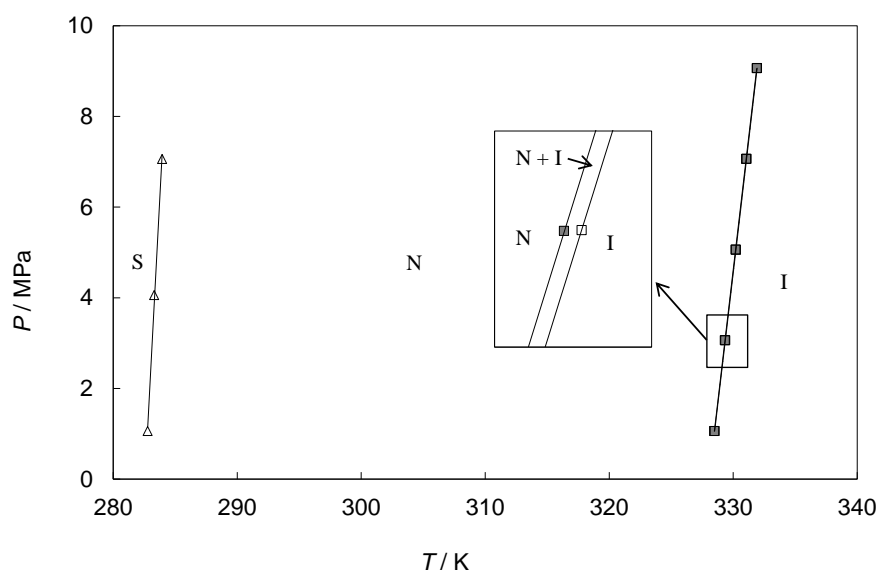


Figure 6.13. P,T -diagram of the binary mixture 4'-propylcyclohexyl-4-benzonitrile + 4'-heptylcyclohexyl-4-benzonitrile, $x_{PCH7}/x_{PCH3} = 3.00$. S denotes the solid phase, N the nematic phase and I the isotropic phase. \triangle $S + N \leftrightarrow N$; \blacksquare $N \leftrightarrow N + I$; \square $N + I \leftrightarrow I$. The lines are linear fits of the data points. The inset shows the two-phase area $N + I$.

equilibria for this system are $S + N \leftrightarrow N$ and $N + I \leftrightarrow N$ and $N + I \leftrightarrow I$. The $N + I$ two phase area is quite small, $\Delta T = 0.04$ K. An inset in Figure 6.13 shows the two-phase area $N + I$. The mixture is liquid at room temperature, for the $S + N \leftrightarrow N$ phase transition is at 282 K.

The pseudo-binary system $PCH3 + PCH7 + CO_2$ at $x_{PCH7}/x_{PCH3} = 3.00$ shows similar behaviour as the pseudo-binary system $5OCB + 7OCB + CO_2$. Phase equilibria measured for this system were the two-phase equilibria $I + G \leftrightarrow I$, $N + G \leftrightarrow N$, $N \leftrightarrow N + I$ and $N + I \leftrightarrow I$. Three-phase equilibria measured are $N + I + G \leftrightarrow N + I$ and $N + I + G \leftrightarrow I + G$ and $N + I + G \leftrightarrow N + G$. Figures 6.14, 6.15 and 6.16 show the results of $x_{CO_2} = 0.138$, 0.244 and 0.332, respectively.

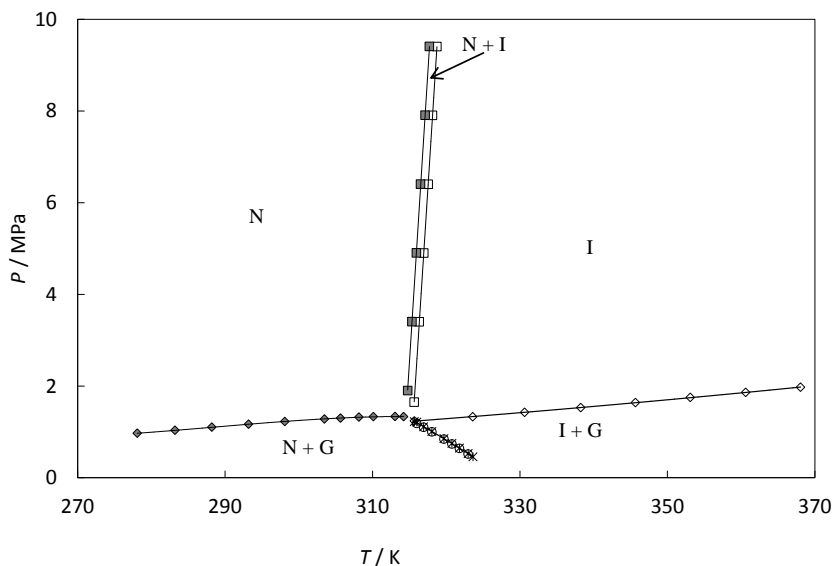


Figure 6.14. P,T -diagram of the ternary mixture 4'-propylcyclohexyl-4-benzonitrile + 4'-heptylcyclohexyl-4-benzonitrile + CO_2 , $x_{\text{PCH7}}/x_{\text{PCH3}} = 2.93$, $x_{\text{CO2}} = 0.138$. N denotes the nematic, I the isotropic and G the gas phase. \blacksquare $N + I \leftrightarrow N$; \square $N + I \leftrightarrow I$; $*$ $I + G \leftrightarrow N + I + G$; \circ $N + G \leftrightarrow N + I + G$; \blacklozenge $N + G \leftrightarrow N$; \diamond $I + G \leftrightarrow I$. The solid lines are polynomial fits through the data points.

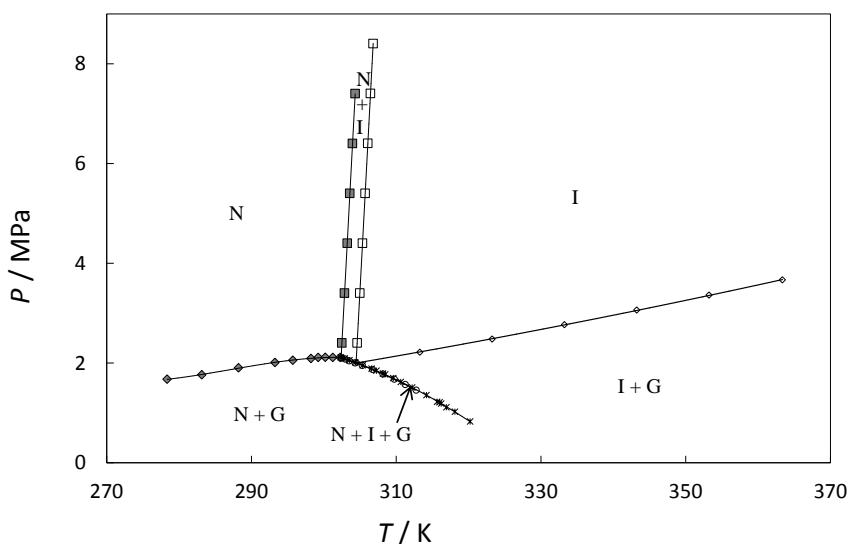


Figure 6.15. P,T -diagram of the ternary mixture 4'-propylcyclohexyl-4-benzonitrile + 4'-heptylcyclohexyl-4-benzonitrile + CO_2 , $x_{\text{PCH7}}/x_{\text{PCH3}} = 2.99$, $x_{\text{CO2}} = 0.244$. N denotes the nematic, I the isotropic and G the gas phase. \blacksquare $N + I \leftrightarrow N$; \square $N + I \leftrightarrow I$; $*$ $I + G \leftrightarrow N + I + G$; \circ $N + G \leftrightarrow N + I + G$; \blacklozenge $N + G \leftrightarrow N$; \diamond $I + G \leftrightarrow I$. The solid lines are polynomial fits through the data points.

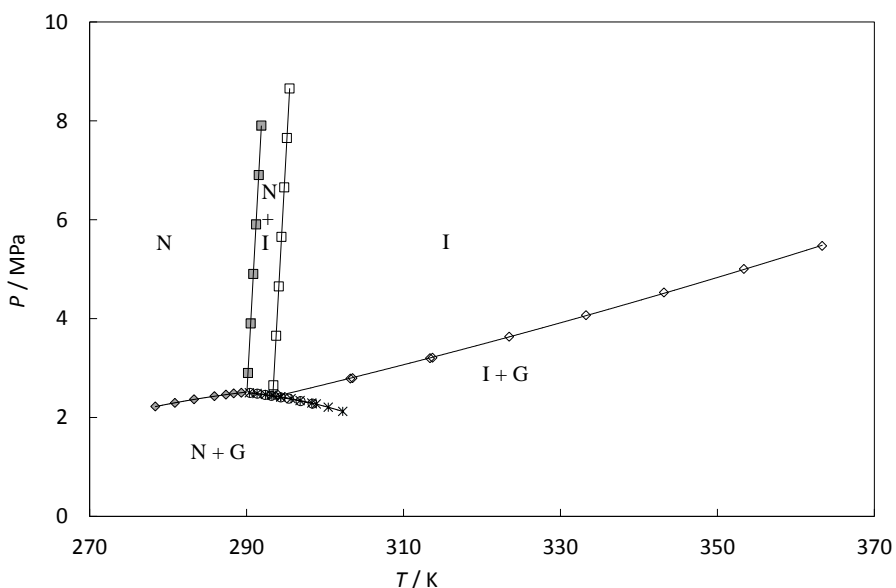


Figure 6.16. P,T -diagram of the ternary mixture 4'-propylcyclohexyl-4-benzonitrile + 4'-heptylcyclohexyl-4-benzonitrile + CO_2 , $x_{\text{PCH7}}/x_{\text{PCH3}} = 3.02$, $x_{\text{CO}_2} = 0.332$. N denotes the nematic phase, I the isotropic phase and G the gas phase. \blacksquare $N + I \leftrightarrow N$; \square $N + I \leftrightarrow I$; $*$ $I + G \leftrightarrow N + I + G$; \circ $N + G \leftrightarrow N + I + G$; \blacklozenge $N + G \leftrightarrow N$; \diamond $I + G \leftrightarrow I$. The solid lines are polynomial fits through the data points.

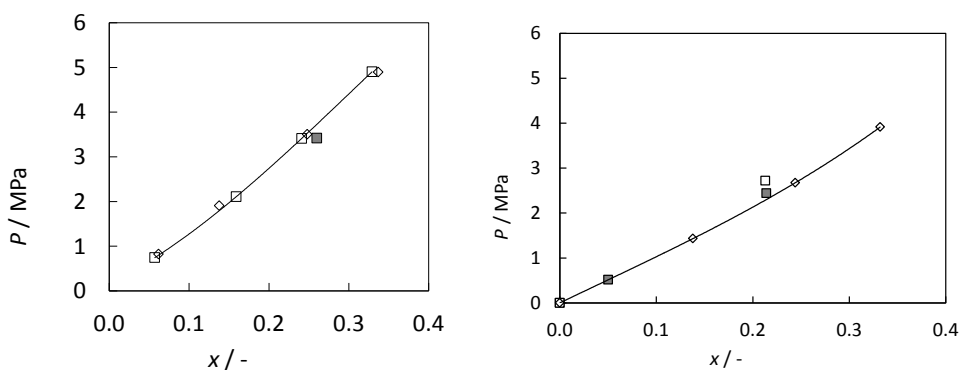


Figure 6.17. Left: P,x -diagram of the $I + G \leftrightarrow I$ equilibria of 5OCB, 7OCB and CO_2 . \blacksquare 7OCB + CO_2 ; \square 5OCB + CO_2 ; \diamond 5OCB + 7OCB + CO_2 . Right: P,x -diagram of the $I + G \leftrightarrow I$ equilibria of PCH3, PCH7 and CO_2 . \blacksquare PCH7 + CO_2 ; \square PCH3 + CO_2 ; \diamond PCH3 + PCH7 + CO_2 .

6.4. Discussion

To determine the best solvent for CO₂ capture, both the overall solubility and the solubility difference between the I and N phases, Δx , should be examined. To compare the solubility of CO₂ for the six different LC solvents, P, x -diagrams at a constant temperature of 330 K are created and shown in Figure 6.17. The solubility of CO₂ is larger in PCH3, PCH7 and the mixture of PCH3 + PCH7 than in the other materials. If we examine the different materials further, it shows that the mixtures of 5OCB + CO₂, 7OCB + CO₂ and 5OCB + 7OCB + CO₂ have an almost comparable CO₂ solubility, whereas for PCH3 + CO₂, PCH7 + CO₂ and PCH3 + PCH7 + CO₂ it seems that mixing the two liquid crystals leads to a lower I + G \leftrightarrow I equilibrium pressure, and thus to a higher CO₂ solubility. This may be explained by the difference in size between PCH3 and PCH7, which is larger than that of 5OCB and 7OCB. Based on this size difference, the mixture of 5OCB and 7OCB is more ideal than of PCH3 and PCH7.

The proposed CO₂ capture process is a process at constant pressure [31]. T, x -diagrams at constant pressure show the total amount of CO₂ which can be removed during one absorption-desorption cycle. In the next paragraphs the T, x -diagram of the binary mixtures of one liquid crystal with CO₂ are compared with the T, x -diagram of its ternary mixture. The pressure of the T, x -diagrams was chosen such that the N + I + G equilibrium was above 300 K. The reason for this is that such a process does not need cryogenic cooling. Therefore, the pressure of T, x -diagram of the ternary mixture 5OCB + 7OCB + CO₂ is $P = 4.00$ MPa, and for the ternary mixture PCH3 + PCH7 + CO₂, $P = 2.00$ MPa.

The data used for creating the T, x -diagram of 5OCB + CO₂ were taken from Chapter 4. In Figure 6.18, the T, x -diagram is shown. Absent in this figure is the N + I + G equilibrium, because the three-phase equilibrium S₂ + N + I is more stable than the N + I + G equilibrium. As explained in the introduction, the presence of the N + I + G equilibrium is essential for the CO₂ capture process. Therefore, at this pressure 5OCB is not suitable for CO₂ capture.

If we examine the T, x -diagram of the ternary mixture of 5OCB + 7OCB + CO₂, shown in Figure 6.19, at the same pressure as the binary mixture of 5OCB + CO₂, it is clear that this ternary mixture at the aforementioned conditions is suitable for CO₂ capture, as the three-phase curve N + I + G is present. The main difference between Figure 6.18 and 6.19 is the phase transition temperature of the solid to nematic phase transition. For the binary mixture of 5OCB + 7OCB measured in this study, with $x_{5OCB}/x_{7OCB} = 1.77$, this melting point is 300 K, whereas the melting

point of pure 5OCB and pure 7OCB are 325 and 327 K, respectively. The $S \leftrightarrow N$ phase equilibria of the binary system 5OCB and 7OCB ends in a eutectic point [45]. This behaviour is analogous to melting point depression. The $N \leftrightarrow I$ phase transition behaves analogous to a zeotropic liquid-vapour equilibrium. The liquid crystals are in both the isotropic and the nematic phase miscible at all compositions. Liquid crystals are in general soluble in all concentrations in the nematic phase. For molecules that are very similar in structure, like the mixture of 5OCB and 7OCB, the temperature of the $N \leftrightarrow I$ phase transition is almost a straight line in the T,x -diagram. Combining this fact with the “melting point depression”, this leads to a larger temperature range of the nematic phase of the binary mixture of two liquid crystals compared to the unary systems. This increases the amount of CO_2 which can be desorbed during one cycle, as the two-phase area $N + I$ becomes wider when more CO_2 is added. Still the maximum amount of CO_2 absorbed and desorbed is small, only 0.008 mol CO_2 /mol.

The schematic T,x -diagram of $\text{PCH3} + \text{CO}_2$ at $P = 2.00$ MPa is shown in Figure 6.20. The basic idea of this T,x -diagram is comparable with the T,x -diagram of 5OCB + CO_2 shown in Figure 6.18. The main difference is that this binary mixture has a smaller temperature range of the nematic phase, leading to an even lower quadruple point concentration, only 0.050 mole CO_2 /mole. At a CO_2 concentration at less than 0.050 mole CO_2 /mole the $N + I + G$ equilibrium is stable, at higher concentration the three-phase equilibria involving the solid phase are more stable, leading to the conclusion that above this concentration PCH3 cannot be used for CO_2 capture. The T,x -diagram of the ternary mixture of $\text{PCH3} + \text{PCH7} + \text{CO}_2$ at $P = 2.00$ MPa is shown in Figure 6.21. At this pressure a stable $N + I + G$ equilibrium is measured. Moreover, the solid phase does not interfere with the $N + I + G$ equilibrium. If one would use this mixture for a CO_2 capture process, the maximum amount of CO_2 released during one desorption cycle is 0.013 mol CO_2 /mol. Compared with the T,x -diagrams of the mixture 5OCB + CO_2 and the ternary mixture of 5OCB + 7OCB + CO_2 , as shown in Figure 6.18 and Figure 6.19 respectively, the T,x -diagram of the ternary mixture $\text{PCH3} + \text{PCH7} + \text{CO}_2$ and the P,x -diagram shown in Figure 6.21 lead to the conclusion that $\text{PCH3} + \text{PCH7}$ is most beneficial for CO_2 capture. First of all, the Δx value is largest of all the liquid crystals measured. Moreover, the solubility of CO_2 in this material is higher than any of the other mixtures. Secondly, the mixture is liquid at room temperature, making the handling more easily than the other mixtures.

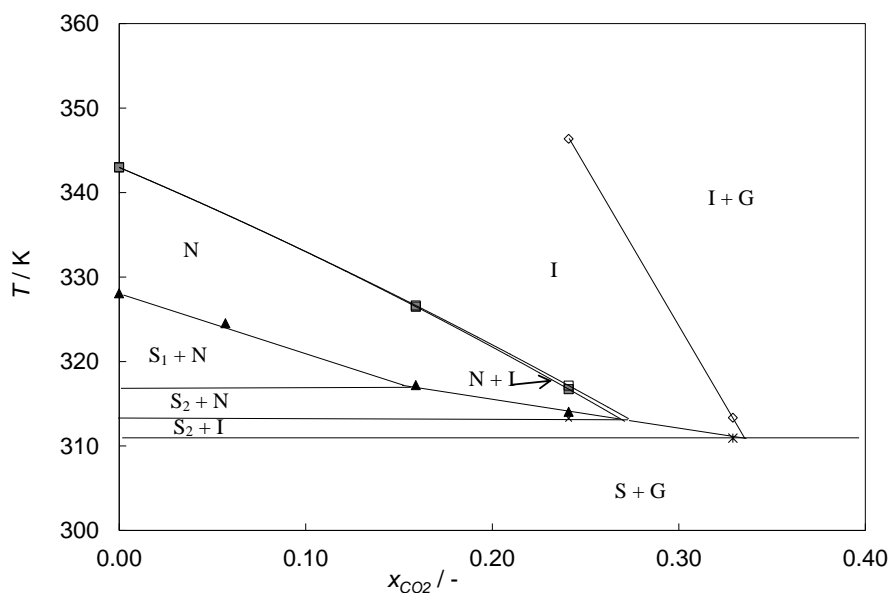


Figure 6.18. T,x -diagram of the binary mixture 4'-pentyloxy-4-cyanobiphenyl + CO₂ at $P = 4.00$ MPa, S_1 and S_2 denote the solid phases, N denotes the nematic phase, I the isotropic phase and G the gas phase.

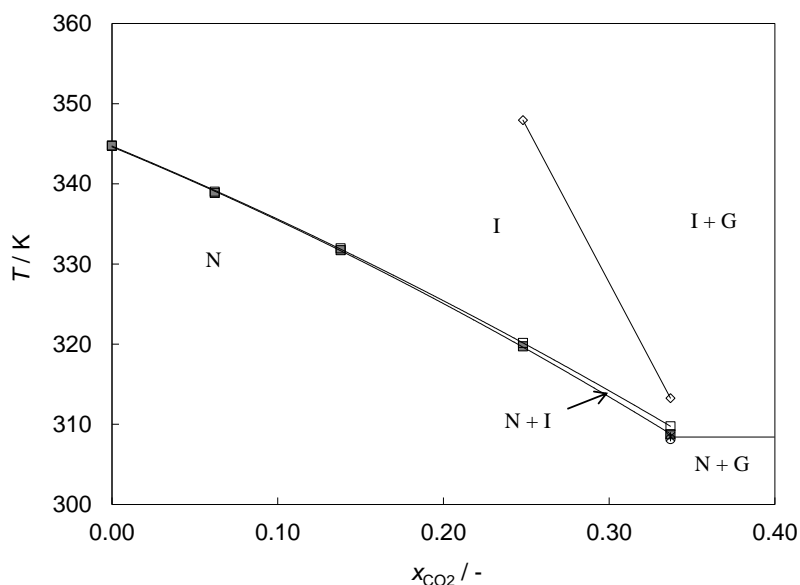


Figure 6.19. T,x -diagram of the ternary mixture 4'-heptyloxy-4-cyanobiphenyl + 4'-pentyloxy-4-cyanobiphenyl + CO₂, $x_{50CB}/x_{70CB} = 1.78$ at $P = 4.00$ MPa. N denotes the nematic phase, I the isotropic phase and G the gas phase.

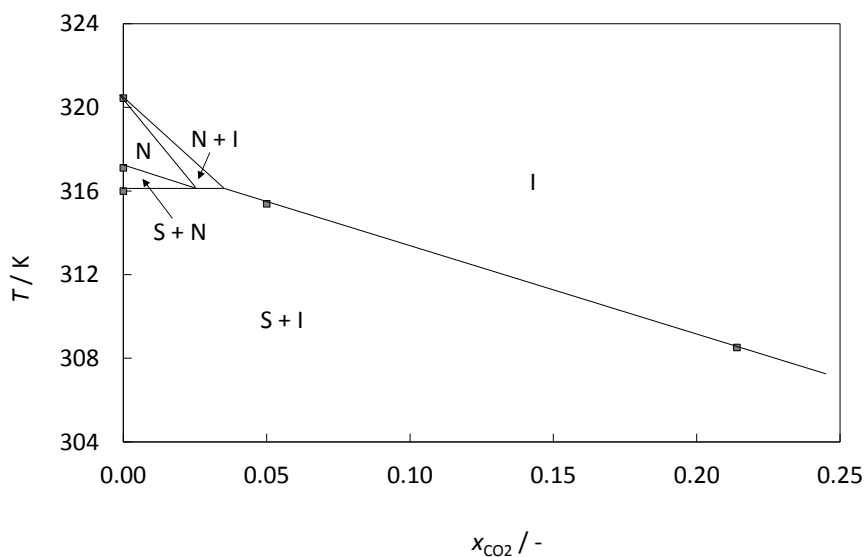


Figure 6.20. Schematic T,x -diagram of the binary mixture 4'-propylcyclohexyl-4-benzonitrile + CO₂, at $P = 2.00$ MPa. S denotes the solid phase, N the nematic phase and I the isotropic phase.

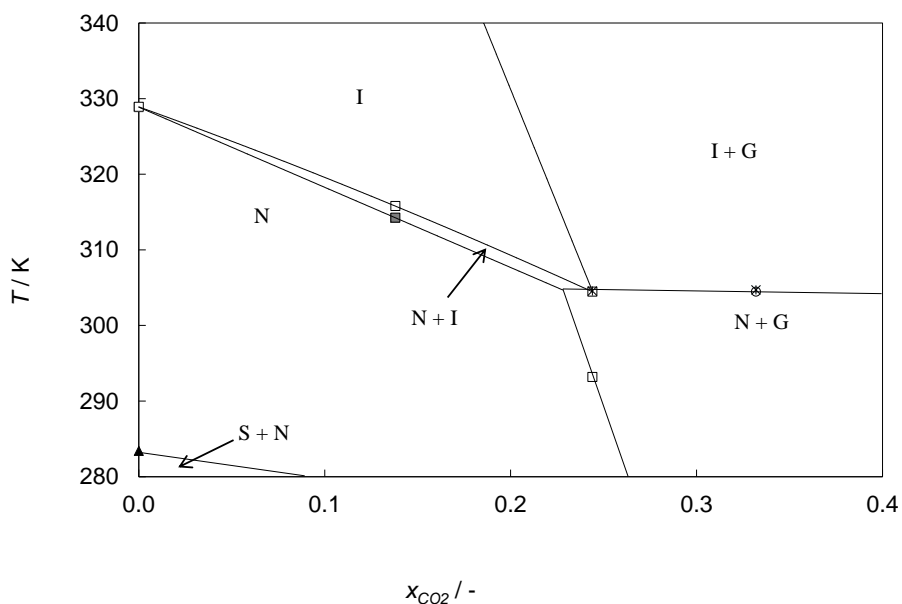


Figure 6.21. T,x -diagram of the ternary mixture 4'-propylcyclohexyl-4-benzonitrile + 4'-heptylcyclohexyl-4-benzonitrile + CO₂, $x_{PCH7}/x_{PCH3} = 3.0 \pm 0.1$ at $P = 2.00$ MPa, S denotes the solid phase, N the nematic phase, I the isotropic phase and G the gas phase.

6.5. Conclusion

The combination of PCH3 and PCH7 is in this case more promising for CO₂ capture than 5OCB and 7OCB because the phase transition enthalpy of the first mentioned system is higher. Also, the CO₂ solubility in PCH3 and PCH7 is lower than for 5OCB + CO₂ and 7OCB + CO₂. The drawback of using liquid crystals for CO₂ capture is the low phase transition enthalpy of the N \leftrightarrow I phase transition. This leads to a small difference of absorbed CO₂ in the two phases, namely $\Delta x = 0.013$.

7. Phase behaviour of binary mixtures of a liquid crystal and methane

This chapter is based on M. de Groen, O. Mesalles Molet, T.J.H. Vlugt, T.W. de Loos, Phase behaviour of binary mixtures of a liquid crystal and methane, submitted to the Journal of Chemical Engineering Data.

7.1. Introduction

Natural gas can contain large amounts of CO₂, leading to corrosivity and increased transportation costs of the gas, and decreased combustion quality [18]. Natural gas sweetening is used to remove CO₂ to avoid these problems. Processes currently applied are processes based on chemical solubility like alkanolamine scrubbing, or physical absorption processes like the Rectisol and Selexol processes [18]. One of the drawbacks of these processes are the high energy use of the regeneration of the solvent [18]. In the case of alkanolamine scrubbing, corrosion and evaporation of the solvent are additional problems related to this process [21].

Of the solubility of methane in liquid crystals practically nothing is known yet. To be able to have a first idea on the ideal selectivity of the separation of CO₂ and CH₄ using liquid crystals, four liquid crystals with different polarity were chosen. The solubility of methane is measured in 4-ethyl-4'-propylbicyclohexyl, 4'-pentylcyclohexyl-4-benzonitrile, 4'-pentyl-4-cyanobiphenyl and 4'-pentyloxy-4-cyanobiphenyl at a weight fraction CH₄ of $w_{\text{CH}_4} = 0.01$. The main conclusion is that the polarity of the liquid crystal has a strong influence on the solubility of methane: the solubility of CH₄ is higher in apolar solvents than in polar solvents.

7.2. Experimental methods

The liquid crystals used in this chapter were obtained from different suppliers. 4-ethyl-4'-propylbicyclohexyl and 4'-pentylcyclohexyl-4-benzonitrile, both with a purity of 98% mass, were provided by Merck KGaA. 4'-pentyl-4-cyanobiphenyl and 4'-pentyloxy-4-cyanobiphenyl, both of purity 99% mass, were obtained from Sigma Aldrich. An overview of the materials is listed in Table 7.1.

Table 7.1. Overview of chemicals used in this chapter.

Chemical name	Source	Purity	Purification
4-ethyl-4'-propyl bicyclohexyl	Merck	$\geq 98\%$ mass	Used as received
4'-pentyl-4-cyanobiphenyl	Alfa Aesar	99% mass	Used as received
4'-pentylcyclohexyl-4- benzonitrile	Merck	$\geq 98\%$ mass	Used as received
4'-pentyloxy-4- cyanobiphenyl	Alfa Aesar	99% mass	Used as received
CO ₂	Linde Gas	Volume fraction 0.99995	Used as received

The phase equilibria of the binary mixtures of a liquid crystal with CH₄ were measured with a Cailletet setup. The procedure followed for sample preparation was similar as described in Chapter 3. The Cailletet setup itself is described in detail in the publication of De Loos *et al.* [51].

Phase equilibria measured in this study were the three-phase equilibria nematic + isotropic + gas (N + I + G), smectic + isotropic + gas (Sm + I + G), and the two-phase equilibria isotropic + gas \leftrightarrow isotropic (I + G \leftrightarrow I), nematic + isotropic \leftrightarrow isotropic (N + I \leftrightarrow I), nematic \leftrightarrow nematic + isotropic (N \leftrightarrow N + I), and smectic + isotropic \leftrightarrow isotropic (Sm + I \leftrightarrow I). The I + G \leftrightarrow I and N + I + G equilibria were measured at constant temperature by changing the pressure with an accuracy of 0.005 MPa and 0.01 K. The phase equilibria involving the smectic phase were measured at constant pressure while changing the temperature, with an accuracy of 0.005 MPa and 0.03 K. The other phase equilibria were measured at constant pressure while changing the temperature, with an accuracy of 0.005 MPa and 0.03 K. The weight fraction of CH₄ chosen was $w_{\text{CH}_4} = 0.010$, because at this concentration the phase equilibria of the investigated systems are below 15 MPa and therefore still measurable in the Cailletet equipment.

7.3. Results

The solubility of methane was measured in four liquid crystals with different polarity. The systems are discussed in the order of increasing polarity of the liquid crystal. The tabulated experimental data is available in Appendix E.

The P,T -phase diagram of a binary mixture of 4-ethyl-4'-propylbicyclohexyl with CH_4 , with $w_{\text{CH}_4} = 0.010$ is shown in Figure 7.1. 4-ethyl-4'-propylbicyclohexyl is a purely apolar molecule with a smectic to isotropic phase transition at 341 K at 0.1 MPa, as shown in Chapter 3. Phase equilibria measured for this liquid crystal were the two-phase equilibria $\text{I} + \text{G} \leftrightarrow \text{I}$, $\text{Sm} + \text{I} \leftrightarrow \text{I}$ and the three-phase equilibrium $\text{Sm} + \text{I} + \text{G}$. The $\text{I} + \text{G} \leftrightarrow \text{I}$ curve has a positive slope. The three-phase curve ends at $P = 0$ MPa at $T = 340$ K, which is close to the pure component phase transition temperature at atmospheric pressure.

The P,T -phase diagram of 4'-pentylcyclohexyl-4-benzonitrile with CH_4 , at $w_{\text{CH}_4} = 0.010$ is shown in Figure 7.2. The molecular structure of this liquid crystal consists of a polar and a nonpolar part. The polar part is a benzene ring with a cyanogroup attached to it at the 4-position, and the nonpolar part consists of a cyclohexane ring with a pentyl carbon chain attached to it. 4'-pentylcyclohexyl-4-benzonitrile is a nematic liquid crystal, with a nematic to isotropic phase transition temperature of $T = 328$ K [37]. Phase equilibria measured for this liquid crystal were the two-phase equilibria $\text{N} + \text{I} \leftrightarrow \text{I}$, $\text{I} + \text{G} \leftrightarrow \text{I}$ and the three-phase equilibrium $\text{N} + \text{I} + \text{G}$. The gas solubility curve has a pressure minimum, and the equilibrium pressure is increasing near the $\text{N} + \text{I} \leftrightarrow \text{I}$ phase transition.

To increase the polarity, a liquid crystal with two benzene rings but with the same side groups was chosen, namely 4'-pentyl-4-cyanobiphenyl. This molecule has a nematic phase as well, the nematic phase is stable up to 308 K [46]. In Figure 7.3 the P,T -diagram is shown of the binary system 4'-pentyl-4-cyanobiphenyl + CH_4 , at $w_{\text{CH}_4} = 0.010$. Phase equilibria measured for this molecule were the two-phase equilibria $\text{N} \leftrightarrow \text{N} + \text{I}$, $\text{N} + \text{I} \leftrightarrow \text{I}$, $\text{I} + \text{G} \leftrightarrow \text{I}$ and the three-phase equilibrium $\text{N} + \text{I} + \text{G}$. The pressure solubility curve $\text{I} + \text{G} \leftrightarrow \text{I}$ is gradually decreasing with increasing T , however, near the phase equilibrium $\text{N} + \text{I} \leftrightarrow \text{I}$ the slope of the equilibrium curve is increasing.

As most polar liquid crystal, 4'-pentyloxy-4-cyanobiphenyl was chosen. This molecule has an oxygen atom in between the carbon chain and the benzene ring. Figure 7.4 shows the P,T -diagram for the binary system of 4'-pentyloxy-4-cyanobiphenyl with CH_4 at $w_{\text{CH}_4} = 0.010$. The two-phase equilibria measured for this system were $\text{N} + \text{I} \leftrightarrow \text{I}$ and $\text{I} + \text{G} \leftrightarrow \text{I}$, and the three-phase curve $\text{N} + \text{I} + \text{G}$

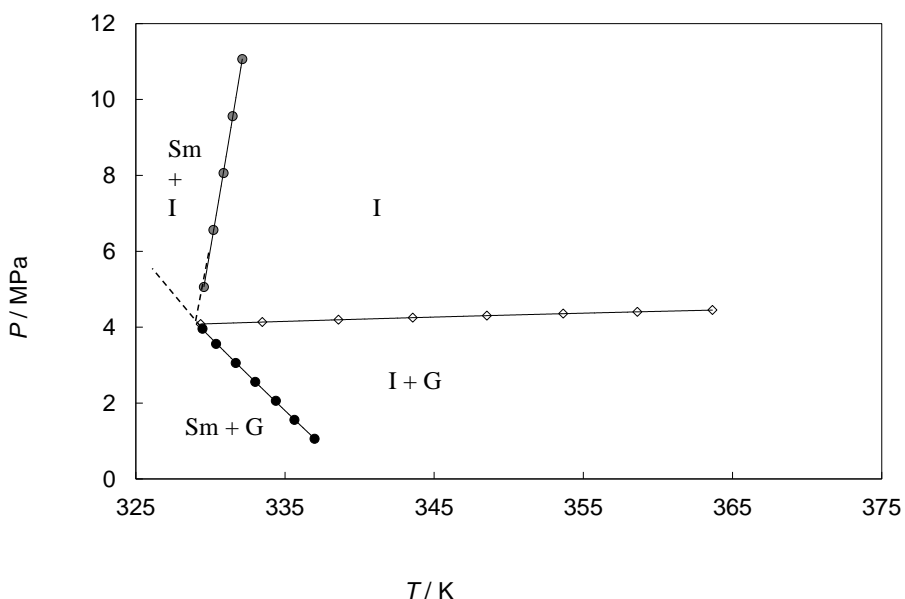


Figure 7.1. P,T -diagram of 4-ethyl-4'-propylbicyclohexyl + CH_4 at $w_{\text{CH}_4} = 0.010$. Sm denotes the smectic phase, I the isotropic phase and G the gas phase. Description of symbols used: \bullet Sm + I \leftrightarrow I, \diamond I + G \leftrightarrow I, \bullet Sm + I + G. The solid lines are first and second order polynomial fits through the data points.

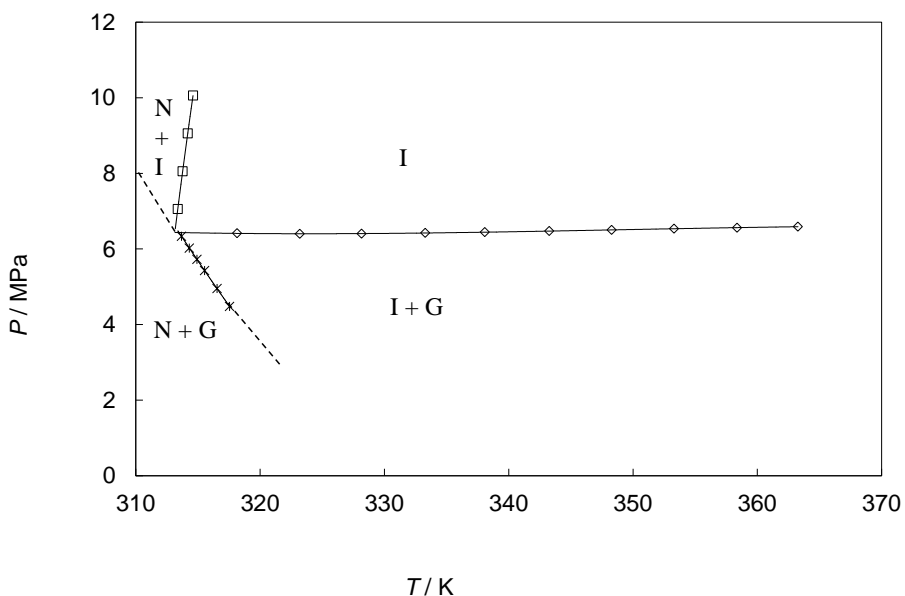


Figure 7.2. P,T -diagram of 4'-pentylcyclohexyl-4-benzonitrile + CH_4 at $w_{\text{CH}_4} = 0.010$. N denotes the nematic phase, I the isotropic phase and G the gas phase. \blacksquare N + I \leftrightarrow N; \square N + I \leftrightarrow I; $*$ N + I + G; \diamond I + G \leftrightarrow I. The solid lines are first and second order polynomial fits through the data points.

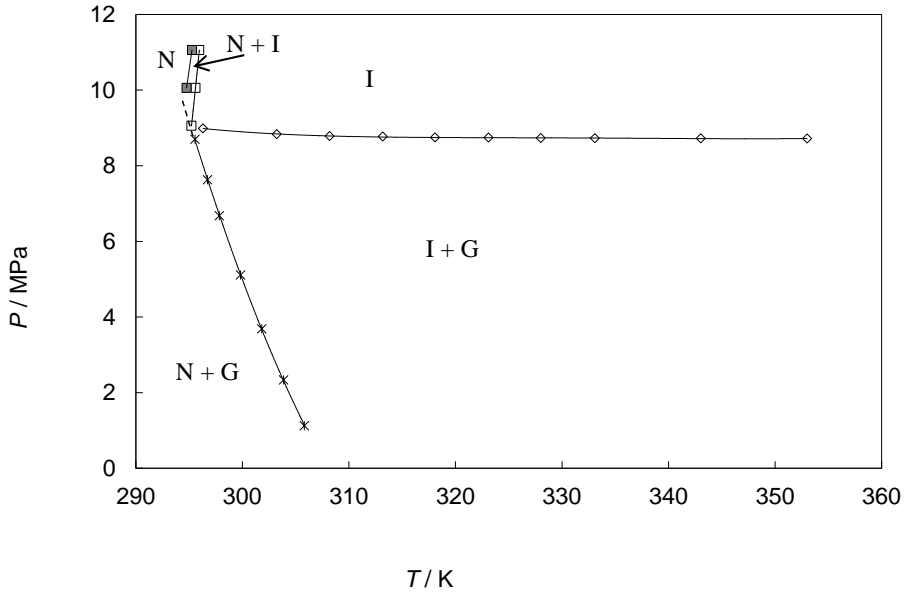


Figure 7.3. P,T -diagram of 4'-pentyl-4-cyanobiphenyl + CH₄ at $w_{CH_4} = 0.010$. N denotes the nematic phase, I the isotropic phase and G the gas phase. \blacksquare $N + I \leftrightarrow N$; \square $N + I \leftrightarrow I$; $*$ $N + I + G$; \diamond $I + G \leftrightarrow I$. The solid lines are first and second order polynomial fits through the data points.

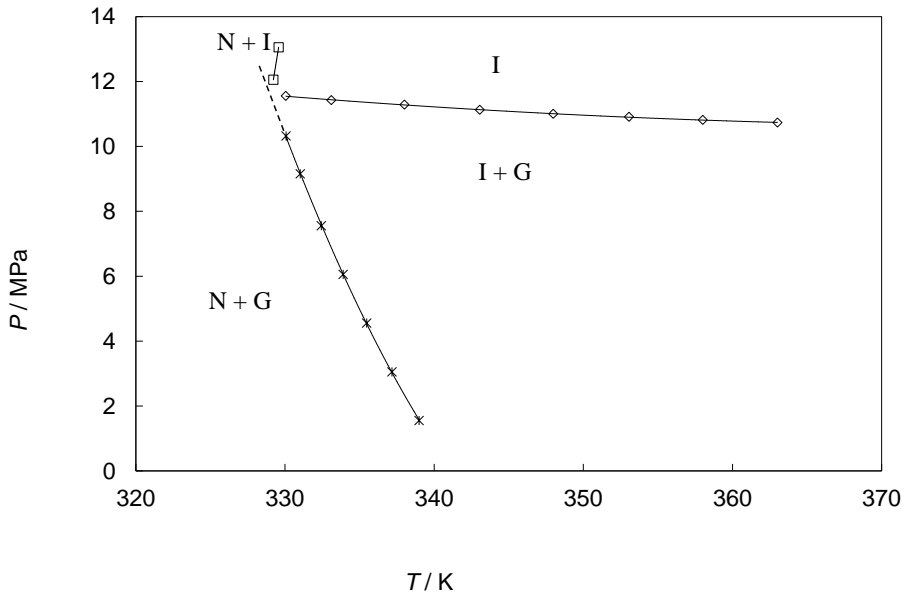


Figure 7.4. P,T -diagram of 4'-pentyloxy-4-cyanobiphenyl + CH₄ at $w_{CH_4} = 0.010$. N denotes the nematic phase, I the isotropic phase and G the gas phase. \square $N + I \leftrightarrow I$; $*$ $N + I + G$; \diamond $I + G \leftrightarrow I$. The solid lines are first and second order polynomial fits through the data points.

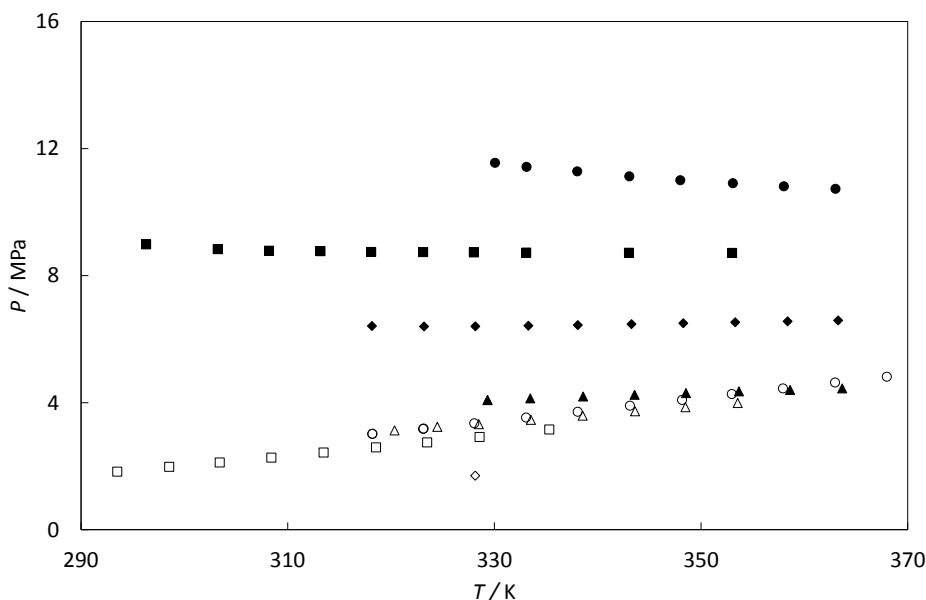


Figure 7.5. Solubility of CH_4 and CO_2 in liquid crystals. The filled symbols correspond to the solubility of CH_4 , and the open symbols to the solubility of CO_2 . Data for CO_2 are taken from Chapter 3, except for the data point of 4'-pentylcyclohexyl-4-benzonitrile, which was estimated from the data published by Chen *et al.* [37]. \circ 4'-pentyloxy-4-cyanobiphenyl \square 4'-pentyl-4-cyanobiphenyl, \triangle 4-ethyl-4'-propylbicyclohexyl, \diamond 4'-pentylcyclohexyl-4-benzonitrile

was measured as well. The nature of the $\text{I} + \text{G} \leftrightarrow \text{I}$ curve of this system is similar as for the system of $\text{CH}_4 + 4'$ -pentyl-4-cyanobiphenyl.

7.4. Discussion

The solubility difference of methane and carbon dioxide is one of the important factors determining the applicability of the solvent for the CO_2 capture process described in the introduction. Therefore, the solubility of both methane and CO_2 is plotted in Figure 7.5. The weight fraction of methane used is $w_{\text{CH}_4} = 0.010$, the weight fraction of CO_2 is $w_{\text{CO}_2} = 0.050$. The results for CO_2 were taken from Chapter 3 and the results of $\text{PCH5} + \text{CO}_2$ from the paper of Chen *et al.* [37]. Important in this figure to see is that the polarity has a clear influence on the solubility of CH_4 in the solvent, but not on the solubility of CO_2 . More polar molecules have a lower solubility for CH_4 . PCH5 has the highest solubility for the

liquid crystal + CO₂ systems [37,56]. An explanation of this behaviour might be the low solvent-solvent interaction of this molecule compared to the other molecules measured.

The shape of the I + G \leftrightarrow I equilibrium curves in the *P,T*-plane at constant composition is varying with the polarity of the solvent. The most apolar liquid crystal, 4-ethyl-4'-propylbicyclohexyl, has a positive slope of the I + G \leftrightarrow I equilibrium curve, comparable to CO₂. The slope of the I + G \leftrightarrow I curve of this system is smaller for CH₄ smaller than of the I + G \leftrightarrow I curve of CO₂. The system of 4'-pentylcyclohexyl-4-benzonitrile + CH₄ and 4'-pentyl-4-cyanobiphenyl + CH₄, both show a minimum in the I + G \leftrightarrow I equilibrium curve. This behaviour is observed as well for systems with type III phase behaviour according to the classification of Van Konyneburg and Scott [62], like systems of CO₂ + *n*-alkanes, with *n* > 13 [63,64]. The most polar liquid crystal, 4'-pentyloxy-4-cyanobiphenyl, shows a decreasing curve. This might also be an effect of type III behaviour.

7.5. Conclusion

The solubility of CH₄ in liquid crystals is clearly influenced by the polarity of the liquid crystal material. This leads to the conclusion that the best solvent, in terms of lowest methane solubility, would be a polar liquid crystal. This does not agree with the results of the solubility of CO₂ in liquid crystals: here, PCH5 has the highest CO₂ solubility. Therefore, there is a trade-off between maximum solubility of CO₂ and ideal selectivity of CH₄ over CO₂. Further research is needed to find the optimum liquid crystal solvent.

8. Concluding remarks

This thesis describes fundamental research on phase equilibria of CO₂ with liquid crystals for CO₂ capture. The main property of using liquid crystals for CO₂ capture is the solubility difference between the nematic and the isotropic phases. The main advantage is that the process only needs minor temperature changes and no pressure changes to separate the CO₂. Measurements of phase equilibria of CO₂-liquid crystal systems showed that the enthalpy change of the nematic-isotropic phase transition and the polarity of the liquid crystals influence the capability of separating the CO₂. Ternary mixtures of two liquid crystals and CO₂ have been proven to have superior properties to binary mixtures of one liquid crystal and CO₂ for CO₂ capture.

However, the technique is not mature. The main drawback is, at the moment, the limited solubility difference between the isotropic and the nematic phase. Only a few mole percent of CO₂ is released during one absorption/desorption cycle. For a practical application this would result in very large process equipment. Furthermore, liquid crystals are specialty chemicals and therefore expensive. Conventional absorption processes will not be suitable for a CO₂ capture process with liquid crystals. Processes involving the smectic phase, a very viscous phase, might be more promising in terms of solubility difference. The drawback of using a very viscous phase is that the released gaseous CO₂ will be trapped as bubbles. Additional effort is needed to separate CO₂ from the smectic phase.

The best direction for this research is increasing the knowledge in theoretical models and molecular simulations of this process, using this experimental study as a basis. This allows a more systematic study on which liquid crystals have optimal properties for being used as process solvent in a CO₂ capture process. Further, CFD simulations of alternative absorption processes will be needed for designing a CO₂ absorption/desorption column.

References

- [1] T.F. Stocker, D. Qin, G.-K. Plattner, M. Tignor, S.K. Allen, J. Boschung, A. Nauels, Y. Xia, V. Bex, P.M. Midgley, *Climate Change 2013: The physical science basis. Contribution of Working Group I to the Fifth Assessment Report of the Intergovernmental Panel on Climate Change*, IPCC, 2013.
- [2] M.E. Boot-Handford, J.C. Abanades, E.J. Anthony, M.J. Blunt, S. Brandani, N. Mac Dowell, J.R. Fernandez, M.C. Ferrari, R. Gross, J.P. Hallett, R.S. Haszeldine, P. Heptonstall, A. Lyngfelt, Z. Makuch, E. Mangano, R.T.J. Porter, M. Pourkashanian, G.T. Rochelle, N. Shah, J.G. Yao, P.S. Fennell, Carbon capture and storage update, *Energy & Environmental Science*, 7 (2014) 130-189.
- [3] International Energy Agency, *Energy, climate change and environment: 2014 insights*, International Energy Agency, 2014.
- [4] R.S. Dhillon, G. von Wuehlisch, Mitigation of global warming through renewable biomass, *Biomass & Bioenergy*, 48 (2013) 75-89.
- [5] T. Abbasi, S.A. Abbasi, Decarbonization of fossil fuels as a strategy to control global warming, *Renewable & Sustainable Energy Reviews*, 15 (2011) 1828-1834.
- [6] B. Li, Y. Duan, D. Luebke, B. Morreale, Advances in CO₂ capture technology: A patent review, *Applied Energy*, 102 (2013) 1439-1447.
- [7] J.C.M. Pires, F.G. Martins, M.C.M. Alvim-Ferraz, M. Simoes, Recent developments on carbon capture and storage: An overview, *Chemical Engineering Research & Design*, 89 (2011) 1446-1460.
- [8] E.S. Rubin, H. Mantripragada, A. Marks, P. Versteeg, J. Kitchin, The outlook for improved carbon capture technology, *Progress in Energy and Combustion Science*, 38 (2012) 630-671.
- [9] E. Levina, S. Bennett, S. McCoy, *Technology roadmap carbon capture and storage*, International Energy Agency, 2013.

- [10] H. Ahn, M. Luberti, Z. Liu, S. Brandani, Process configuration studies of the amine capture process for coal-fired power plants, *International Journal of Greenhouse Gas Control*, 16 (2013) 29-40.
- [11] S. Topham, A. Bazzanella, S. Schiebahn, S. Luhr, L. Zhao, A. Otto, D. Stolten, Carbon dioxide, in: *Ullmann's Encyclopedia of Industrial Chemistry*, Wiley-VCH Verlag GmbH & Co. KGaA, 2000.
- [12] V. Scherer, D. Stolten, J. Franz, E. Riensche, CCS-Abscheidetechniken: Stand der Technik und Entwicklungen; CCS separation techniques – Review on existing technologies and developments, *Chemie Ingenieur Technik*, 84 (2012) 1026-1040.
- [13] B.P. Spigarelli, S.K. Kawatra, Opportunities and challenges in carbon dioxide capture, *Journal of CO₂ Utilization*, 1 (2013) 69-87.
- [14] A.A. Olajire, CO₂ capture and separation technologies for end-of-pipe applications - A review, *Energy*, 35 (2010) 2610-2628.
- [15] M.K. Mondal, H.K. Balsora, P. Varshney, Progress and trends in CO₂ capture/separation technologies: A review, *Energy*, 46 (2012) 431-441.
- [16] J.C. Meerman, E.S. Hamborg, T. van Keulen, A. Ramírez, W.C. Turkenburg, A.P.C. Faaij, Techno-economic assessment of CO₂ capture at steam methane reforming facilities using commercially available technology, *International Journal of Greenhouse Gas Control*, 9 (2012) 160-171.
- [17] M.Z. Jacobson, Review of solutions to global warming, air pollution, and energy security, *Energy & Environmental Science*, 2 (2009) 148-173.
- [18] G. Hammer, T. Lübcke, R. Kettner, M.R. Pillarella, H. Recknagel, A. Commichau, H.-J. Neumann, B. Paczynska-Lahme, Natural gas, in: *Ullmann's Encyclopedia of Industrial Chemistry*, Wiley-VCH Verlag GmbH & Co. KGaA, 2000.
- [19] G.T. Rochelle, Amine scrubbing for CO₂ capture, *Science*, 325 (2009) 1652-1654.

- [20] M. Wang, A. Lawal, P. Stephenson, J. Sidders, C. Ramshaw, Post-combustion CO₂ capture with chemical absorption: A state-of-the-art review, *Chemical Engineering Research & Design*, 89 (2011) 1609-1624.
- [21] P. Khakharia, L. Brachert, J. Mertens, A. Huizinga, B. Schallert, K. Schaber, T.J.H. Vlugt, E. Goetheer, Investigation of aerosol based emission of MEA due to sulphuric acid aerosol and soot in a post-combustion CO₂ capture process, *International Journal of Greenhouse Gas Control*, 19 (2013) 138-144.
- [22] J. Kittel, S. Gonzalez, Corrosion in CO₂ post-combustion capture with alkanolamines - A review, *Oil & Gas Science and Technology-Revue D IFP Energies Nouvelles*, 69 (2014) 915-929.
- [23] E.F. da Silva, H. Kolderup, E. Goetheer, K.W. Hjarbo, A. Huizinga, P. Khakharia, I. Tuinman, T. Mejdell, K. Zahlsen, K. Vernstad, A. Hyldbakk, T. Holten, H.M. Kvamsdal, P. van Os, A. Einbu, Emission studies from a CO₂ capture pilot plant, *Greenhouse Gas Technology-11*, 37 (2013) 778-783.
- [24] S.D. Kenarsari, D.L. Yang, G.D. Jiang, S.J. Zhang, J.J. Wang, A.G. Russell, Q. Wei, M.H. Fan, Review of recent advances in carbon dioxide separation and capture, *RSC Advances*, 3 (2013) 22739-22773.
- [25] S. Seo, L.D. Simoni, M. Ma, M.A. DeSilva, Y. Huang, M.A. Stadtherr, J.F. Brennecke, Phase-change ionic liquids for post-combustion CO₂ capture, *Energy & Fuels*, 28 (2014) 5968-5977.
- [26] D.M. D'Alessandro, B. Smit, J.R. Long, Carbon dioxide capture: Prospects for new materials, *Angewandte Chemie-International Edition*, 49 (2010) 6058-6082.
- [27] A. Samanta, A. Zhao, G.K.H. Shimizu, P. Sarkar, R. Gupta, Post-combustion CO₂ capture using solid sorbents: A review, *Industrial & Engineering Chemistry Research*, 51 (2012) 1438-1463.
- [28] M. Ramdin, T.W. de Loos, T.J.H. Vlugt, State-of-the-art of CO₂ capture with ionic liquids, *Industrial & Engineering Chemistry Research*, 51 (2012) 8149-8177.

- [29] B. Smit, J.A. Reimer, C.M. Oldenburg, I.C. Bourg, Introduction to geological sequestration, Imperial College Press, London, 2014.
- [30] F. Karadas, M. Atilhan, S. Aparicio, Review on the use of ionic liquids (ILs) as alternative fluids for CO₂ capture and natural gas sweetening, *Energy & Fuels*, 24 (2010) 5817-5828.
- [31] J. Gross, P.J. Jansens, Removal of component, preferably carbon dioxide, from process gas stream by using isotropic liquid crystals as solvent, patent application, 2008, WO2008147181-A1, NL2000654-C2.
- [32] S. Pestov, Group VIII Advanced Materials and Technologies, V. Vill (Ed.), Landolt-Börnstein Database, Springer Berlin Heidelberg, 2003.
- [33] B. Oyarzun, T. van Westen, T.J.H. Vlugt, The phase behavior of linear and partially flexible hard-sphere chain fluids and the solubility of hard spheres in hard-sphere chain fluids, *Journal of Chemical Physics*, 138 (2013).
- [34] T. van Westen, B. Oyarzun, T.J.H. Vlugt, J. Gross, The isotropic-nematic phase transition of tangent hard-sphere chain fluids-Pure components, *Journal of Chemical Physics*, 139 (2013).
- [35] D.S. Chen, G.H. Hsiue, J.D. Schultze, B.H. Song, J. Springer, Gas sorption properties and molecular-states of a liquid-crystal, *Molecular Crystals and Liquid Crystals Science and Technology Section a-Molecular Crystals and Liquid Crystals*, 237 (1993) 85-95.
- [36] G.H. Hsiue, D.S. Chen, C.J. Hsieh, Gas sorption properties in a smectic liquid-crystal, *Molecular Crystals and Liquid Crystals Science and Technology Section a-Molecular Crystals and Liquid Crystals*, 241 (1994) 187-193.
- [37] G.H. Chen, J. Springer, Sorption and diffusion of gases in liquid crystalline substances, *Molecular Crystals and Liquid Crystals*, 339 (2000) 31-44.
- [38] H. Orendi, M. Ballauff, Complete phase-diagrams of mixtures of a nematic liquid crystal with normal-alkanes, *Liquid Crystals*, 6 (1989) 497-500.

- [39] H. Orendi, M. Ballauff, Analysis of the phase-diagrams of mixtures of a nematic liquid with normal-alkanes, *Berichte Der Bunsen-Gesellschaft-Physical Chemistry Chemical Physics*, 96 (1992) 96-100.
- [40] S.M. Pestov, V.A. Molotchko, R.A. Lidine, Solubility of liquid-crystals in organic solvents, *Thermochimica Acta*, 236 (1994) 131-139.
- [41] Z.A. Tchoraia, V.A. Molotchko, E.I. Smarina, R.A. Lidine, Polymorphism of nematogenes in the solid-state - normal-butyl-4-phenyl-normal-4'-hexyloxy-benzoate - organic-solvents, *Journal of Thermal Analysis*, 21 (1981) 263-270.
- [42] J. Zernike, *Chemical Phase Theory*, Kluwer, 1955.
- [43] G.N. Lewis, M. Randall, K.S. Pitzer, L. Brewer, *Thermodynamics*, McGraw-Hill, United States, 1961.
- [44] T.W. de Loos, On the phase behaviour of asymmetric systems: The three-phase curve solid-liquid-gas, *Journal of Supercritical Fluids*, 39 (2006) 154-159.
- [45] D.S. Hulme, E.P. Raynes, Eutectic mixtures of nematic 4'-substituted 4-cyanobiphenyls, *Journal of the Chemical Society-Chemical Communications*, (1974) 98-99.
- [46] G.A. Oweimreen, M.A. Morsey, DSC studies on p-(n-alkyl)-p'-cyanobiphenyl (RCB's) and p-(n-alkoxy)-p'-cyanobiphenyl (ROCB's) liquid crystals, *Thermochimica Acta*, 346 (2000) 37-47.
- [47] R.A. Orwoll, V.J. Sullivan, G.C. Campbell, Thermal pressure coefficients and specific volumes of cyanobiphenyls and their transition entropies at constant volume, *Molecular Crystals and Liquid Crystals*, 149 (1987) 121-140.
- [48] L.L. Lai, J.J. Chen, Y.G. Lin, Y.C. Lin, W.S. Tzeng, K.L. Cheng, N,N-Disubstituted-4-aminophenylazostyrylformate derivatives: Their synthesis, mesogenic behaviour and photostability, *Liquid Crystals*, 30 (2003) 1449-1454.

- [49] S.J. Picken, Personal communication, 2011.
- [50] D.S. Chen, G.H. Hsiue, Gas sorption in side-chain liquid-crystalline polymers, *Polymer*, 35 (1994) 2808-2814.
- [51] T.W. de Loos, H.J. van der Kooij, P.L. Ott, Vapor-liquid critical curve of the system ethane + 2-methylpropane, *Journal of Chemical and Engineering Data*, 31 (1986) 166-168.
- [52] M.J. Muldoon, S.N.V.K. Aki, J.L. Anderson, J.K. Dixon, J.F. Brennecke, Improving carbon dioxide solubility in ionic liquids, *Journal of Physical Chemistry B*, 111 (2007) 9001-9009.
- [53] M. Besnard, M.I. Cabaco, D. Talaga, Y. Danten, Raman spectroscopy and ab initio investigations of transient complex formation in CO₂-benzene mixtures, *Journal of Chemical Physics*, 129 (2008).
- [54] R. Span, W. Wagner, A new equation of state for carbon dioxide covering the fluid region from the triple-point temperature to 1100 K at pressures up to 800 MPa, *Journal of Physical and Chemical Reference Data*, 25 (1996) 1509-1596.
- [55] G.W. Gray, K.J. Harrison, J.A. Nash, Recent developments concerning biphenyl mesogens and structurally related compounds, *Pramana Supplement*, 1 (1975) 381-396.
- [56] M. de Groen, T.J.H. Vlugt, T.W. de Loos, Phase behavior of liquid crystals with CO₂, *Journal of Physical Chemistry B*, 116 (2012) 9101-9106.
- [57] O.P. Chernova, V.A. Molochko, G.M. Kurdyumov, I.N. Kashcheev, Phase-equilibria in systems formed by 4-alkyl-4'-cyanobiphenyls and 4-alkoxy-4'-cyanobiphenyls, *Journal of Applied Chemistry of the USSR*, 55 (1982) 473-476.
- [58] T. Engel, P. Reid, *Physical Chemistry*, Pearson/Benjamin/Cummings, 2006.
- [59] G.W. Smith, Thermal parameters of some liquid-crystals, *Molecular Crystals and Liquid Crystals*, 41 (1977) 89-95.

- [60] J.F. Ely, J.W. Magee, W.M. Haynes, Thermophysical properties for special high CO₂ content mixtures, Gas Processors Association, 1987.
- [61] V.A. Molotchko, S.M. Pestov, R.A. Lidine, Classification of nematic liquid crystal systems, Molecular Crystals and Liquid Crystals Science and Technology Section a-Molecular Crystals and Liquid Crystals, 287 (1996) 47-56.
- [62] G. Schneider, Z. Alwani, W. Heim, E. Horvath, E.U. Franck, Phase equilibria and critical phenomena in binary mixtures (CO₂ with n-octane, n-undecane, n-tridecane and n-hexadecane up to 1500 bar), Chemie Ingenieur Technik, 39 (1967) 649-656.
- [63] C.J. Peters, L.J. Florusse, S. Hahre, J. de Swaan Arons, Fluid multiphase equilibria and critical phenomena in binary and ternary mixtures of carbon dioxide, certain n-alkanols and tetradecane, Fluid Phase Equilibria, 110 (1995) 157-173.
- [64] M.M. Miller, K.D. Luks, Observations on multiphase equilibria behavior of CO₂-rich and ethane-rich mixtures, Fluid Phase Equilibria, 44 (1989) 295-304.

Summary

Research to the prevention of global warming has remained important during the last decade. It is widely recognised that greenhouse gases, amongst others CO_2 are one of the main causes. As renewable energy is not available at a large scale yet, CO_2 capture is needed to lower the emission of greenhouse gases. Conventional methods like pre- and post-combustion CO_2 capture consume a lot of energy. Therefore, research to new materials for CO_2 capture and new processes is a key to reduce emissions on a short time scale.

Liquid crystals are one of the new possible materials for pre-combustion CO_2 capture. When heating a liquid crystal from the solid phase (S), first an ordered liquid phase exists before the material becomes an isotropic liquid (I). The ordered phase can either be a nematic phase (N) or a smectic phase (Sm). CO_2 is better soluble in the ordered liquid phase than in the isotropic phase. A possible explanation for this solubility change is the difference in free volume between the structured and isotropic liquid. CO_2 is dissolved in the isotropic liquid, then the mixture is cooled down until the nematic phase is reached. At this point, part of the absorbed CO_2 can be separated as a gas. The main feature of a CO_2 capture process using liquid crystals as a solvent is that the process should run at constant pressure, whereas conventional pre-combustion needs a pressure swing process. Furthermore, the liquid crystal solvent can be regenerated by increasing the temperature only a few degrees Kelvin. This is in sharp contrast to the solvent regeneration of a post-combustion process: high regeneration temperatures are necessary to remove the CO_2 .

As hardly any experimental data is available for binary systems of CO_2 and liquid crystals, phase equilibria measurements are needed for designing a CO_2 capture process with liquid crystals as a solvent. In this thesis, research is carried out using the Cailletet apparatus, which is of the synthetic visual type. With this apparatus, P, T -diagrams of samples with known amounts of liquid crystal and gas (G) were measured to understand the phase behaviour of these systems.

To have a first idea of the properties of liquid crystal + CO_2 systems, the influence of the molecular structure on the solubility of CO_2 was studied (Chapter 3). Parameters taken into account were the influence of the length of the side group of the liquid crystal and of the polarity of the side group. For this first check, a concentration of 5% mass CO_2 was taken. Comparison of the measured P, T -phase diagrams leads to the conclusion that a longer side group of the liquid crystal

increases the molar solubility of CO₂, but not the mass-based solubility. The polarity does not have a clear influence on the solubility of CO₂. Apolar liquid crystals like 4-ethyl-4'-propyl-biphenyl and liquid crystals with a polar side chain like 4'-pentyloxy-4-cyanobiphenyl seem to have a lower solubility than 4'-pentyloxy-4-cyanobiphenyl.

One of the aforementioned liquid crystals studied, 4'-pentyloxy-4-cyanobiphenyl, was studied in more detail (Chapter 4). The phase behaviour of the system of 4'-pentyloxy-4-cyanobiphenyl + CO₂ was studied for CO₂ mole fractions up to 0.72, in temperature range 280–360 K and at pressures up to 12 MPa. Two different solid phases were found, S₁ and S₂, of which S₂ is metastable. Furthermore, liquid-liquid demixing was found at high CO₂ concentration. Three quadruplepoints were found: S₁S₂IG, S₂NIG and S₂I₁I₂G. The relation between the fugacity and CO₂ concentration of the isotropic + gas \leftrightarrow isotropic phase equilibrium is fairly linear, leading to the conclusion that the Henry coefficient can be estimated using a finite concentration. Therefore, the solubility of CO₂ in various liquid crystals can be compared using the Henry coefficients calculated from measurements with approximately 1% mass CO₂. This method was then used for various liquid crystal + CO₂ systems (Chapter 5). These measurements confirmed that liquid crystals with benzene rings, but without a polar sidegroup have a higher CO₂ solubility.

None of the binary systems studied had optimal properties for designing a CO₂ capture process. Either the overall solubility is too low, or the temperature range in which the nematic phase is stable is too small. In the last case, the three-phase curve NIG, which is used for the separation process, has a small temperature range. This leads to a small solubility difference between the isotropic and the nematic phase. Therefore, research to ternary mixture of two liquid crystals + CO₂ was performed, and compared with the corresponding binary systems (Chapter 6). Compared to the corresponding binary mixtures, ternary mixtures have a lower phase transition temperature from the solid to the nematic phase. This is only the case for the solid phase. The nematic \leftrightarrow isotropic transition is not subject to lowering of the phase transition temperature. This leads to an increased temperature range of the nematic phase. Two different ternary mixtures were studied: 4'-pentyloxy-4-cyanobiphenyl + 4'-heptyloxy-4-cyanobiphenyl + CO₂ and 4'-propylcyclohexyl-4-benzonitrile + 4'-heptylcyclohexyl-4-benzonitrile + CO₂. Of these liquid crystals, the liquid crystals of the cyclohexyl benzonitrile type had a higher CO₂ solubility and a higher CO₂ solubility difference between the isotropic and nematic phase. Due to the lowering of the solid to nematic phase transition temperature, the

quadruplepoint SNIG is at a lower temperature for the ternary mixture than for the binary mixture. This leads to an increased CO₂ capacity of the solvent and a larger maximum solubility difference between the isotropic and nematic phase. Furthermore, the liquid crystals in the mixture can be chosen such that the mixture of the liquid crystals is liquid at room temperature, resulting in easier handling of the solvent. Unfortunately, the CO₂ solubility difference between the isotropic and the nematic phase is too small for designing a process with competitive properties compared to the conventional CO₂ capture processes. At this moment, the costs for liquid crystals are very high compared with other solvents used.

The last part of this thesis focuses on the solubility of methane in liquid crystals (Chapter 7). The major reason for choosing methane is the ability to check the ideal selectivity of CO₂ and another gas. The solubility of methane in liquid crystals was not studied in literature before. As expected, the solubility of methane is lower than the solubility of CO₂ in liquid crystals. The polarity has a clear influence on the solubility of methane in liquid crystals. Apolar liquid crystals have a higher solubility of methane, and the more polar the liquid crystal is, the lower the solubility. 4-Ethyl-4'-propyl-bicyclohexyl had the highest methane solubility.

Samenvatting

Het laatste decennium is het onderzoek naar het voorkomen van opwarming van de aarde steeds in de belangstelling blijven staan. Het wordt algemeen aangenomen dat de uitstoot van broeikasgassen, waar CO_2 er één van is, hiervoor een van de belangrijkste oorzaken is. Aangezien er op korte termijn nog niet voldoende energie uit hernieuwbare bronnen gewonnen kan worden is het afvangen van CO_2 noodzakelijk om de uitstoot van broeikasgassen te beperken. De nu gangbare processen voor het afvangen van CO_2 gebruiken een te grote hoeveelheid energie. Om de uitstoot van broeikasgassen op korte termijn te verlagen is het van het grootste belang dat er voortdurend onderzoek wordt gedaan naar nieuwe materialen en nieuwe processen voor het afvangen van CO_2 .

Vloeibare kristallen zijn een van deze nieuwe materialen die mogelijk geschikt kunnen zijn voor het afvangen van CO_2 na de water-gas-shift reactor, maar voor de verbrandingsinstallatie. Het verschil tussen vloeibare kristallen en gewone vloeistoffen is dat vloeibare kristallen na het smelten van de vaste fase (S) geen isotrope vloeistof (I) vormen, maar eerst een geordende vloeistof. Deze geordende fase kan een nematische (N) of een smectische (Sm) fase zijn. Als de temperatuur vervolgens verder wordt verhoogd, ontstaat er een isotrope vloeistof. De oplosbaarheid van CO_2 is hoger in de isotrope fase dan in de geordende fase. Een mogelijke verklaring voor dit verschil in oplosbaarheid is het verschil in vrij volume tussen de geordende en de isotrope fase. CO_2 wordt in de isotrope fase opgelost, vervolgens wordt het mengsel afgekoeld totdat het mengsel nematisch is. Dan wordt een deel van het opgeloste CO_2 als een gas gescheiden. Het belangrijkste voordeel van het afvangen van CO_2 met een proces dat gebruik maakt van vloeibare kristallen als oplosmiddel voor CO_2 , is dat dit proces isobaar is. Voor de conventionele processen die onder verhoogde druk werken is dit niet het geval, en is verlaging van de druk nodig om het oplosmiddel te regenereren. De vloeibare kristallen kunnen worden geregenereerd door de temperatuur een paar graden Kelvin te verhogen, waardoor er opnieuw een isotrope vloeistof ontstaat. Voor een conventioneel CO_2 -afvang proces dat plaatsvindt na de verbranding, zoals een amine-proces, is een hoge regeneratietemperatuur vereist om de CO_2 uit het oplosmiddel te verwijderen.

Om een proces te ontwerpen voor het toepassen van vloeibare kristallen als oplosmiddel voor het afvangen van CO_2 zijn gegevens nodig over het fasengedrag van deze systemen. In de literatuur is nog weinig data bekend over binaire systemen van CO_2 met een vloeibaar kristal. Dit proefschrift richt zich op

experimentele data op het gebied van thermodynamische fasenevenwichten. Voor de metingen in dit proefschrift is gebruik gemaakt van de zogenaamde Cailletet-apparatuur. Deze apparatuur is van het synthetisch-visuele type. Met dit apparaat kunnen P,T -fasenevenwichten van mengsels gemeten worden met een vooraf bepaalde hoeveelheid van het vloeibaar kristal en het gedoseerde gas (G). Middels deze metingen kan het fasendiagram van dit soort systemen bestudeerd worden.

Allereerst is de invloed van de moleculaire structuur van vloeibare kristallen op de oplosbaarheid van CO_2 bestudeerd (Hoofdstuk 3). De bestudeerde parameters voor de oplosbaarheid van CO_2 waren de invloed van de lengte van de zijgroep van het vloeibare kristal en de polariteit van deze zijgroep. Voor een eerste screening is 5 massaprocent CO_2 gebruikt. Het vergelijken van de verkregen P,T -fasendiagrammen leidde tot de conclusie dat de molaire oplosbaarheid van CO_2 wel hoger wordt als er een langere zijgroep gebruikt wordt, maar de oplosbaarheid gebaseerd op het gewicht niet. De polariteit heeft geen eenduidige invloed op de oplosbaarheid van CO_2 . Het lijkt erop dat apolaire en sterk polaire vloeibare kristallen zoals 4-ethyl-4'-propyl-bifenyl en 4'-pentyloxy-4-cyanobifenyl een lagere oplosbaarheid van CO_2 hebben dan 4'-penty-4-cyanobifenyl.

Een van de hiervoor genoemde vloeibare kristallen, 4'-pentyloxy-4-cyanobifenyl, is uitgebreider bestudeerd (Hoofdstuk 4). Het fasengedrag van het systeem 4'-pentyloxy-4-cyanobifenyl + CO_2 is bestudeerd tot een CO_2 molfractie van 0.72 in het temperatuurbereik van 280 tot 360 K, en drukken tot 12 MPa. Voor dit vloeibare kristal zijn twee vaste stoffen gevonden, S_1 en S_2 , waarvan S_1 metastabiël is. Ook treedt er vloeistof-vloeistof ontmenging op bij hoge CO_2 concentratie. In het binaire systeem zijn drie quadrupelpunten gevonden: $S_1S_2\text{IG}$, $S_2\text{NIG}$ en $S_2\text{I}_1\text{I}_2\text{G}$. De relatie tussen de fugaciteit en de gemeten oplosbaarheid van CO_2 is lineair. Dit leidt tot de conclusie dat de Henry coëfficiënt bepaald kan worden door een eindige concentratie te gebruiken. Deze methode is vervolgens gebruikt om de Henry coëfficiënten van een aantal vloeibare kristallen te bepalen bij een concentratie van één gewichtsprocent CO_2 (Hoofdstuk 5). De metingen bevestigen de eerste resultaten, namelijk dat vloeibare kristallen met een benzeenring, maar zonder zuurstofatoom in de zijgroep, een hogere oplosbaarheid hebben.

Geen van de bestudeerde vloeibare kristallen was goed genoeg voor commercialisatie van het voorgestelde CO_2 afvang proces. Van de bestudeerde vloeibare kristallen was óf de oplosbaarheid te laag, óf het temperatuurbereik

van de nematische fase te klein. Dit laatste geeft problemen doordat het verschil in oplosbaarheid evenredig is met het temperatuurbereik van de nematische fase. Daarom zijn ternaire systemen onderzocht, bestaande uit een mengsel van twee vloeibare kristallen met CO₂ (Hoofdstuk 6). Deze zijn vergeleken met de bijbehorende binaire systemen. De overgangstemperatuur van de vaste naar de nematische fase van ternaire systemen is lager dan van binaire systemen. Dit is niet het geval voor de nematisch-isotrope fasenovergangstemperatuur. Dit leidt ertoe dat het temperatuurbereik van de nematische fase voor mengsels van vloeibare kristallen groter is. Twee verschillende ternaire systemen zijn bestudeerd: 4'-pentyloxy-4'-cyanobifenyl + 4'-heptyloxy-4'-cyanobifenyl + CO₂ en 4'-propylcyclohexyl-4-benzonitril + 4'-heptylcyclohexyl-4-benzonitril. Van deze twee mengsels is de laatste het meest veelbelovend, aangezien de oplosbaarheid en het verschil in oplosbaarheid tussen de isotrope en nematische fase het grootste is. Vanwege de verlaging van de overgangstemperatuur van de vaste fase naar de nematische fase is het quadrupelpunt lager in vergelijking met het binaire mengsel. Daarnaast is het mogelijk om de verhouding van de vloeibare kristallen zodanig te kiezen dat het mengsel vloeibaar is bij kamertemperatuur. Hierdoor wordt het gebruik van het mengsel in het proces eenvoudiger. Helaas is het oplosbaarheidsverschil tussen de isotrope en nematische fase van het mengsel niet voldoende om een proces te ontwerpen dat kan concurreren met de reeds toegepaste methodes. Verder zijn de kosten voor vloeibare kristallen op dit moment hoog in vergelijking met commerciële oplosmiddelen.

Het laatste gedeelte van het proefschrift beschrijft een studie naar de oplosbaarheid van methaan in vloeibare kristallen (Hoofdstuk 7). De belangrijkste reden om de oplosbaarheid van methaan te meten was dat dit de mogelijkheid gaf om de ideale selectiviteit te berekenen tussen CO₂ en een ander gas. De oplosbaarheid van methaan in vloeibare kristallen is nog niet eerder onderzocht in de literatuur. Zoals verwacht is de oplosbaarheid van methaan in vloeibare kristallen lager dan van CO₂. De mate van polariteit heeft duidelijk invloed op de oplosbaarheid van methaan: hoe polairder het vloeibare kristal is, des te lager de oplosbaarheid. CO₂ is het beste oplosbaar in het vloeibaar kristal 4-ethyl-4'-propylbicyclohexyl.

Curriculum Vitae

Name: Mariëtte de Groen

Date of birth: 26-05-1986

Place of birth: Voorburg

Education:

2010-2015 PhD, TU Delft

2007-2010 Master Chemical Engineering, TU Delft

2004-2009 Bachelor Scheikundige Technologie en Bioprocestechnologie,
TU Delft

1998-2004 VWO (Gymnasium), Driestar College, Gouda

Published work

M. de Groen, O. Mesalles Molet, T.J.H. Vlugt, T.W. de Loos, *Phase behaviour of binary mixtures of a liquid crystal and methane*, submitted to Journal of Chemical Engineering Data.

M. de Groen, T.J.H. Vlugt, T.W. de Loos, *Binary and ternary mixtures of liquid crystals with CO₂*, submitted to AIChE journal.

M. de Groen, B.C. Ramaker, T.J.H. Vlugt, T.W. de Loos, *Phase Behavior of Liquid Crystal + CO₂ Mixtures*, Journal of Chemical and Engineering Data, 59 (2014) 1667-1672.

M. de Groen, H. Matsuda, T.J.H. Vlugt, T.W. de Loos, *Phase behaviour of the system 4'-pentyloxy-4-cyanobiphenyl + CO₂*, Journal of Chemical Thermodynamics, 59 (2013) 20-27.

M. de Groen, T.J.H. Vlugt, T.W. de Loos, *Phase Behavior of Liquid Crystals with CO₂*, Journal of Physical Chemistry B, 116 (2012) 9101-9106.

Acknowledgement

At the end of my PhD thesis, I would like to take the opportunity to look back at the whole process, especially at the support I got from everyone around me. I am very grateful that the number of persons who helped me is far larger than I can possibly thank in this chapter. A few persons I would like to name in person.

First of all, I would like to thank my promotor and co-promotor, Thijs Vlugt and Theo de Loos. Theo, you were most special to me of all persons I worked with. You did not only teach me performing research, writing articles and applying phase theory, but you took care of teaching me lessons worthy for my future life and career as well. Thijs, you were the best promotor I could wish for. You challenged me continuously and it is remarkable for me how fast you gave your comments back. You both helped me when I needed motivation and support.

This research is supported by the Dutch Technology Foundation STW, applied science division of NWO and the Technology Program of the Ministry of Economic Affairs. I would like to thank STW and the user committee for the financial support and discussions.

Without the thermolab, my research would not have been possible. I would like to thank all my peers, too many to mention here, for fruitful discussions. Especially Eugène Straver, our research technician and lab supervisor, who taught me all ins and outs of both the equipment (especially the gasrek!) and the CO₂-liquid crystal systems. I would like to thank my co-worker Dr. Matsuda, and my master students Oriol, Bo, and Olcay for all research for the project. Mahinder, thanks for all the help and fruitful discussions. And last but not least, Mayte, thanks for being a great friend and peer.

When having a job as PhD, your fellow researchers are of great importance. Bernardo and Thijs vW, thank you for the discussions and new insights from the simulations and modeling. Furthermore, I would like to thank all my officemates, especially Dennis and Julia, for all support. Wim and Rob, your personal support was beyond helpful.

Of course, the support I got from everyone outside university was of great importance too. Familie van der Struif, I would like to thank you from the bottom of my heart for all help you gave me. And Bas de Vroome, your insights and personal support gave me new strength for my research. At last, I would like to thank my parents and André, Berdien and William. Your support was so special that I am not able to express it in words. Without your help I would not have been able to finish my thesis.

Appendix A. Experimental data of Chapter 3

Table A.1. P, T data of measured phase equilibria of 4-ethyl-4'-propyl-bicyclohexyl with CO_2 , $w_{\text{CO}_2} = 0.050$. I denotes the isotropic, G the gas phase and Sm the smectic phase. The uncertainties of temperature and pressure are denoted by $u(T)$ and $u(P)$, respectively.

T / K	P / MPa	Phase boundary
328.49	3.324	$(I + G) \leftrightarrow I^a$
333.54	3.459	$(I + G) \leftrightarrow I^a$
338.55	3.594	$(I + G) \leftrightarrow I^a$
343.62	3.729	$(I + G) \leftrightarrow I^a$
348.49	3.859	$(I + G) \leftrightarrow I^a$
353.54	3.989	$(I + G) \leftrightarrow I^a$
320.34	3.127	$(I + G) \leftrightarrow I^a$
324.48	3.238	$(I + G) \leftrightarrow I^a$
328.56	1.838	$(Sm + I + G)^b$
330.13	1.593	$(Sm + I + G)^b$
331.5	1.379	$(Sm + I + G)^b$
332.55	1.214	$(Sm + I + G)^b$
333.49	1.065	$(Sm + I + G)^b$
334.57	0.881	$(Sm + I + G)^b$
336.04	0.634	$(Sm + I + G)^b$
326.44	2.152	$(Sm + I + G)^b$
324.02	2.502	$(Sm + I + G)^b$
322.44	2.727	$(Sm + I + G)^b$
320.34	3.007	$(Sm + I + G)^b$
319.78	3.558	$(Sm + I) \leftrightarrow I^b$
319.88	4.059	$(Sm + I) \leftrightarrow I^b$
320.34	5.060	$(Sm + I) \leftrightarrow I^b$
320.78	6.060	$(Sm + I) \leftrightarrow I^b$
321.1	7.061	$(Sm + I) \leftrightarrow I^b$
321.55	8.561	$(Sm + I) \leftrightarrow I^b$
322.09	9.562	$(Sm + I) \leftrightarrow I^b$

^a: $u(P) = 0.005 \text{ MPa}$, $u(T) = 0.01 \text{ K}$ ^b: $u(P) = 0.005 \text{ MPa}$, $u(T) = 0.05 \text{ K}$

Table A.2. P, T data of measured phase equilibria of 4-propyl-4'-butyl-bicyclohexyl with CO_2 , $w_{\text{CO}_2} = 0.050$. I denotes the isotropic, G the gas phase and Sm the smectic phase. The uncertainties of temperature and pressure are denoted by $u(T)$ and $u(P)$, respectively.

T / K	P / MPa	Phase boundary
363.47	4.582	$(I + G) \leftrightarrow I^a$
362.24	4.556	$(I + G) \leftrightarrow I^a$
360.06	4.491	$(I + G) \leftrightarrow I^a$
356.45	4.401	$(I + G) \leftrightarrow I^a$
353.9	4.341	$(I + G) \leftrightarrow I^a$
358.28	4.452	$(I + G) \leftrightarrow I^a$
351.49	4.282	$(I + G) \leftrightarrow I^a$
349.70	4.242	$(I + G) \leftrightarrow I^a$
352.11	3.666	$(Sm + I + G)^b$
352.50	3.586	$(Sm + I + G)^b$
353.07	3.466	$(Sm + I + G)^b$
354.12	3.236	$(Sm + I + G)^b$
356.11	2.801	$(Sm + I + G)^b$
358.26	2.331	$(Sm + I + G)^b$
360.51	1.826	$(Sm + I + G)^b$
362.23	1.432	$(Sm + I + G)^b$
351.49	3.782	$(Sm + I + G)^b$
349.70	4.157	$(Sm + I + G)^b$
364.67	0.857	$(Sm + I + G)^b$
365.49	0.659	$(Sm + I + G)^b$
349.91	5.563	$(Sm + I) \leftrightarrow I^b$
350.59	7.064	$(Sm + I) \leftrightarrow I^b$
351.01	8.065	$(Sm + I) \leftrightarrow I^b$
351.45	9.066	$(Sm + I) \leftrightarrow I^b$
351.87	10.066	$(Sm + I) \leftrightarrow I^b$
350.15	6.064	$(Sm + I) \leftrightarrow I^b$
350.37	6.564	$(Sm + I) \leftrightarrow I^b$
349.72	5.064	$(Sm + I) \leftrightarrow I^b$
349.47	4.414	$(Sm + I) \leftrightarrow I^b$
^a : $u(P) = 0.005 \text{ MPa}$, $u(T) = 0.01 \text{ K}$ ^b : $u(P) = 0.005 \text{ MPa}$, $u(T) = 0.05 \text{ K}$		

Table A.3. P, T data of measured phase equilibria of 4-propyl-4'-butyl-bicyclohexyl with CO_2 , $w_{\text{CO}_2} = 0.050$. I denotes the isotropic, G the gas phase, N the nematic phase and Sm the smectic phase. The uncertainties of temperature and pressure are denoted by $u(T)$ and $u(P)$, respectively.

T / K	P / MPa	Phase boundary	T / K	P / MPa	Phase boundary
333.98	3.666	(I + G) to I ^a	332.87	3.762	(N + I + G) ^a
337.42	3.751	(I + G) to I ^a	332.97	3.742	(N + I + G) ^a
341.71	3.867	(I + G) to I ^a	333.19	3.712	(N + I + G) ^a
345.59	3.977	(I + G) to I ^a	333.59	3.647	(N + I + G) ^a
350.23	4.128	(I + G) to I ^a	334.28	3.537	(N + I + G) ^a
335.35	3.692	(I + G) to I ^a	335.18	3.392	(N + I + G) ^a
333.59	3.662	(I + G) to I ^a	336.08	3.247	(N + I + G) ^a
333.57	3.912	(N + I) to I ^a	337.47	3.017	(N + I + G) ^a
333.94	5.163	(N + I) to I ^a	339.14	2.737	(N + I + G) ^a
334.30	6.414	(N + I) to I ^a	341.32	2.357	(N + I + G) ^a
335.01	8.915	(N + I) to I ^a	327.59	3.912	(Sm + I) to I ^b
334.72	7.915	(N + I) to I ^a	327.80	4.913	(Sm + I) to I ^b
335.44	10.416	(N + I) to I ^a	327.95	5.914	(Sm + I) to I ^b
332.82	3.913	N to (N + I) ^a	328.13	6.914	(Sm + I) to I ^b
333.10	4.913	N to (N + I) ^a	328.32	7.914	(Sm + I) to I ^b
333.42	5.914	N to (N + I) ^a	328.50	8.915	(Sm + I) to I ^b
333.70	6.915	N to (N + I) ^a	327.67	3.802	(Sm + N + G) ^b
333.99	7.915	N to (N + I) ^a	328.07	3.702	(Sm + N + G) ^b
334.30	8.916	N to (N + I) ^a	329.07	3.467	(Sm + N + G) ^b
334.59	9.916	N to (N + I) ^a	330.44	3.117	(Sm + N + G) ^b
332.13	3.802	(N + G) to N ^a	331.72	2.787	(Sm + N + G) ^b
331.49	3.812	(N + G) to N ^a	333.22	2.442	(Sm + N + G) ^b
330.19	3.812	(N + G) to N ^a	334.08	2.187	(Sm + N + G) ^b
328.08	3.812	(N + G) to N ^a			
332.57	3.787	(N + G) to N ^a			

^a: $u(P) = 0.005 \text{ MPa}$, $u(T) = 0.01 \text{ K}$ ^b: $u(P) = 0.005 \text{ MPa}$, $u(T) = 0.05 \text{ K}$

Table A.4. P, T data of measured phase equilibria of 4-propyl-4'-butyl-bicyclohexyl with CO_2 , $w_{\text{CO}_2} = 0.050$. I denotes the isotropic, G the gas phase, N the nematic phase, and S the solid phase. The uncertainties of temperature and pressure are denoted by $u(T)$ and $u(P)$, respectively.

T / K	P / MPa	Phase boundary	T / K	P / MPa	Phase boundary
318.19	3.017	(I + G) to I ^a	313.50	3.055	(S ₂ + N) to N ^b
323.10	3.177	(I + G) to I ^a	314.64	6.908	(S ₂ + N) to N ^b
328.06	3.353	(I + G) to I ^a	315.30	9.410	(S ₂ + N) to N ^b
333.06	3.534	(I + G) to I ^a	314.05	4.905	(S ₂ + N) to N ^b
338.07	3.716	(I + G) to I ^a	315.63	2.155	(S ₂ + N) to N ^b
343.11	3.904	(I + G) to I ^a	316.31	1.905	(S ₂ + N) to N ^b
348.16	4.088	(I + G) to I ^a	316.93	1.655	(S ₂ + N) to N ^b
352.98	4.274	(I + G) to I ^a	317.52	1.406	(S ₂ + N) to N ^b
357.92	4.452	(I + G) to I ^a	315.05	2.404	(S ₂ + N) to N ^b
362.96	4.635	(I + G) to I ^a	317.65	1.331	(S ₂ + N) to N ^b
367.97	4.817	(I + G) to I ^a	314.25	2.780	(S ₂ + N) to N ^b
318.18	3.020	(I + G) to I ^a	314.55	2.657	(S ₂ + N) to N ^b
323.15	3.184	(I + G) to I ^a	321.60	1.157	(S ₁ + N + G) ^b
316.55	3.005	(N + I) to I ^a	322.82	0.908	(S ₁ + N + G) ^b
317.53	5.907	(N + I) to I ^a	323.93	0.661	(S ₁ + N + G) ^b
318.55	8.909	(N + I) to I ^a	318.57	1.806	(S ₁ + N + G) ^b
316.15	3.105	(N + I) to I ^a	319.38	1.658	(S ₁ + N + G) ^b
316.60	4.406	(N + I) to I ^a	317.31	2.057	(S ₁ + N + G) ^b
317.10	5.907	(N + I) to I ^a	315.87	2.307	(S ₁ + N + G) ^b
317.56	7.207	(N + I) to I ^a	312.50	3.351	(S ₂ + I + G) ^b
318.10	8.908	(N + I) to I ^a	313.25	4.905	(S ₂ + I + G) ^b
315.62	3.020	(N + I) to N ^a	313.53	5.906	(S ₂ + I + G) ^b
313.14	2.979	(N + I) to N ^a	313.80	6.907	(S ₂ + I + G) ^b
314.10	3.003	(N + I) to N ^a	314.09	7.908	(S ₂ + I + G) ^b
316.76	2.960	(N + I + G) ^a	314.36	8.909	(S ₂ + I + G) ^b
317.14	2.925	(N + I + G) ^a			
321.11	2.540	(N + I + G) ^a			
325.92	2.025	(N + I + G) ^a			
330.21	1.516	(N + I + G) ^a			
333.18	1.132	(N + I + G) ^a			

^a: $u(P) = 0.005 \text{ MPa}$, $u(T) = 0.01 \text{ K}$ ^b: $u(P) = 0.005 \text{ MPa}$, $u(T) = 0.05 \text{ K}$

Table A.5. P, T data of measured phase equilibria of 4-propyl-4'-butyl-bicyclohexyl with CO_2 , $w_{\text{CO}_2} = 0.050$. I denotes the isotropic, G the gas phase, N the nematic phase, and S the solid phase. The uncertainties of temperature and pressure are denoted by $u(T)$ and $u(P)$, respectively.

T / K	P / MPa	Phase boundary	T / K	P / MPa	Phase boundary
313.47	2.431	(I + G) to I ^a	284.58	1.578	(N + I + G) ^a
318.54	2.591	(I + G) to I ^a	283.35	1.614	(N + I + G) ^a
323.49	2.751	(I + G) to I ^a	283.69	1.604	(N + I + G) ^a
328.57	2.921	(I + G) to I ^a	284.03	1.594	(N + I + G) ^a
335.31	3.156	(I + G) to I ^a	284.38	1.569	(N + I + G) ^a
298.53	1.983	(I + G) to I ^a	285.36	1.549	(N + I + G) ^a
303.42	2.118	(I + G) to I ^a	286.53	1.504	(N + I + G) ^a
308.42	2.268	(I + G) to I ^a	287.74	1.454	(N + I + G) ^a
293.51	1.827	(I + G) to I ^a	288.81	1.404	(N + I + G) ^a
288.40	1.687	(I + G) to I ^a	289.90	1.354	(N + I + G) ^a
284.58	1.588	(I + G) to I ^a	291.21	1.290	(N + I + G) ^a
286.45	1.639	(I + G) to I ^a	292.49	1.220	(N + I + G) ^a
284.32	1.647	(N + I) to I ^a	294.05	1.125	(N + I + G) ^a
284.77	2.898	(N + I) to I ^a	286.67	1.899	(S + I) to I ^b
285.31	4.399	(N + I) to I ^a	287.34	3.900	(S + I) to I ^b
285.84	5.900	(N + I) to I ^a	288.34	7.402	(S + I) to I ^b
286.37	7.401	(N + I) to I ^a	289.16	10.404	(S + I) to I ^b
287.09	9.402	(N + I) to I ^a	286.88	1.624	(S + I + G) ^b
283.29	1.799	(N + I) to N ^a	287.55	1.514	(S + I + G) ^b
283.70	2.900	(N + I) to N ^a	286.35	1.699	(S + I + G) ^b
284.11	4.150	(N + I) to N ^a	286.04	1.739	(S + I + G) ^b
284.49	5.402	(N + I) to N ^a	285.40	1.809	(S + I + G) ^b
284.93	6.652	(N + I) to N ^a	284.95	1.854	(S + I + G) ^b
285.52	8.153	(N + I) to N ^a	283.60	1.999	(S + I + G) ^b
279.65	1.578	(N + G) to N ^a	288.63	1.398	(S + N + G) ^b
281.80	1.613	(N + G) to N ^a	290.09	1.150	(S + N + G) ^b
283.00	1.619	(N + G) to N ^a	289.16	1.300	(S + N + G) ^b
280.92	1.599	(N + G) to N ^a	289.65	1.225	(S + N + G) ^b
278.93	1.559	(N + G) to N ^a	290.55	1.075	(S + N + G) ^b
277.62	1.539	(N + G) to N ^a	291.02	1.001	(S + N + G) ^b
276.13	1.509	(N + G) to N ^a	292.61	0.728	(S + N + G) ^b
274.66	1.474	(N + G) to N ^a	291.71	0.877	(S + N + G) ^b

^a: $u(P) = 0.005 \text{ MPa}$, $u(T) = 0.01 \text{ K}$ ^b: $u(P) = 0.005 \text{ MPa}$, $u(T) = 0.05 \text{ K}$

Appendix B. Experimental data of Chapter 4

Table B.1. Experimental data for pure 5OCB at temperature T and pressure P . S_1 denotes the solid phase, N the nematic phase and I_2 the isotropic liquid. The uncertainties of temperature and pressure are denoted by $u(T)$ and $u(P)$, respectively.

T / K	P / MPa	Phase boundary
326.84	0.399	$S_1 \leftrightarrow N^a$
327.21	1.399	$S_1 \leftrightarrow N^a$
328.20	4.401	$S_1 \leftrightarrow N^a$
327.72	3.001	$S_1 \leftrightarrow N^a$
327.52	2.400	$S_1 \leftrightarrow N^a$
327.86	3.400	$S_1 \leftrightarrow N^a$
328.54	5.401	$S_1 \leftrightarrow N^a$
328.84	6.402	$S_1 \leftrightarrow N^a$
329.23	7.403	$S_1 \leftrightarrow N^a$
329.55	8.403	$S_1 \leftrightarrow N^a$
329.86	9.405	$S_1 \leftrightarrow N^a$
330.08	10.005	$S_1 \leftrightarrow N^a$
341.58	0.399	$N \leftrightarrow I_2^b$
341.96	1.399	$N \leftrightarrow I_2^b$
342.38	2.400	$N \leftrightarrow I_2^b$
342.75	3.401	$N \leftrightarrow I_2^b$
343.13	4.401	$N \leftrightarrow I_2^b$
342.91	3.901	$N \leftrightarrow I_2^b$
343.32	4.902	$N \leftrightarrow I_2^b$
343.51	5.402	$N \leftrightarrow I_2^b$
343.90	6.403	$N \leftrightarrow I_2^b$
344.30	7.404	$N \leftrightarrow I_2^b$
344.70	8.404	$N \leftrightarrow I_2^b$
345.10	9.405	$N \leftrightarrow I_2^b$
345.33	10.005	$N \leftrightarrow I_2^b$

^a: $u(T) = 0.05 \text{ K}$, $u(P) = 0.005 \text{ MPa}$
^b: $u(T) = 0.01 \text{ K}$, $u(P) = 0.005 \text{ MPa}$.

Table B.2. Experimental data for the system 5OCB (1) + CO₂ (2) for mole fraction $x_2 = 0.057$. I_2 denotes the isotropic phase, G the gas phase, S_1 the solid phase, N the nematic phase. The uncertainties of temperature and pressure are denoted by $u(T)$ and $u(P)$, respectively.^a

T / K	P / MPa	Phase boundary
344.11	0.829	$(I_2 + G) \leftrightarrow I_2^a$
348.92	0.864	$(I_2 + G) \leftrightarrow I_2^a$
354.05	0.898	$(I_2 + G) \leftrightarrow I_2^a$
358.31	0.923	$(I_2 + G) \leftrightarrow I_2^a$
364.01	0.963	$(I_2 + G) \leftrightarrow I_2^a$
338.85	0.798	$(I_2 + G) \leftrightarrow I_2^a$
336.12	0.783	$(I_2 + G) \leftrightarrow I_2^a$
335.22	0.800	$(N + G) \leftrightarrow N^a$
330.24	0.790	$(N + G) \leftrightarrow N^a$
325.30	0.764	$(N + G) \leftrightarrow N^a$
320.27	0.729	$(N + G) \leftrightarrow N^a$
324.06	2.905	$(S_1 + N) \leftrightarrow N^b$
324.66	4.906	$(S_1 + N) \leftrightarrow N^b$
325.46	6.909	$(S_1 + N) \leftrightarrow N^b$
326.16	8.911	$(S_1 + N) \leftrightarrow N^b$
335.86	0.904	$N \leftrightarrow (N + I_2)^c$
336.63	2.905	$N \leftrightarrow (N + I_2)^c$
337.39	4.906	$N \leftrightarrow (N + I_2)^c$
338.17	6.908	$N \leftrightarrow (N + I_2)^c$
338.94	8.909	$N \leftrightarrow (N + I_2)^c$
339.72	10.910	$N \leftrightarrow (N + I_2)^c$
335.98	0.903	$(N + I_2) \leftrightarrow I_2^a$
336.75	2.904	$(N + I_2) \leftrightarrow I_2^a$
337.52	4.906	$(N + I_2) \leftrightarrow I_2^a$
338.29	6.908	$(N + I_2) \leftrightarrow I_2^a$
339.06	8.909	$(N + I_2) \leftrightarrow I_2^a$
339.82	10.910	$(N + I_2) \leftrightarrow I_2^a$
^a : $u(T) = 0.01 \text{ K}$, $u(P) = 0.005 \text{ MPa}$		
^b : $u(T) = 0.05 \text{ K}$, $u(P) = 0.005 \text{ MPa}$		
^c : $u(T) = 0.02 \text{ K}$, $u(P) = 0.005 \text{ MPa}$		

Table B.3. Experimental data for the system 5OCB (1) + CO₂ (2) for mole fraction $x_2 = 0.159$. I_2 denotes the isotropic phase, G the gas phase, S_1 the solid phase, N the nematic phase. The uncertainties of temperature and pressure are denoted by $u(T)$ and $u(P)$, respectively.^a

T / K	P / MPa	Phase boundary	T / K	P / MPa	Phase boundary
328.26	2.066	$(I_2 + G) \leftrightarrow I_2^b$	325.97	2.033	$(N + I_2 + G)^b$
338.25	2.283	$(I_2 + G) \leftrightarrow I_2^b$	325.86	2.046	$(N + I_2 + G)^b$
358.24	2.717	$(I_2 + G) \leftrightarrow I_2^b$	325.76	2.069	$(N + I_2 + G)^b$
368.31	2.932	$(I_2 + G) \leftrightarrow I_2^b$	330.51	1.523	$(N + I_2 + G)^b$
326.97	2.039	$(I_2 + G) \leftrightarrow I_2^b$	331.33	1.403	$(N + I_2 + G)^b$
326.88	2.039	$(I_2 + G) \leftrightarrow I_2^b$	331.02	1.453	$(N + I_2 + G)^b$
326.24	2.031	$(I_2 + G) \leftrightarrow I_2^b$	330.58	1.503	$(N + I_2 + G)^b$
323.23	2.061	$(N + G) \leftrightarrow N^b$	330.14	1.553	$(N + I_2 + G)^b$
321.25	2.036	$(N + G) \leftrightarrow N^b$	329.74	1.603	$(N + I_2 + G)^b$
322.26	2.044	$(N + G) \leftrightarrow N^b$	328.93	1.702	$(N + I_2 + G)^b$
320.18	2.014	$(N + G) \leftrightarrow N^b$	328.13	1.802	$(N + I_2 + G)^b$
319.22	2.000	$(N + G) \leftrightarrow N^b$	327.30	1.902	$(N + I_2 + G)^b$
318.25	1.984	$(N + G) \leftrightarrow N^b$	326.47	2.002	$(N + I_2 + G)^b$
317.23	1.963	$(N + G) \leftrightarrow N^b$	326.08	2.050	$(N + I_2 + G)^b$
316.24	1.949	$(N + G) \leftrightarrow N^b$	326.73	1.950	$(N + I_2 + G)^b$
315.25	1.929	$(N + G) \leftrightarrow N^b$	327.72	1.851	$(N + I_2 + G)^b$
325.23	2.069	$(N + G) \leftrightarrow N^b$	328.48	1.751	$(N + I_2 + G)^b$
324.25	2.066	$(N + G) \leftrightarrow N^b$	329.33	1.651	$(N + I_2 + G)^b$
313.17	1.891	$(N + G) \leftrightarrow N^b$	316.58	2.401	$(S_1 + N) \leftrightarrow N^d$
325.78	2.151	$N \leftrightarrow (N + I_2)^c$	316.80	2.902	$(S_1 + N) \leftrightarrow N^d$
325.89	2.402	$N \leftrightarrow (N + I_2)^c$	317.13	3.902	$(S_1 + N) \leftrightarrow N^d$
325.98	2.652	$N \leftrightarrow (N + I_2)^c$	316.69	2.652	$(S_1 + N) \leftrightarrow N^d$
326.09	2.902	$N \leftrightarrow (N + I_2)^c$	316.92	3.152	$(S_1 + N) \leftrightarrow N^d$
326.18	3.152	$N \leftrightarrow (N + I_2)^c$	316.97	3.402	$(S_1 + N) \leftrightarrow N^d$
326.27	3.402	$N \leftrightarrow (N + I_2)^c$	317.02	3.652	$(S_1 + N) \leftrightarrow N^d$
326.36	3.652	$N \leftrightarrow (N + I_2)^c$	316.47	2.101	$(S_1 + N) \leftrightarrow N^d$
326.51	3.652	$(N + I_2) \leftrightarrow I_2^c$	316.43	2.051	$(S_1 + N) \leftrightarrow N^d$
326.42	3.402	$(N + I_2) \leftrightarrow I_2^c$	316.53	2.251	$(S_1 + N) \leftrightarrow N^d$
326.32	3.152	$(N + I_2) \leftrightarrow I_2^c$			
326.23	2.902	$(N + I_2) \leftrightarrow I_2^c$			
326.13	2.652	$(N + I_2) \leftrightarrow I_2^c$			
326.06	2.402	$(N + I_2) \leftrightarrow I_2^c$			
325.96	2.152	$(N + I_2) \leftrightarrow I_2^c$			

^a: $u(P) = 0.005 \text{ MPa}$, ^b: $u(T) = 0.01 \text{ K}$, ^c: $u(T) = 0.02 \text{ K}$, ^d: $u(T) = 0.05 \text{ K}$

Table B.4. Experimental data for the system 5OCB (1) + CO₂ (2) for mole fraction $x_2 = 0.241$, reproduced from Chapter 3. I_2 denotes the isotropic phase, G the gas phase, S_1 and S_2 solid phases, N the nematic phase. The uncertainties of temperature and pressure are denoted by $u(T)$ and $u(P)$, respectively.^a

T / K	P / MPa	Phase boundary	T / K	P / MPa	Phase boundary
318.43	3.017	$(I_2 + G) \leftrightarrow I_2^b$	315.86	3.020	$(N + G) \leftrightarrow N^b$
323.34	3.177	$(I_2 + G) \leftrightarrow I_2^b$	313.38	2.979	$(N + G) \leftrightarrow N^b$
328.30	3.353	$(I_2 + G) \leftrightarrow I_2^b$	314.34	3.003	$(N + G) \leftrightarrow N^b$
333.30	3.534	$(I_2 + G) \leftrightarrow I_2^b$	313.74	3.055	$(S_2 + N) \leftrightarrow N^d$
338.30	3.716	$(I_2 + G) \leftrightarrow I_2^b$	314.89	6.908	$(S_2 + N) \leftrightarrow N^d$
343.35	3.904	$(I_2 + G) \leftrightarrow I_2^b$	315.55	9.410	$(S_2 + N) \leftrightarrow N^d$
348.39	4.088	$(I_2 + G) \leftrightarrow I_2^b$	314.30	4.905	$(S_2 + N) \leftrightarrow N^d$
353.21	4.274	$(I_2 + G) \leftrightarrow I_2^b$	315.87	2.155	$(S_2 + N + G)^d$
358.16	4.452	$(I_2 + G) \leftrightarrow I_2^b$	316.55	1.905	$(S_2 + N + G)^d$
363.21	4.635	$(I_2 + G) \leftrightarrow I_2^b$	317.18	1.655	$(S_2 + N + G)^d$
368.22	4.817	$(I_2 + G) \leftrightarrow I_2^b$	317.77	1.406	$(S_2 + N + G)^d$
318.43	3.020	$(I_2 + G) \leftrightarrow I_2^b$	315.29	2.404	$(S_2 + N + G)^d$
323.39	3.184	$(I_2 + G) \leftrightarrow I_2^b$	317.89	1.331	$(S_2 + N + G)^d$
316.79	3.005	$(N + I_2) \leftrightarrow I_2^b$	321.84	1.157	$(S_1 + N + G)^d$
317.78	5.907	$(N + I_2) \leftrightarrow I_2^b$	323.06	0.908	$(S_1 + N + G)^d$
318.79	8.909	$(N + I_2) \leftrightarrow I_2^b$	324.17	0.661	$(S_1 + N + G)^d$
316.39	3.105	$N \leftrightarrow (N + I_2)^c$	318.57	1.806	$(S_1 + N + G)^d$
316.85	4.406	$N \leftrightarrow (N + I_2)^c$	319.38	1.658	$(S_1 + N + G)^d$
317.34	5.907	$N \leftrightarrow (N + I_2)^c$	317.31	2.057	$(S_1 + N + G)^d$
317.80	7.207	$N \leftrightarrow (N + I_2)^c$	315.87	2.307	$(S_1 + N + G)^d$
318.34	8.908	$N \leftrightarrow (N + I_2)^c$	312.50	3.351	$(S_2 + I_2 + G)^d$
317.00	2.960	$(N + I_2 + G)^b$	313.49	4.905	$(S_2 + N + I_2)^e$
317.38	2.925	$(N + I_2 + G)^b$	313.78	4.905	$(S_2 + N + I_2)^e$
321.35	2.540	$(N + I_2 + G)^b$	314.04	4.905	$(S_2 + N + I_2)^e$
326.16	2.025	$(N + I_2 + G)^b$	314.33	4.905	$(S_2 + N + I_2)^e$
330.44	1.516	$(N + I_2 + G)^b$	314.60	4.905	$(S_2 + N + I_2)^e$
333.41	1.132	$(N + I_2 + G)^b$			

^a: $u(P) = 0.005 \text{ MPa}$, ^b: $u(T) = 0.01 \text{ K}$, ^c: $u(T) = 0.02 \text{ K}$, ^d: $u(T) = 0.05 \text{ K}$, ^e: $u(T) = 0.1 \text{ K}$

Table B.5. Experimental data for the system 5OCB (1) + CO₂ (2) for mole fraction $x_2 = 0.329$. I_2 denotes the isotropic phase, G the gas phase, S_2 the solid phase, N the nematic phase. The uncertainties of temperature and pressure are denoted by $u(T)$ and $u(P)$, respectively.^a

T / K	P / MPa	Phase boundary	T / K	P / MPa	Phase boundary
323.45	4.522	$(I_2 + G) \leftrightarrow I_2^b$	305.44	3.642	$(N + I_2 + G)^b$
328.40	4.794	$(I_2 + G) \leftrightarrow I_2^b$	305.53	3.636	$(N + I_2 + G)^b$
333.47	5.086	$(I_2 + G) \leftrightarrow I_2^b$	305.64	3.629	$(N + I_2 + G)^b$
343.38	5.649	$(I_2 + G) \leftrightarrow I_2^b$	305.77	3.624	$(N + I_2 + G)^b$
348.49	5.940	$(I_2 + G) \leftrightarrow I_2^b$	323.42	2.313	$(N + I_2 + G)^b$
353.47	6.225	$(I_2 + G) \leftrightarrow I_2^b$	321.42	2.507	$(N + I_2 + G)^b$
358.42	6.503	$(I_2 + G) \leftrightarrow I_2^b$	319.38	2.703	$(N + I_2 + G)^b$
338.44	5.365	$(I_2 + G) \leftrightarrow I_2^b$	318.39	2.787	$(N + I_2 + G)^b$
363.45	6.788	$(I_2 + G) \leftrightarrow I_2^b$	317.51	2.863	$(N + I_2 + G)^b$
368.37	7.071	$(I_2 + G) \leftrightarrow I_2^b$	315.48	3.027	$(N + I_2 + G)^b$
318.55	4.260	$(I_2 + G) \leftrightarrow I_2^b$	313.36	3.182	$(N + I_2 + G)^b$
313.49	3.994	$(I_2 + G) \leftrightarrow I_2^b$	311.24	3.322	$(N + I_2 + G)^b$
308.50	3.734	$(I_2 + G) \leftrightarrow I_2^b$	309.63	3.422	$(N + I_2 + G)^b$
306.02	3.626	$(I_2 + G) \leftrightarrow I_2^b$	308.61	3.466	$(N + I_2 + G)^b$
306.49	3.646	$(I_2 + G) \leftrightarrow I_2^b$	307.54	3.532	$(N + I_2 + G)^b$
303.53	3.604	$(N + G) \leftrightarrow N^b$	306.52	3.576	$(N + I_2 + G)^b$
301.46	3.588	$(N + G) \leftrightarrow N^b$	306.21	3.596	$(N + I_2 + G)^b$
297.53	3.373	$(N + G) \leftrightarrow N^b$	313.82	2.904	$(S_2 + N + G)^d$
303.53	3.604	$(N + G) \leftrightarrow N^b$	314.58	2.654	$(S_2 + N + G)^d$
305.29	3.853	$N \leftrightarrow (N + I_2)^c$	315.22	2.405	$(S_2 + N + G)^d$
306.32	6.855	$N \leftrightarrow (N + I_2)^c$	311.48	3.804	$(S_2 + I_2 + G)^d$
307.25	9.857	$N \leftrightarrow (N + I_2)^c$	311.90	3.604	$(S_2 + I_2 + G)^d$
306.77	8.407	$N \leftrightarrow (N + I_2)^c$	312.45	3.404	$(S_2 + I_2 + G)^d$
305.80	3.704	$(N + I_2) \leftrightarrow N^c$	310.55	4.053	$(S_2 + I_2 + G)^d$
306.76	6.705	$(N + I_2) \leftrightarrow N^c$	309.48	4.398	$(S_2 + I_2 + G)^d$
306.25	5.204	$(N + I_2) \leftrightarrow N^c$	308.23	4.789	$(S_2 + I_2 + G)^d$
307.44	8.907	$(N + I_2) \leftrightarrow N^c$	311.25	4.003	$(S_2 + I_2) \leftrightarrow I_2^d$
307.98	10.658	$(N + I_2) \leftrightarrow N^c$	311.47	5.004	$(S_2 + I_2) \leftrightarrow I_2^d$
			312.00	7.005	$(S_2 + I_2) \leftrightarrow I_2^d$
			312.29	8.055	$(S_2 + I_2) \leftrightarrow I_2^d$
			312.80	10.007	$(S_2 + I_2) \leftrightarrow I_2^d$
			311.74	6.005	$(S_2 + I_2) \leftrightarrow I_2^d$

^a: $u(P) = 0.005 \text{ MPa}$, ^b: $u(T) = 0.01 \text{ K}$, ^c: $u(T) = 0.02 \text{ K}$, ^d: $u(T) = 0.05 \text{ K}$

Table B.6. Experimental data for the system 5OCB (1) + CO₂ (2) for mole fraction $x_2 = 0.400$ l_2 denotes the isotropic phase, G the gas phase, S_2 the solid phase, N the nematic phase. The uncertainties of temperature and pressure are denoted by $u(T)$ and $u(P)$, respectively.

T / K	P / MPa	Phase boundary	T / K	P / MPa	Phase boundary
333.35	6.687	$(l_2 + G) \leftrightarrow l_2^a$	309.70	3.408	$(N + I + G)^a$
338.36	7.077	$(l_2 + G) \leftrightarrow l_2^a$	309.52	3.421	$(N + I + G)^a$
343.37	7.478	$(l_2 + G) \leftrightarrow l_2^a$	308.46	3.474	$(N + I + G)^a$
348.26	7.868	$(l_2 + G) \leftrightarrow l_2^a$	307.47	3.528	$(N + I + G)^a$
353.19	8.263	$(l_2 + G) \leftrightarrow l_2^a$	306.49	3.576	$(N + I + G)^a$
358.40	8.683	$(l_2 + G) \leftrightarrow l_2^a$	305.42	3.624	$(N + I + G)^a$
328.32	6.268	$(l_2 + G) \leftrightarrow l_2^a$	304.32	3.668	$(N + I + G)^a$
363.37	9.069	$(l_2 + G) \leftrightarrow l_2^a$	303.50	3.704	$(N + I + G)^a$
368.41	9.465	$(l_2 + G) \leftrightarrow l_2^a$	302.44	3.738	$(N + I + G)^a$
318.39	5.512	$(l_2 + G) \leftrightarrow l_2^a$	301.45	3.771	$(N + I + G)^a$
313.46	5.128	$(l_2 + G) \leftrightarrow l_2^a$	300.51	3.798	$(N + I + G)^a$
308.44	4.761	$(l_2 + G) \leftrightarrow l_2^a$	299.43	3.823	$(N + I + G)^a$
303.47	4.404	$(l_2 + G) \leftrightarrow l_2^a$	298.44	3.845	$(N + I + G)^a$
323.38	5.879	$(l_2 + G) \leftrightarrow l_2^a$	297.50	3.863	$(N + I + G)^a$
296.52	3.940	$(l_2 + G) \leftrightarrow l_2^a$	313.43	3.171	$(N + I + G)^a$
295.75	3.895	$(l_2 + G) \leftrightarrow l_2^a$	311.49	3.300	$(N + I + G)^a$
298.52	4.091	$(l_2 + G) \leftrightarrow l_2^a$	308.55	5.157	$(S_2 + l_2) \leftrightarrow l_2^b$
297.46	4.018	$(l_2 + G) \leftrightarrow l_2^a$	308.90	6.408	$(S_2 + l_2) \leftrightarrow l_2^b$
			309.12	7.408	$(S_2 + l_2) \leftrightarrow l_2^b$
			308.51	4.906	$(S_2 + l_2) \leftrightarrow l_2^b$
			309.39	8.408	$(S_2 + l_2) \leftrightarrow l_2^b$

^a: $u(P) = 0.005 \text{ MPa}$, $u(T) = 0.01 \text{ K}$ ^b: $u(P) = 0.005 \text{ MPa}$, $u(T) = 0.05 \text{ K}$

Table B.7. Experimental data for the system 5OCB (1) + CO₂ (2) for mole fraction $x_2 = 0.497$. l_2 denotes the isotropic phase, G the gas phase, S_2 the solid phase. The uncertainties of temperature and pressure are denoted by $u(T)$ and $u(P)$, respectively.

T / K	P / MPa	Phase boundary
328.58	7.614	$(l_2 + G) \leftrightarrow l_2^a$
333.26	8.095	$(l_2 + G) \leftrightarrow l_2^a$
338.45	8.630	$(l_2 + G) \leftrightarrow l_2^a$
306.82	5.478	$(l_2 + G) \leftrightarrow l_2^a$
308.27	5.618	$(l_2 + G) \leftrightarrow l_2^a$
313.32	6.093	$(l_2 + G) \leftrightarrow l_2^a$
318.26	6.569	$(l_2 + G) \leftrightarrow l_2^a$
323.35	7.079	$(l_2 + G) \leftrightarrow l_2^a$
338.42	8.612	$(l_2 + G) \leftrightarrow l_2^a$
343.48	9.158	$(l_2 + G) \leftrightarrow l_2^a$
348.46	9.678	$(l_2 + G) \leftrightarrow l_2^a$
306.50	6.157	$(S_2 + l_2) \leftrightarrow l_2^b$
306.99	8.157	$(S_2 + l_2) \leftrightarrow l_2^b$
307.61	10.158	$(S_2 + l_2) \leftrightarrow l_2^b$
^a : $u(P) = 0.005 \text{ MPa}$, $u(T) = 0.01 \text{ K}$		
^b : $u(P) = 0.005 \text{ MPa}$, $u(T) = 0.05 \text{ K}$		

Table B.8. Experimental data for the system 5OCB (1) + CO₂ (2) for mole fraction $x_2 = 0.720$. l_2 denotes the 5OCB-rich isotropic phase, l_1 the CO₂-rich isotropic phase, G the gas phase, S_2 the solid phase, N the nematic phase. The uncertainties of temperature and pressure are denoted by $u(T)$ and $u(P)$, respectively.

T / K	P / MPa	Phase boundary
302.29	7.073	$(l_1 + l_2 + G)^a$
301.23	6.903	$(l_1 + l_2 + G)^a$
301.84	7.003	$(l_1 + l_2 + G)^a$
302.85	7.163	$(l_1 + l_2 + G)^a$
303.31	7.237	$(l_1 + l_2 + G)^a$
303.81	7.322	$(l_1 + l_2 + G)^a$
301.73	7.153	$(S_2 + l_1 + l_2)^b$
301.75	9.155	$(S_2 + l_1 + l_2)^b$
301.84	6.904	$(S_2 + l_1 + G)^a$
303.28	6.405	$(S_2 + l_1 + G)^a$
304.84	5.905	$(S_2 + l_1 + G)^a$
306.41	5.405	$(S_2 + l_1 + G)^a$
307.91	4.905	$(S_2 + l_1 + G)^a$
311.50	3.755	$(S_2 + l_1 + G)^a$
278.58	4.021	$(S + l_2 + G)^b$
283.17	4.506	$(S + l_2 + G)^b$
288.36	5.112	$(S + l_2 + G)^b$
293.16	5.727	$(S + l_2 + G)^b$
^a : $u(P) = 0.005 \text{ MPa}$, $u(T) = 0.01 \text{ K}$		
^b : $u(P) = 0.005 \text{ MPa}$, $u(T) = 0.05 \text{ K}$		

Appendix C. Experimental data of Chapter 5

Table C.1. Experimental P, T -data of 4-ethyl-4'-propyl bicyclohexyl + CO_2 , mole fraction $x_{\text{CO}_2} = 0.052$. Uncertainties u are provided below the table.

T / K	P / MPa	Phase boundary
336.10	0.703	$\text{I} + \text{G} \leftrightarrow \text{I}^{\text{a}}$
340.35	0.719	$\text{I} + \text{G} \leftrightarrow \text{I}^{\text{a}}$
344.48	0.744	$\text{I} + \text{G} \leftrightarrow \text{I}^{\text{a}}$
348.74	0.764	$\text{I} + \text{G} \leftrightarrow \text{I}^{\text{a}}$
352.76	0.784	$\text{I} + \text{G} \leftrightarrow \text{I}^{\text{a}}$
357.19	0.805	$\text{I} + \text{G} \leftrightarrow \text{I}^{\text{a}}$
361.78	0.830	$\text{I} + \text{G} \leftrightarrow \text{I}^{\text{a}}$
366.96	0.860	$\text{I} + \text{G} \leftrightarrow \text{I}^{\text{a}}$
335.51	0.754	$\text{Sm} + \text{I} \leftrightarrow \text{I}^{\text{b}}$
335.87	1.553	$\text{Sm} + \text{I} \leftrightarrow \text{I}^{\text{b}}$
336.33	2.553	$\text{Sm} + \text{I} \leftrightarrow \text{I}^{\text{b}}$
336.79	3.554	$\text{Sm} + \text{I} \leftrightarrow \text{I}^{\text{b}}$
337.23	4.554	$\text{Sm} + \text{I} \leftrightarrow \text{I}^{\text{b}}$
337.67	5.555	$\text{Sm} + \text{I} \leftrightarrow \text{I}^{\text{b}}$
338.12	6.556	$\text{Sm} + \text{I} \leftrightarrow \text{I}^{\text{b}}$
338.59	7.556	$\text{Sm} + \text{I} \leftrightarrow \text{I}^{\text{b}}$
339.03	8.557	$\text{Sm} + \text{I} \leftrightarrow \text{I}^{\text{b}}$
337.15	0.441	$\text{Sm} + \text{I} + \text{G}^{\text{a}}$
336.76	0.511	$\text{Sm} + \text{I} + \text{G}^{\text{a}}$
336.14	0.620	$\text{Sm} + \text{I} + \text{G}^{\text{a}}$

Sm = smectic, I = isotropic and G = gas.

^a: $u(P) = 0.005 \text{ MPa}$, $u(T) = 0.01 \text{ K}$, $u(x) = 0.001$

^b: $u(P) = 0.005 \text{ MPa}$, $u(T) = 0.02 \text{ K}$, $u(x) = 0.001$

Table C.2. Experimental P, T -data of 4-propyl-4'-butyl bicyclohexyl + CO_2 , mole fraction $x_{\text{CO}_2} = 0.057$. Uncertainties u are provided below the table.

T / K	P / MPa	Phase boundary
367.98	0.927	$\text{I} + \text{G} \leftrightarrow \text{I}^{\text{a}}$
373.80	0.953	$\text{I} + \text{G} \leftrightarrow \text{I}^{\text{a}}$
379.93	0.988	$\text{I} + \text{G} \leftrightarrow \text{I}^{\text{a}}$
385.81	1.023	$\text{I} + \text{G} \leftrightarrow \text{I}^{\text{a}}$
391.88	1.059	$\text{I} + \text{G} \leftrightarrow \text{I}^{\text{a}}$
397.78	1.084	$\text{I} + \text{G} \leftrightarrow \text{I}^{\text{a}}$
403.79	1.114	$\text{I} + \text{G} \leftrightarrow \text{I}^{\text{a}}$
409.83	1.135	$\text{I} + \text{G} \leftrightarrow \text{I}^{\text{a}}$
416.31	1.160	$\text{I} + \text{G} \leftrightarrow \text{I}^{\text{a}}$
422.85	1.185	$\text{I} + \text{G} \leftrightarrow \text{I}^{\text{a}}$
364.04	1.057	$\text{Sm} + \text{I} \leftrightarrow \text{I}^{\text{b}}$
364.58	2.058	$\text{Sm} + \text{I} \leftrightarrow \text{I}^{\text{b}}$
365.27	3.058	$\text{Sm} + \text{I} \leftrightarrow \text{I}^{\text{b}}$
365.89	4.059	$\text{Sm} + \text{I} \leftrightarrow \text{I}^{\text{b}}$
366.51	5.060	$\text{Sm} + \text{I} \leftrightarrow \text{I}^{\text{b}}$
366.93	6.060	$\text{Sm} + \text{I} \leftrightarrow \text{I}^{\text{b}}$
367.46	7.061	$\text{Sm} + \text{I} \leftrightarrow \text{I}^{\text{b}}$
368.08	8.061	$\text{Sm} + \text{I} \leftrightarrow \text{I}^{\text{b}}$
366.60	0.439	$\text{Sm} + \text{I} + \text{G}^{\text{a}}$
366.11	0.568	$\text{Sm} + \text{I} + \text{G}^{\text{a}}$
365.63	0.678	$\text{Sm} + \text{I} + \text{G}^{\text{a}}$
365.10	0.792	$\text{Sm} + \text{I} + \text{G}^{\text{a}}$
364.59	0.907	$\text{Sm} + \text{I} + \text{G}^{\text{a}}$

Sm = smectic, I = isotropic and G = gas.

^a: $u(P) = 0.005 \text{ MPa}$, $u(T) = 0.01 \text{ K}$, $u(x) = 0.001$

^b: $u(P) = 0.005 \text{ MPa}$, $u(T) = 0.02 \text{ K}$, $u(x) = 0.001$

Table C.3. Experimental P,T -data of 4,4'-hexyloxy benzylidene aminobenzonitrile + CO_2 , mole fraction $x_{\text{CO}_2} = 0.066$. Uncertainties u are provided below the table.

T / K	P / MPa	Phase boundary	T / K	P / MPa	Phase boundary
368.01	1.064	$\text{I} + \text{G} \leftrightarrow \text{I}^{\text{a}}$	326.73	1.153	$\text{S} + \text{N} \leftrightarrow \text{N}^{\text{c}}$
373.38	1.099	$\text{I} + \text{G} \leftrightarrow \text{I}^{\text{a}}$	327.12	2.054	$\text{S} + \text{N} \leftrightarrow \text{N}^{\text{c}}$
378.92	1.129	$\text{I} + \text{G} \leftrightarrow \text{I}^{\text{a}}$	327.53	3.054	$\text{S} + \text{N} \leftrightarrow \text{N}^{\text{c}}$
384.33	1.165	$\text{I} + \text{G} \leftrightarrow \text{I}^{\text{a}}$	327.94	4.055	$\text{S} + \text{N} \leftrightarrow \text{N}^{\text{c}}$
389.93	1.200	$\text{I} + \text{G} \leftrightarrow \text{I}^{\text{a}}$	328.33	5.055	$\text{S} + \text{N} \leftrightarrow \text{N}^{\text{c}}$
395.33	1.235	$\text{I} + \text{G} \leftrightarrow \text{I}^{\text{a}}$	328.71	6.056	$\text{S} + \text{N} \leftrightarrow \text{N}^{\text{c}}$
400.83	1.271	$\text{I} + \text{G} \leftrightarrow \text{I}^{\text{a}}$	329.12	7.056	$\text{S} + \text{N} \leftrightarrow \text{N}^{\text{c}}$
406.28	1.306	$\text{I} + \text{G} \leftrightarrow \text{I}^{\text{a}}$	329.52	8.057	$\text{S} + \text{N} \leftrightarrow \text{N}^{\text{c}}$
411.75	1.341	$\text{I} + \text{G} \leftrightarrow \text{I}^{\text{a}}$	328.92	0.913	$\text{N} + \text{G} \leftrightarrow \text{N}^{\text{a}}$
417.22	1.371	$\text{I} + \text{G} \leftrightarrow \text{I}^{\text{a}}$	332.76	0.938	$\text{N} + \text{G} \leftrightarrow \text{N}^{\text{a}}$
422.70	1.407	$\text{I} + \text{G} \leftrightarrow \text{I}^{\text{a}}$	336.83	0.969	$\text{N} + \text{G} \leftrightarrow \text{N}^{\text{a}}$
366.65	1.156	$\text{N} + \text{I} \leftrightarrow \text{I}^{\text{a}}$	340.80	0.999	$\text{N} + \text{G} \leftrightarrow \text{N}^{\text{a}}$
366.98	2.056	$\text{N} + \text{I} \leftrightarrow \text{I}^{\text{a}}$	344.81	1.023	$\text{N} + \text{G} \leftrightarrow \text{N}^{\text{a}}$
367.38	3.057	$\text{N} + \text{I} \leftrightarrow \text{I}^{\text{a}}$	348.90	1.053	$\text{N} + \text{G} \leftrightarrow \text{N}^{\text{a}}$
367.78	4.057	$\text{N} + \text{I} \leftrightarrow \text{I}^{\text{a}}$	352.86	1.073	$\text{N} + \text{G} \leftrightarrow \text{N}^{\text{a}}$
368.19	5.058	$\text{N} + \text{I} \leftrightarrow \text{I}^{\text{a}}$	356.82	1.088	$\text{N} + \text{G} \leftrightarrow \text{N}^{\text{a}}$
368.57	6.059	$\text{N} + \text{I} \leftrightarrow \text{I}^{\text{a}}$	360.85	1.099	$\text{N} + \text{G} \leftrightarrow \text{N}^{\text{a}}$
368.98	7.059	$\text{N} + \text{I} \leftrightarrow \text{I}^{\text{a}}$	364.75	1.099	$\text{N} + \text{G} \leftrightarrow \text{N}^{\text{a}}$
369.39	8.060	$\text{N} + \text{I} \leftrightarrow \text{I}^{\text{a}}$	369.25	0.560	$\text{N} + \text{I} + \text{G}^{\text{a}}$
366.00	1.355	$\text{N} \leftrightarrow \text{N} + \text{I}^{\text{b}}$	368.95	0.629	$\text{N} + \text{I} + \text{G}^{\text{a}}$
366.30	2.055	$\text{N} \leftrightarrow \text{N} + \text{I}^{\text{b}}$	368.66	0.685	$\text{N} + \text{I} + \text{G}^{\text{a}}$
366.72	3.056	$\text{N} \leftrightarrow \text{N} + \text{I}^{\text{b}}$	368.41	0.734	$\text{N} + \text{I} + \text{G}^{\text{a}}$
367.10	4.056	$\text{N} \leftrightarrow \text{N} + \text{I}^{\text{b}}$	368.17	0.779	$\text{N} + \text{I} + \text{G}^{\text{a}}$
367.50	5.057	$\text{N} \leftrightarrow \text{N} + \text{I}^{\text{b}}$	367.89	0.824	$\text{N} + \text{I} + \text{G}^{\text{a}}$
367.91	6.057	$\text{N} \leftrightarrow \text{N} + \text{I}^{\text{b}}$	367.74	0.849	$\text{N} + \text{I} + \text{G}^{\text{a}}$
368.31	7.058	$\text{N} \leftrightarrow \text{N} + \text{I}^{\text{b}}$	367.44	0.909	$\text{N} + \text{I} + \text{G}^{\text{a}}$
368.71	8.059	$\text{N} \leftrightarrow \text{N} + \text{I}^{\text{b}}$	366.80	1.029	$\text{N} + \text{I} + \text{G}^{\text{a}}$

^a: $u(P) = 0.005 \text{ MPa}$, $u(T) = 0.01 \text{ K}$, $u(x) = 0.001$, ^b: $u(P) = 0.005 \text{ MPa}$, $u(T) = 0.02 \text{ K}$, $u(x) = 0.001$, ^c: $u(P) = 0.005 \text{ MPa}$, $u(T) = 0.1 \text{ K}$, $u(x) = 0.001$

Table C.4. Experimental P, T -data of 4'-heptyloxy-4-cyanobiphenyl + CO_2 , mole fraction $x_{\text{CO}_2} = 0.063$. Uncertainties u are provided below the table.

T / K	P / MPa	Phase boundary
343.14	0.810	$\text{I} + \text{G} \leftrightarrow \text{I}^{\text{a}}$
345.36	0.825	$\text{I} + \text{G} \leftrightarrow \text{I}^{\text{a}}$
348.64	0.840	$\text{I} + \text{G} \leftrightarrow \text{I}^{\text{a}}$
351.67	0.855	$\text{I} + \text{G} \leftrightarrow \text{I}^{\text{a}}$
356.15	0.885	$\text{I} + \text{G} \leftrightarrow \text{I}^{\text{a}}$
360.53	0.911	$\text{I} + \text{G} \leftrightarrow \text{I}^{\text{a}}$
366.14	0.941	$\text{I} + \text{G} \leftrightarrow \text{I}^{\text{a}}$
342.85	0.910	$\text{N} + \text{I} \leftrightarrow \text{I}^{\text{a}}$
343.18	1.910	$\text{N} + \text{I} \leftrightarrow \text{I}^{\text{a}}$
343.54	2.911	$\text{N} + \text{I} \leftrightarrow \text{I}^{\text{a}}$
343.89	3.912	$\text{N} + \text{I} \leftrightarrow \text{I}^{\text{a}}$
344.23	4.912	$\text{N} + \text{I} \leftrightarrow \text{I}^{\text{a}}$
344.58	5.912	$\text{N} + \text{I} \leftrightarrow \text{I}^{\text{a}}$
344.93	6.913	$\text{N} + \text{I} \leftrightarrow \text{I}^{\text{a}}$
345.26	7.914	$\text{N} + \text{I} \leftrightarrow \text{I}^{\text{a}}$
342.73	0.910	$\text{N} \leftrightarrow \text{N} + \text{I}^{\text{b}}$
343.09	1.910	$\text{N} \leftrightarrow \text{N} + \text{I}^{\text{b}}$
343.44	2.911	$\text{N} \leftrightarrow \text{N} + \text{I}^{\text{b}}$
343.79	3.912	$\text{N} \leftrightarrow \text{N} + \text{I}^{\text{b}}$
344.14	4.912	$\text{N} \leftrightarrow \text{N} + \text{I}^{\text{b}}$
344.50	5.913	$\text{N} \leftrightarrow \text{N} + \text{I}^{\text{b}}$
344.86	6.913	$\text{N} \leftrightarrow \text{N} + \text{I}^{\text{b}}$
345.19	7.914	$\text{N} \leftrightarrow \text{N} + \text{I}^{\text{b}}$
326.46	0.784	$\text{N} + \text{G} \leftrightarrow \text{N}^{\text{a}}$
329.52	0.804	$\text{N} + \text{G} \leftrightarrow \text{N}^{\text{a}}$
332.59	0.819	$\text{N} + \text{G} \leftrightarrow \text{N}^{\text{a}}$
335.39	0.834	$\text{N} + \text{G} \leftrightarrow \text{N}^{\text{a}}$
338.54	0.845	$\text{N} + \text{G} \leftrightarrow \text{N}^{\text{a}}$
341.57	0.845	$\text{N} + \text{G} \leftrightarrow \text{N}^{\text{a}}$
345.75	0.308	$\text{N} + \text{I} + \text{G}^{\text{a}}$
345.20	0.412	$\text{N} + \text{I} + \text{G}^{\text{a}}$
344.55	0.521	$\text{N} + \text{I} + \text{G}^{\text{a}}$
343.96	0.625	$\text{N} + \text{I} + \text{G}^{\text{a}}$
343.59	0.695	$\text{N} + \text{I} + \text{G}^{\text{a}}$
342.74	0.835	$\text{N} + \text{I} + \text{G}^{\text{a}}$
^a : $u(P) = 0.005 \text{ MPa}$, $u(T) = 0.01 \text{ K}$, $u(x) = 0.001$		
^b : $u(P) = 0.005 \text{ MPa}$, $u(T) = 0.02 \text{ K}$, $u(x) = 0.001$		

Appendix D. Experimental data of Chapter 6

Table D.1. Phase equilibria data of pure 4'-heptyloxy-4-cyanobiphenyl at temperature T and pressure P . S denotes the solid phase, N the nematic phase and I the isotropic liquid. The uncertainties of temperature and pressure are denoted by $u(T)$ and $u(P)$, respectively.

T / K	P / MPa	Phase change	T / K	P / MPa	Phase change
327.92	0.406	$S \leftrightarrow N^a$	347.42	0.405	$N \leftrightarrow I^b$
328.33	1.406	$S \leftrightarrow N^a$	347.99	1.906	$N \leftrightarrow I^b$
328.67	2.407	$S \leftrightarrow N^a$	348.54	3.407	$N \leftrightarrow I^b$
329.26	4.409	$S \leftrightarrow N^a$	349.07	4.908	$N \leftrightarrow I^b$
329.83	6.410	$S \leftrightarrow N^a$	349.61	6.409	$N \leftrightarrow I^b$
330.34	8.411	$S \leftrightarrow N^a$	350.16	7.910	$N \leftrightarrow I^b$
330.90	10.411	$S \leftrightarrow N^a$	350.69	9.411	$N \leftrightarrow I^b$
			351.23	10.912	$N \leftrightarrow I^b$
^a : $u(T) = 0.05 \text{ K}$, $u(P) = 0.005 \text{ MPa}$					
^b : $u(T) = 0.02 \text{ K}$, $u(P) = 0.005 \text{ MPa}$					

Table D.2. Phase equilibria data of the binary mixture 4'-heptyloxy-4-cyanobiphenyl + CO_2 at $x_{\text{CO}_2} = 0.260$ at temperature T and pressure P . N denotes the nematic phase, I the isotropic liquid and G the gas phase. The uncertainties of temperature and pressure are denoted by $u(T)$ and $u(P)$, respectively.

T / K	P / MPa	Phase change	T / K	P / MPa	Phase change
327.73	3.346	$I + G \leftrightarrow I^a$	325.51	4.971	$N + I \leftrightarrow I^a$
335.98	3.615	$I + G \leftrightarrow I^a$	325.84	6.050	$N + I \leftrightarrow I^a$
339.38	3.726	$I + G \leftrightarrow I^a$	326.18	7.201	$N + I \leftrightarrow I^a$
344.70	3.906	$I + G \leftrightarrow I^a$	326.40	7.936	$N + I \leftrightarrow I^a$
350.87	4.122	$I + G \leftrightarrow I^a$	326.59	8.582	$N + I \leftrightarrow I^a$
356.32	4.312	$I + G \leftrightarrow I^a$	325.59	3.215	$N + I + G^a$
361.74	4.502	$I + G \leftrightarrow I^a$	326.98	3.045	$N + I + G^a$
324.80	4.150	$N + I \leftrightarrow N^b$	328.69	2.825	$N + I + G^a$
325.23	5.651	$N + I \leftrightarrow N^b$	330.48	2.580	$N + I + G^a$
325.71	7.152	$N + I \leftrightarrow N^b$	331.54	2.435	$N + I + G^a$
326.08	8.903	$N + I \leftrightarrow N^b$	333.88	2.100	$N + I + G^a$
326.61	10.404	$N + I \leftrightarrow N^b$	335.92	1.790	$N + I + G^a$
			337.87	1.481	$N + I + G^a$
^a : $u(T) = 0.02 \text{ K}$, $u(P) = 0.005 \text{ MPa}$					
^b : $u(T) = 0.07 \text{ K}$, $u(P) = 0.005 \text{ MPa}$					

Table D.3. Phase equilibria data of the binary mixture 4'-heptyloxy-4-cyanobiphenyl + 4'-pentyloxy-4-cyanobiphenyl, $x_{50CB}/x_{70CB} = 1.79$. *N* denotes the nematic phase, *I* the isotropic phase. The uncertainties of temperature and pressure are denoted by $u(T)$ and $u(P)$, respectively.

<i>T</i> / K	<i>P</i> / MPa	Phase change	<i>T</i> / K	<i>P</i> / MPa	Phase change
343.55	0.907	N + I \leftrightarrow N	343.61	0.907	N + I \leftrightarrow I
343.94	1.908	N + I \leftrightarrow N	343.99	1.907	N + I \leftrightarrow I
344.32	2.908	N + I \leftrightarrow N	344.38	2.908	N + I \leftrightarrow I
344.71	3.909	N + I \leftrightarrow N	344.75	3.909	N + I \leftrightarrow I
345.09	4.910	N + I \leftrightarrow N	345.14	4.909	N + I \leftrightarrow I
345.46	5.910	N + I \leftrightarrow N	345.50	5.910	N + I \leftrightarrow I
345.85	6.911	N + I \leftrightarrow N	345.89	6.910	N + I \leftrightarrow I
346.23	7.911	N + I \leftrightarrow N	346.27	7.911	N + I \leftrightarrow I
346.61	8.912	N + I \leftrightarrow N	346.65	8.912	N + I \leftrightarrow I
			347.03	9.912	N + I \leftrightarrow I
$u(T) = 0.02$ K, $u(P) = 0.005$ MPa					

Table D.4. Phase equilibria data of the ternary mixture 4'-heptyloxy-4-cyanobiphenyl + 4'-pentyloxy-4-cyanobiphenyl + CO₂, $x_{50CB}/x_{70CB} = 1.77$, $x_{CO_2} = 0.062$. N denotes the nematic phase, I the isotropic phase and G the gas phase. The uncertainties of temperature and pressure are denoted by $u(T)$ and $u(P)$, respectively.

T / K	P / MPa	Phase change	T / K	P / MPa	Phase change
339.17	0.825	I + G \leftrightarrow I ^a	337.88	0.906	N + I \leftrightarrow I ^b
344.24	0.851	I + G \leftrightarrow I ^a	338.43	2.407	N + I \leftrightarrow I ^b
349.45	0.891	I + G \leftrightarrow I ^a	338.99	3.908	N + I \leftrightarrow I ^b
354.24	0.921	I + G \leftrightarrow I ^a	339.54	5.409	N + I \leftrightarrow I ^b
359.33	0.956	I + G \leftrightarrow I ^a	340.11	6.910	N + I \leftrightarrow I ^b
364.40	0.991	I + G \leftrightarrow I ^a	340.65	8.411	N + I \leftrightarrow I ^b
293.48	0.575	N + G \leftrightarrow N ^a	341.20	9.912	N + I \leftrightarrow I ^b
298.42	0.615	N + G \leftrightarrow N ^a	337.73	0.907	N + I \leftrightarrow N ^b
303.40	0.650	N + G \leftrightarrow N ^a	338.29	2.406	N + I \leftrightarrow N ^b
308.37	0.686	N + G \leftrightarrow N ^a	338.84	3.907	N + I \leftrightarrow N ^b
313.35	0.726	N + G \leftrightarrow N ^a	339.38	5.407	N + I \leftrightarrow N ^b
318.36	0.756	N + G \leftrightarrow N ^a	339.93	6.908	N + I \leftrightarrow N ^b
323.35	0.791	N + G \leftrightarrow N ^a			
328.32	0.816	N + G \leftrightarrow N ^a			
333.32	0.841	N + G \leftrightarrow N ^a			
337.73	0.840	N + I + G \leftrightarrow I + G ^a			
338.03	0.795	N + I + G \leftrightarrow I + G ^a			
338.42	0.735	N + I + G \leftrightarrow I + G ^a			
338.74	0.691	N + I + G \leftrightarrow I + G ^a			
339.07	0.641	N + I + G \leftrightarrow I + G ^a			
339.41	0.591	N + I + G \leftrightarrow I + G ^a			
339.73	0.541	N + I + G \leftrightarrow I + G ^a			
340.24	0.468	N + I + G \leftrightarrow I + G ^a			
340.74	0.389	N + I + G \leftrightarrow I + G ^a			
341.18	0.320	N + I + G \leftrightarrow I + G ^a			
341.73	0.236	N + I + G \leftrightarrow I + G ^a			
^a : $u(T) = 0.02 \text{ K}$, $u(P) = 0.005 \text{ MPa}$					
^b : $u(T) = 0.05 \text{ K}$, $u(P) = 0.005 \text{ MPa}$					

Table D.5. Phase equilibria data of the ternary mixture 4'-heptyloxy-4-cyanobiphenyl + 4'-pentyloxy-4-cyanobiphenyl + CO₂, $x_{50CB}/x_{70CB} = 1.77$, $x_{CO_2} = 0.138$. N denotes the nematic phase, I the isotropic phase and G the gas phase. The uncertainties of temperature and pressure are denoted by $u(T)$ and $u(P)$, respectively.

T / K	P / MPa	Phase change	T / K	P / MPa	Phase change
333.41	1.888	I + G \leftrightarrow I	331.26	1.904	N + I \leftrightarrow I
338.55	1.958	I + G \leftrightarrow I	331.72	3.155	N + I \leftrightarrow I
343.51	2.033	I + G \leftrightarrow I	332.15	4.406	N + I \leftrightarrow I
348.53	2.114	I + G \leftrightarrow I	332.61	5.656	N + I \leftrightarrow I
353.55	2.194	I + G \leftrightarrow I	333.04	6.907	N + I \leftrightarrow I
358.48	2.262	I + G \leftrightarrow I	333.59	8.405	N + I \leftrightarrow I
363.65	2.347	I + G \leftrightarrow I	334.03	9.656	N + I \leftrightarrow I
			331.04	1.901	N + I \leftrightarrow N
293.35	1.366	N + G \leftrightarrow N	331.47	3.151	N + I \leftrightarrow N
298.14	1.451	N + G \leftrightarrow N	331.91	4.402	N + I \leftrightarrow N
303.48	1.537	N + G \leftrightarrow N	332.35	5.654	N + I \leftrightarrow N
308.41	1.622	N + G \leftrightarrow N	332.80	6.905	N + I \leftrightarrow N
313.47	1.702	N + G \leftrightarrow N	333.33	8.405	N + I \leftrightarrow N
318.47	1.773	N + G \leftrightarrow N	333.78	9.656	N + I \leftrightarrow N
323.46	1.838	N + G \leftrightarrow N	331.43	1.789	N + I + G \leftrightarrow I + G
			332.14	1.688	N + I + G \leftrightarrow I + G
331.38	1.803	N + I + G \leftrightarrow N + G	333.44	1.498	N + I + G \leftrightarrow I + G
332.14	1.653	N + I + G \leftrightarrow N + G	334.48	1.344	N + I + G \leftrightarrow I + G
333.29	1.503	N + I + G \leftrightarrow N + G	335.50	1.199	N + I + G \leftrightarrow I + G
334.33	1.354	N + I + G \leftrightarrow N + G	332.51	1.629	N + I + G \leftrightarrow I + G
335.40	1.204	N + I + G \leftrightarrow N + G	333.39	1.499	N + I + G \leftrightarrow I + G
$u(T) = 0.02 \text{ K}$, $u(P) = 0.005 \text{ MPa}$					

Table D.6. Phase equilibria data of the ternary mixture 4'-heptyloxy-4-cyanobiphenyl + 4'-pentyloxy-4-cyanobiphenyl + CO₂, $x_{50CB}/x_{70CB} = 1.76$, $x_{CO_2} = 0.248$. N denotes the nematic phase, I the isotropic phase and G the gas phase. The uncertainties of temperature and pressure are denoted by $u(T)$ and $u(P)$, respectively.

T / K	P / MPa	Phase change	T / K	P / MPa	Phase change
320.22	3.051	I + G \leftrightarrow I	320.04	3.026	N + I + G \leftrightarrow I + G
323.76	3.157	I + G \leftrightarrow I	321.05	2.927	N + I + G \leftrightarrow I + G
328.21	3.306	I + G \leftrightarrow I	322.75	2.756	N + I + G \leftrightarrow I + G
333.43	3.487	I + G \leftrightarrow I	324.20	2.601	N + I + G \leftrightarrow I + G
338.34	3.657	I + G \leftrightarrow I	325.68	2.436	N + I + G \leftrightarrow I + G
343.54	3.847	I + G \leftrightarrow I	326.96	2.292	N + I + G \leftrightarrow I + G
348.54	4.023	I + G \leftrightarrow I	328.25	2.137	N + I + G \leftrightarrow I + G
353.56	4.207	I + G \leftrightarrow I	329.54	1.977	N + I + G \leftrightarrow I + G
358.31	4.378	I + G \leftrightarrow I	330.45	1.862	N + I + G \leftrightarrow I + G
363.33	4.558	I + G \leftrightarrow I	332.37	1.608	N + I + G \leftrightarrow I + G
293.42	2.321	N + G \leftrightarrow N	319.73	3.050	N + I + G \leftrightarrow N + G
298.41	2.492	N + G \leftrightarrow N	321.26	2.902	N + I + G \leftrightarrow N + G
303.45	2.669	N + G \leftrightarrow N	322.74	2.751	N + I + G \leftrightarrow N + G
308.33	2.833	N + G \leftrightarrow N	324.14	2.601	N + I + G \leftrightarrow N + G
313.30	2.979	N + G \leftrightarrow N	325.51	2.451	N + I + G \leftrightarrow N + G
318.32	3.084	N + G \leftrightarrow N	326.79	2.302	N + I + G \leftrightarrow N + G
319.95	3.402	N + I \leftrightarrow I	328.05	2.152	N + I + G \leftrightarrow N + G
320.36	4.653	N + I \leftrightarrow I	329.26	2.002	N + I + G \leftrightarrow N + G
320.77	5.904	N + I \leftrightarrow I	330.45	1.852	N + I + G \leftrightarrow N + G
321.18	7.154	N + I \leftrightarrow I	331.93	1.653	N + I + G \leftrightarrow N + G
321.59	8.405	N + I \leftrightarrow I			
321.99	9.656	N + I \leftrightarrow I			
319.53	3.401	N + I \leftrightarrow N			
319.93	4.652	N + I \leftrightarrow N			
320.33	5.903	N + I \leftrightarrow N			
320.73	7.154	N + I \leftrightarrow N			
321.13	8.404	N + I \leftrightarrow N			
321.53	9.655	N + I \leftrightarrow N			
$u(T) = 0.02 \text{ K}$, $u(P) = 0.005 \text{ MPa}$					

Table D.7. Phase equilibria of the ternary mixture 4'-heptyloxy-4-cyanobiphenyl + 4'-pentyloxy-4-cyanobiphenyl + CO₂, $x_{50CB}/x_{70CB} = 1.77$, $x_{CO_2} = 0.337$. N denotes the nematic phase, I the isotropic phase and G the gas phase. The uncertainties of temperature and pressure are denoted by $u(T)$ and $u(P)$, respectively.

T / K	P / MPa	Phase change	T / K	P / MPa	Phase change
310.84	3.883	I + G \leftrightarrow I	309.83	3.836	N + I + G \leftrightarrow I + G
310.97	3.883	I + G \leftrightarrow I	310.34	3.806	N + I + G \leftrightarrow I + G
318.24	4.251	I + G \leftrightarrow I	310.83	3.773	N + I + G \leftrightarrow I + G
325.86	4.662	I + G \leftrightarrow I	311.83	3.708	N + I + G \leftrightarrow I + G
332.57	5.036	I + G \leftrightarrow I	313.38	3.603	N + I + G \leftrightarrow I + G
340.88	5.497	I + G \leftrightarrow I	314.84	3.493	N + I + G \leftrightarrow I + G
348.45	5.921	I + G \leftrightarrow I	316.38	3.373	N + I + G \leftrightarrow I + G
355.94	6.337	I + G \leftrightarrow I	317.96	3.238	N + I + G \leftrightarrow I + G
363.51	6.763	I + G \leftrightarrow I	319.37	3.108	N + I + G \leftrightarrow I + G
309.72	3.900	N + I \leftrightarrow I	320.91	2.966	N + I + G \leftrightarrow I + G
310.17	5.400	N + I \leftrightarrow I	322.34	2.823	N + I + G \leftrightarrow I + G
310.62	6.901	N + I \leftrightarrow I	323.94	2.653	N + I + G \leftrightarrow I + G
311.06	8.402	N + I \leftrightarrow I	325.44	2.488	N + I + G \leftrightarrow I + G
311.51	9.904	N + I \leftrightarrow I	310.34	3.799	N + I + G \leftrightarrow N + G
308.70	3.898	N + I \leftrightarrow N	311.90	3.697	N + I + G \leftrightarrow N + G
309.26	5.402	N + I \leftrightarrow N	313.38	3.597	N + I + G \leftrightarrow N + G
309.82	6.901	N + I \leftrightarrow N	315.36	3.448	N + I + G \leftrightarrow N + G
310.37	8.401	N + I \leftrightarrow N	317.75	3.250	N + I + G \leftrightarrow N + G
310.90	9.902	N + I \leftrightarrow N	320.49	3.000	N + I + G \leftrightarrow N + G
			322.50	2.800	N + I + G \leftrightarrow N + G
			324.39	2.600	N + I + G \leftrightarrow N + G
$u(T) = 0.02 \text{ K}$, $u(P) = 0.005 \text{ MPa}$					

Table D.8. Phase equilibria data of pure 4'-heptylcyclohexyl-4-benzonitrile at temperature T and pressure P . S denotes the solid phase, N the nematic phase and I the isotropic liquid. The uncertainties of temperature and pressure are denoted by $u(T)$ and $u(P)$, respectively.

T / K	P / MPa	Phase change	T / K	P / MPa	Phase change
331.35	0.400	$N \leftrightarrow I$	303.78	0.400	$S \leftrightarrow N$
331.78	1.401	$N \leftrightarrow I$	304.11	1.401	$S \leftrightarrow N$
332.41	2.902	$N \leftrightarrow I$	304.63	2.900	$S \leftrightarrow N$
333.04	4.402	$N \leftrightarrow I$	305.09	4.403	$S \leftrightarrow N$
333.67	5.903	$N \leftrightarrow I$	305.59	5.902	$S \leftrightarrow N$
334.30	7.404	$N \leftrightarrow I$	306.08	7.405	$S \leftrightarrow N$
334.92	8.905	$N \leftrightarrow I$	306.57	8.905	$S \leftrightarrow N$
335.55	10.406	$N \leftrightarrow I$	307.03	10.406	$S \leftrightarrow N$
$u(T) = 0.02 \text{ K}$, $u(P) = 0.005 \text{ MPa}$					

Table D.9. Phase equilibria data of pure 4'-propylcyclohexyl-4-benzonitrile at temperature T and pressure P . S denotes the solid phase, N the nematic phase and I the isotropic liquid. The uncertainties of temperature and pressure are denoted by $u(T)$ and $u(P)$, respectively.

T / K	P / MPa	Phase change	T / K	P / MPa	Phase change
319.66	0.412	$N \leftrightarrow I$	316.62	0.413	$S \leftrightarrow N$
320.41	1.913	$N \leftrightarrow I$	317.09	1.914	$S \leftrightarrow N$
321.12	3.414	$N \leftrightarrow I$	317.52	3.413	$S \leftrightarrow N$
321.86	4.915	$N \leftrightarrow I$	317.99	4.914	$S \leftrightarrow N$
322.58	6.416	$N \leftrightarrow I$	318.46	6.416	$S \leftrightarrow N$
323.29	7.916	$N \leftrightarrow I$	319.35	9.417	$S \leftrightarrow N$
324.00	9.417	$N \leftrightarrow I$	318.92	7.916	$S \leftrightarrow N$
324.74	10.918	$N \leftrightarrow I$	319.83	10.918	$S \leftrightarrow N$
$u(T) = 0.02 \text{ K}$, $u(P) = 0.005 \text{ MPa}$					

Table D.10. Phase equilibria data of the binary mixture 4'-heptylcyclohexyl-4-benzonitrile + CO₂, $x_{\text{CO}_2} = 0.213$, at temperature T and pressure P . S denotes the solid phase, N the nematic phase, I the isotropic liquid and G the gas phase. The uncertainties of temperature and pressure are denoted by $u(T)$ and $u(P)$, respectively.

T / K	P / MPa	Phase change	T / K	P / MPa	Phase change
308.10	2.167	$I + G \leftrightarrow I^a$	283.71	1.957	$S + N \leftrightarrow N^b$
308.35	2.171	$I + G \leftrightarrow I^a$	284.13	3.407	$S + N \leftrightarrow N^b$
311.55	2.237	$I + G \leftrightarrow I^a$	284.60	4.908	$S + N \leftrightarrow N^b$
313.85	2.291	$I + G \leftrightarrow I^a$	285.04	6.409	$S + N \leftrightarrow N^b$
315.81	2.342	$I + G \leftrightarrow I^a$	285.81	9.411	$S + N \leftrightarrow N^b$
319.25	2.426	$I + G \leftrightarrow I^a$	308.09	2.207	$N + I \leftrightarrow I^a$
321.73	2.497	$I + G \leftrightarrow I^a$	308.44	3.157	$N + I \leftrightarrow I^a$
325.30	2.592	$I + G \leftrightarrow I^a$	308.89	4.408	$N + I \leftrightarrow I^a$
332.17	2.787	$I + G \leftrightarrow I^a$	309.34	5.659	$N + I \leftrightarrow I^a$
339.31	2.997	$I + G \leftrightarrow I^a$	309.80	6.909	$N + I \leftrightarrow I^a$
344.88	3.173	$I + G \leftrightarrow I^a$	310.25	8.160	$N + I \leftrightarrow I^a$
353.10	3.413	$I + G \leftrightarrow I^a$	310.79	9.661	$N + I \leftrightarrow I^a$
306.24	2.273	$N + I + G^a$	306.10	2.407	$N + I \leftrightarrow N^a$
306.68	2.248	$N + I + G^a$	306.55	3.658	$N + I \leftrightarrow N^a$
307.04	2.228	$N + I + G^a$	307.01	4.908	$N + I \leftrightarrow N^a$
307.42	2.208	$N + I + G^a$	307.46	6.159	$N + I \leftrightarrow N^a$
307.75	2.188	$N + I + G^a$	307.91	7.410	$N + I \leftrightarrow N^a$
308.10	2.162	$N + I + G^a$	308.62	9.412	$N + I \leftrightarrow N^a$
308.60	2.133	$N + I + G^a$	283.30	1.992	$S + N + G^b$
309.43	2.083	$N + I + G^a$	285.12	1.658	$S + N + G^b$
310.23	2.028	$N + I + G^a$	286.25	1.408	$S + N + G^b$
311.22	1.963	$N + I + G^a$	287.34	1.159	$S + N + G^b$
312.29	1.883	$N + I + G^a$	288.36	0.911	$S + N + G^b$
313.68	1.778	$N + I + G^a$	289.25	0.663	$S + N + G^b$
314.90	1.684	$N + I + G^a$	286.89	2.292	$N + G \leftrightarrow N^a$
316.08	1.584	$N + I + G^a$	292.36	2.263	$N + G \leftrightarrow N^a$
317.53	1.459	$N + I + G^a$	296.80	2.187	$N + G \leftrightarrow N^a$
319.13	1.315	$N + I + G^a$	301.18	2.097	$N + G \leftrightarrow N^a$
320.96	1.140	$N + I + G^a$	305.85	1.972	$N + G \leftrightarrow N^a$
322.41	0.996	$N + I + G^a$			
324.94	0.729	$N + I + G^a$			
^a : $u(T) = 0.02 \text{ K}$, $u(P) = 0.005 \text{ MPa}$					
^b : $u(T) = 0.05 \text{ K}$, $u(P) = 0.005 \text{ MPa}$					

Table D.11. Phase equilibria data of the binary mixture 4'-propylcyclohexyl-4-benzonitrile + CO₂, $x_{\text{CO}_2} = 0.050$, at temperature T and pressure P . S denotes the solid phase, N the nematic phase, I the isotropic liquid and G the gas phase. The uncertainties of temperature and pressure are denoted by $u(T)$ and $u(P)$, respectively.

T / K	P / MPa	Phase change	T / K	P / MPa	Phase change
315.07	0.443	I + G \leftrightarrow I	315.53	2.556	S + I \leftrightarrow I
321.58	0.474	I + G \leftrightarrow I	315.96	4.057	S + I \leftrightarrow I
327.57	0.504	I + G \leftrightarrow I	316.20	5.058	S + I \leftrightarrow I
333.62	0.539	I + G \leftrightarrow I	316.82	7.059	S + N + I
339.58	0.569	I + G \leftrightarrow I	314.01	0.658	N + I \leftrightarrow I
345.67	0.600	I + G \leftrightarrow I	314.45	1.558	N + I \leftrightarrow I
351.69	0.635	I + G \leftrightarrow I	314.92	2.559	N + I \leftrightarrow I
357.72	0.670	I + G \leftrightarrow I	315.40	3.560	N + I \leftrightarrow I
363.87	0.710	I + G \leftrightarrow I	315.87	4.560	N + I \leftrightarrow I
308.53	0.491	N + G \leftrightarrow N	316.35	5.560	N + I \leftrightarrow I
310.00	0.491	N + G \leftrightarrow N	316.83	6.560	N + I \leftrightarrow I
311.52	0.491	N + G \leftrightarrow N	317.31	7.561	N + I \leftrightarrow I
312.75	0.491	N + G \leftrightarrow N	317.78	8.562	N + I \leftrightarrow I
303.48	0.475	N + G \leftrightarrow N	313.04	0.657	N + I \leftrightarrow N
297.48	0.450	N + G \leftrightarrow N	313.48	1.557	N + I \leftrightarrow N
284.49	0.389	N + G \leftrightarrow N	313.96	2.558	N + I \leftrightarrow N
313.30	0.486	N + I + G	314.43	3.558	N + I \leftrightarrow N
313.78	0.451	N + I + G	314.90	4.559	N + I \leftrightarrow N
314.14	0.426	N + I + G	315.39	5.559	N + I \leftrightarrow N
314.79	0.381	N + I + G	315.86	6.560	N + I \leftrightarrow N
315.36	0.331	N + I + G	316.34	7.561	N + I \leftrightarrow N
315.96	0.287	N + I + G	316.81	8.561	N + I \leftrightarrow N
$u(T) = 0.02 \text{ K}$, $u(P) = 0.005 \text{ MPa}$					

Table D.12. Phase equilibria data of the binary mixture 4'-propylcyclohexyl-4-benzonitrile + CO₂, $x_{\text{CO}_2} = 0.214$, at temperature T and pressure P . S denotes the solid phase, N the nematic phase, I the isotropic liquid and G the gas phase. The uncertainties of temperature and pressure are denoted by $u(T)$ and $u(P)$, respectively.

T / K	P / MPa	Phase change	T / K	P / MPa	Phase change
308.53	2.052	$S + I \leftrightarrow I$	309.22	1.876	$I + G \leftrightarrow I$
308.94	3.403	$S + I \leftrightarrow I$	315.76	2.052	$I + G \leftrightarrow I$
309.40	4.904	$S + I \leftrightarrow I$	321.72	2.207	$I + G \leftrightarrow I$
309.87	6.405	$S + I \leftrightarrow I$	327.61	2.377	$I + G \leftrightarrow I$
310.34	7.905	$S + I \leftrightarrow I$	335.34	2.597	$I + G \leftrightarrow I$
310.75	9.406	$S + I \leftrightarrow I$	341.51	2.777	$I + G \leftrightarrow I$
309.50	1.652	$S + I + G$	347.70	2.952	$I + G \leftrightarrow I$
310.69	1.402	$S + I + G$	353.43	3.118	$I + G \leftrightarrow I$
311.83	1.153	$S + I + G$	358.64	3.273	$I + G \leftrightarrow I$
312.88	0.904	$S + I + G$			
313.96	0.656	$S + I + G$			
314.96	0.411	$S + I + G$			
$u(T) = 0.02 \text{ K}$, $u(P) = 0.005 \text{ MPa}$					

Table D.13. Experimental data of the binary mixture 4'-propylcyclohexyl-4-benzonitrile + 4'-heptylcyclohexyl-4-benzonitrile, $x_{\text{PCH7}}/x_{\text{PCH3}} = 3.00$. N denotes the nematic phase, I the isotropic phase. The uncertainties of temperature and pressure are denoted by $u(T)$ and $u(P)$, respectively.

T / K	P / MPa	Phase change	T / K	P / MPa	Phase change
282.78	0.907	$S + N \leftrightarrow N$	328.51	1.061	$N + I \leftrightarrow I$
283.30	1.908	$S + N \leftrightarrow N$	329.37	3.062	$N + I \leftrightarrow I$
283.94	2.908	$S + N \leftrightarrow N$	330.22	5.063	$N + I \leftrightarrow I$
328.47	1.060	$N + I \leftrightarrow N$	331.08	7.065	$N + I \leftrightarrow I$
329.33	3.061	$N + I \leftrightarrow N$	331.93	9.066	$N + I \leftrightarrow I$
330.19	5.062	$N + I \leftrightarrow N$			
331.05	7.064	$N + I \leftrightarrow N$			
331.90	9.064	$N + I \leftrightarrow N$			
$a: u(T) = 0.02 \text{ K}$, $u(P) = 0.005 \text{ MPa}$					

Table D.14. Phase equilibria data of the ternary mixture 4'-propylcyclohexyl-4-benzonitrile + 4'-heptylcyclohexyl-4-benzonitrile + CO₂, $x_{PCH7}/x_{PCH3} = 2.93$, $x_{CO2} = 0.138$. N denotes the nematic phase, I the isotropic phase and G the gas phase. The uncertainties of temperature and pressure are denoted by $u(T)$ and $u(P)$, respectively.

T / K	P / MPa	Phase change	T / K	P / MPa	Phase change
316.34	3.400	N + I \leftrightarrow I	315.67	1.329	I + G \leftrightarrow I
316.95	4.901	N + I \leftrightarrow I	323.60	1.329	I + G \leftrightarrow I
317.55	6.402	N + I \leftrightarrow I	330.64	1.425	I + G \leftrightarrow I
318.14	7.904	N + I \leftrightarrow I	338.25	1.530	I + G \leftrightarrow I
318.74	9.405	N + I \leftrightarrow I	345.66	1.640	I + G \leftrightarrow I
314.23	1.900	N + I \leftrightarrow N	353.10	1.750	I + G \leftrightarrow I
314.77	3.403	N + I \leftrightarrow N	360.61	1.860	I + G \leftrightarrow I
315.35	4.904	N + I \leftrightarrow N	368.05	1.975	I + G \leftrightarrow I
315.96	6.405	N + I \leftrightarrow N	315.67	1.224	N + I + G \leftrightarrow I + G
316.52	7.906	N + I \leftrightarrow N	316.01	1.214	N + I + G \leftrightarrow I + G
317.14	9.407	N + I \leftrightarrow N	316.94	1.111	N + I + G \leftrightarrow I + G
278.09	0.970	N + G \leftrightarrow N	318.05	1.006	N + I + G \leftrightarrow I + G
283.21	1.035	N + G \leftrightarrow N	319.70	0.852	N + I + G \leftrightarrow I + G
288.20	1.102	N + G \leftrightarrow N	320.77	0.748	N + I + G \leftrightarrow I + G
293.19	1.167	N + G \leftrightarrow N	321.80	0.644	N + I + G \leftrightarrow I + G
298.11	1.227	N + G \leftrightarrow N	322.98	0.525	N + I + G \leftrightarrow I + G
303.48	1.282	N + G \leftrightarrow N	323.63	0.456	N + I + G \leftrightarrow I + G
305.66	1.301	N + G \leftrightarrow N	316.00	1.184	N + I + G \leftrightarrow N + G
308.16	1.321	N + G \leftrightarrow N	316.94	1.101	N + I + G \leftrightarrow N + G
310.12	1.331	N + G \leftrightarrow N	318.05	1.001	N + I + G \leftrightarrow N + G
311.63	1.336	N + G \leftrightarrow N	319.70	0.841	N + I + G \leftrightarrow N + G
313.05	1.337	N + G \leftrightarrow N	320.77	0.736	N + I + G \leftrightarrow N + G
314.23	1.332	N + G \leftrightarrow N	321.79	0.639	N + I + G \leftrightarrow N + G
314.23			322.98	0.515	N + I + G \leftrightarrow N + G
$u(T) = 0.02 \text{ K}$, $u(P) = 0.005 \text{ MPa}$					

Table D.15. Phase equilibria data of the ternary mixture 4'-propylcyclohexyl-4-benzonitrile + 4'-heptylcyclohexyl-4-benzonitrile + CO₂, $x_{PCH7}/x_{PCH3} = 2.99$, $x_{CO2} = 0.244$. N denotes the nematic phase, I the isotropic phase and G the gas phase. The uncertainties of temperature and pressure are denoted by $u(T)$ and $u(P)$, respectively.

T / K	P / MPa	Phase change	T / K	P / MPa	Phase change
304.57	2.012	I + G \leftrightarrow I	278.34	1.676	N + G \leftrightarrow N
304.58	2.012	I + G \leftrightarrow I	283.13	1.766	N + G \leftrightarrow N
308.31	2.093	I + G \leftrightarrow I	288.21	1.906	N + G \leftrightarrow N
313.20	2.213	I + G \leftrightarrow I	293.26	2.011	N + G \leftrightarrow N
313.28	2.215	I + G \leftrightarrow I	295.71	2.056	N + G \leftrightarrow N
323.24	2.483	I + G \leftrightarrow I	298.23	2.091	N + G \leftrightarrow N
323.26	2.482	I + G \leftrightarrow I	299.24	2.111	N + G \leftrightarrow N
333.24	2.767	I + G \leftrightarrow I	300.21	2.116	N + G \leftrightarrow N
333.28	2.763	I + G \leftrightarrow I	301.24	2.111	N + G \leftrightarrow N
343.18	3.062	I + G \leftrightarrow I	302.26	2.111	N + G \leftrightarrow N
343.25	3.062	I + G \leftrightarrow I	305.38	1.956	N + I + G \leftrightarrow I + G
353.24	3.363	I + G \leftrightarrow I	306.61	1.886	N + I + G \leftrightarrow I + G
353.33	3.362	I + G \leftrightarrow I	307.28	1.846	N + I + G \leftrightarrow I + G
363.30	3.662	I + G \leftrightarrow I	308.47	1.771	N + I + G \leftrightarrow I + G
363.37	3.668	I + G \leftrightarrow I	309.61	1.696	N + I + G \leftrightarrow I + G
304.60	2.402	N + I \leftrightarrow I	310.64	1.621	N + I + G \leftrightarrow I + G
304.98	3.403	N + I \leftrightarrow I	312.22	1.510	N + I + G \leftrightarrow I + G
305.35	4.404	N + I \leftrightarrow I	314.18	1.356	N + I + G \leftrightarrow I + G
305.71	5.404	N + I \leftrightarrow I	316.24	1.187	N + I + G \leftrightarrow I + G
306.08	6.405	N + I \leftrightarrow I	318.13	1.023	N + I + G \leftrightarrow I + G
306.45	7.406	N + I \leftrightarrow I	320.22	0.829	N + I + G \leftrightarrow I + G
306.82	8.406	N + I \leftrightarrow I	308.19	1.789	N + I + G \leftrightarrow N + G
302.49	2.402	N + I \leftrightarrow N	304.33	2.001	N + I + G \leftrightarrow N + G
302.86	3.403	N + I \leftrightarrow N	305.31	1.951	N + I + G \leftrightarrow N + G
303.24	4.403	N + I \leftrightarrow N	306.73	1.872	N + I + G \leftrightarrow N + G
303.60	5.404	N + I \leftrightarrow N	308.18	1.780	N + I + G \leftrightarrow N + G
303.96	6.404	N + I \leftrightarrow N	309.75	1.675	N + I + G \leftrightarrow N + G
304.33	7.404	N + I \leftrightarrow N	311.26	1.570	N + I + G \leftrightarrow N + G
302.38	2.111	N + I + G \leftrightarrow N + I	312.76	1.456	N + I + G \leftrightarrow N + G
302.89	2.091	N + I + G \leftrightarrow N + I	302.44	2.105	N + I + G \leftrightarrow N + G
303.55	2.056	N + I + G \leftrightarrow N + I	302.95	2.080	N + I + G \leftrightarrow N + G
304.34	2.016	N + I + G \leftrightarrow N + I	303.50	2.045	N + I + G \leftrightarrow N + G
$u(T) = 0.02 \text{ K}$, $u(P) = 0.005 \text{ MPa}$					

Table D.16. Phase equilibria data of the ternary mixture 4'-propylcyclohexyl-4-benzonitrile + 4'-heptylcyclohexyl-4-benzonitrile + CO₂, $x_{PCH7}/x_{PCH3} = 3.02$, $x_{CO2} = 0.332$. N denotes the nematic phase, I the isotropic phase and G the gas phase. The uncertainties of temperature and pressure are denoted by $u(T)$ and $u(P)$, respectively.

T / K	P / MPa	Phase change	T / K	P / MPa	Phase change
293.98	2.461	I + G \leftrightarrow I	278.37	2.221	N + G \leftrightarrow N
303.24	2.786	I + G \leftrightarrow I	280.86	2.296	N + G \leftrightarrow N
303.52	2.797	I + G \leftrightarrow I	283.31	2.366	N + G \leftrightarrow N
313.38	3.197	I + G \leftrightarrow I	285.91	2.430	N + G \leftrightarrow N
313.71	3.207	I + G \leftrightarrow I	287.37	2.460	N + G \leftrightarrow N
323.46	3.633	I + G \leftrightarrow I	288.35	2.485	N + G \leftrightarrow N
333.26	4.068	I + G \leftrightarrow I	289.33	2.500	N + G \leftrightarrow N
343.20	4.528	I + G \leftrightarrow I	293.39	2.445	N + I + G \leftrightarrow I + G
353.38	5.004	I + G \leftrightarrow I	294.35	2.416	N + I + G \leftrightarrow I + G
363.36	5.469	I + G \leftrightarrow I	294.37	2.414	N + I + G \leftrightarrow I + G
293.42	2.651	N + I \leftrightarrow I	295.67	2.381	N + I + G \leftrightarrow I + G
293.76	3.652	N + I \leftrightarrow I	296.82	2.341	N + I + G \leftrightarrow I + G
294.11	4.652	N + I \leftrightarrow I	298.32	2.292	N + I + G \leftrightarrow I + G
294.45	5.653	N + I \leftrightarrow I	298.89	2.272	N + I + G \leftrightarrow I + G
294.79	6.653	N + I \leftrightarrow I	300.42	2.207	N + I + G \leftrightarrow I + G
295.14	7.654	N + I \leftrightarrow I	302.26	2.122	N + I + G \leftrightarrow I + G
295.48	8.655	N + I \leftrightarrow I	294.37	2.404	N + I + G \leftrightarrow N + G
290.18	2.901	N + I \leftrightarrow N	295.40	2.379	N + I + G \leftrightarrow N + G
290.51	3.902	N + I \leftrightarrow N	296.88	2.329	N + I + G \leftrightarrow N + G
290.85	4.903	N + I \leftrightarrow N	298.40	2.279	N + I + G \leftrightarrow N + G
291.21	5.903	N + I \leftrightarrow N	290.44	2.495	N + I + G \leftrightarrow N + G
291.54	6.904	N + I \leftrightarrow N	291.37	2.480	N + I + G \leftrightarrow N + G
291.88	7.905	N + I \leftrightarrow N	292.36	2.455	N + I + G \leftrightarrow N + G
290.36	2.499	N + I + G \leftrightarrow N + I	293.18	2.436	N + I + G \leftrightarrow N + G
291.33	2.484	N + I + G \leftrightarrow N + I			
292.40	2.464	N + I + G \leftrightarrow N + I			
293.23	2.449	N + I + G \leftrightarrow N + I			
$u(T) = 0.02 \text{ K}$, $u(P) = 0.005 \text{ MPa}$					

Appendix E. Experimental data of Chapter 7

Table E.1. Experimental P, T -data of 4-ethyl-4'-propyl bicyclohexyl + CH_4 , mass fraction $w_{CH_4} = 0.010$. Uncertainties u are provided below the table.

T / K	P / MPa	Phase boundary	T / K	P / MPa	Phase boundary
329.34	4.081	I + G \leftrightarrow I ^a	329.56	5.057	Sm + I \leftrightarrow I ^b
333.48	4.136	I + G \leftrightarrow I ^a	330.20	6.558	Sm + I \leftrightarrow I ^b
338.59	4.197	I + G \leftrightarrow I ^a	330.88	8.059	Sm + I \leftrightarrow I ^b
343.57	4.251	I + G \leftrightarrow I ^a	331.49	9.560	Sm + I \leftrightarrow I ^b
348.54	4.301	I + G \leftrightarrow I ^a	332.14	11.061	Sm + I \leftrightarrow I ^b
353.66	4.356	I + G \leftrightarrow I ^a	329.47	3.958	Sm + I + G ^b
358.62	4.402	I + G \leftrightarrow I ^a	330.39	3.558	Sm + I + G ^b
363.66	4.451	I + G \leftrightarrow I ^a	331.70	3.057	Sm + I + G ^b
329.34	4.081	I + G \leftrightarrow I ^a	333.01	2.557	Sm + I + G ^b
			334.39	2.057	Sm + I + G ^b
			335.64	1.557	Sm + I + G ^b
			336.99	1.058	Sm + I + G ^b

Sm = smectic, I = isotropic and G = gas.
^a: $u(P) = 0.005$ MPa, $u(T) = 0.01$ K, $u(x) = 0.001$
^b: $u(P) = 0.005$ MPa, $u(T) = 0.05$ K, $u(x) = 0.001$

Table E.2. Experimental P, T -data of 4'-pentylcyclohexyl-4-benzonitrile + CH_4 , mass fraction $w_{CH_4} = 0.010$. Uncertainties u are provided below the table.

T / K	P / MPa	Phase boundary	T / K	P / MPa	Phase boundary
318.15	6.414	I + G \leftrightarrow I ^a	313.37	7.055	I + N \leftrightarrow I ^b
323.19	6.399	I + G \leftrightarrow I ^a	313.77	8.055	I + N \leftrightarrow I ^b
328.16	6.404	I + G \leftrightarrow I ^a	314.18	9.056	I + N \leftrightarrow I ^b
333.29	6.425	I + G \leftrightarrow I ^a	314.60	10.056	I + N \leftrightarrow I ^b
338.08	6.445	I + G \leftrightarrow I ^a	313.68	6.333	I + N + G ^a
343.26	6.474	I + G \leftrightarrow I ^a	314.31	6.023	I + N + G ^a
348.28	6.504	I + G \leftrightarrow I ^a	314.92	5.722	I + N + G ^a
353.30	6.534	I + G \leftrightarrow I ^a	315.53	5.427	I + N + G ^a
358.37	6.561	I + G \leftrightarrow I ^a	316.53	4.952	I + N + G ^a
363.27	6.591	I + G \leftrightarrow I ^a	317.55	4.477	I + N + G ^a

N = nematic, I = isotropic and G = gas.
^a: $u(P) = 0.005$ MPa, $u(T) = 0.01$ K, $u(x) = 0.001$
^b: $u(P) = 0.005$ MPa, $u(T) = 0.02$ K, $u(x) = 0.001$

Table E.3. Experimental P,T -data of 4'-pentyl-4-cyanobiphenyl + CH_4 , mass fraction $w_{CH_4} = 0.010$. Uncertainties u are provided below the table.

T / K	P / MPa	Phase boundary	T / K	P / MPa	Phase boundary
296.31	8.988	I + G \leftrightarrow I ^a	295.22	9.056	I + N \leftrightarrow I ^b
303.23	8.833	I + G \leftrightarrow I ^a	295.60	10.058	I + N \leftrightarrow I ^b
308.20	8.783	I + G \leftrightarrow I ^a	295.96	11.058	I + N \leftrightarrow I ^b
313.18	8.773	I + G \leftrightarrow I ^a	294.76	10.058	I + N \leftrightarrow N ^b
318.08	8.747	I + G \leftrightarrow I ^a	295.28	11.059	I + N \leftrightarrow N ^b
323.11	8.742	I + G \leftrightarrow I ^a	295.56	8.697	I + N + G ^a
328.02	8.732	I + G \leftrightarrow I ^a	296.73	7.627	I + N + G ^a
333.08	8.727	I + G \leftrightarrow I ^a	297.84	6.677	I + N + G ^a
343.02	8.723	I + G \leftrightarrow I ^a	299.83	5.111	I + N + G ^a
353.01	8.718	I + G \leftrightarrow I ^a	301.82	3.685	I + N + G ^a
			303.87	2.334	I + N + G ^a
			305.82	1.125	I + N + G ^a

N = nematic, I = isotropic and G = gas.
^a: $u(P) = 0.005$ MPa, $u(T) = 0.01$ K, $u(x) = 0.001$
^b: $u(P) = 0.005$ MPa, $u(T) = 0.02$ K, $u(x) = 0.001$

Table E.4. Experimental P,T -data of 4'-pentyloxy-4-cyanobiphenyl + CH_4 , mass fraction $w_{CH_4} = 0.010$. Uncertainties u are provided below the table.

T / K	P / MPa	Phase boundary	T / K	P / MPa	Phase boundary
330.06	11.555	I + G \leftrightarrow I ^a	329.22	12.055	I + N \leftrightarrow I ^b
333.11	11.426	I + G \leftrightarrow I ^a	329.57	13.056	I + N \leftrightarrow I ^b
338.01	11.286	I + G \leftrightarrow I ^a	329.22	12.055	I + N + G ^a
343.06	11.126	I + G \leftrightarrow I ^a	329.57	13.056	I + N + G ^a
347.99	11.004	I + G \leftrightarrow I ^a	330.07	10.320	I + N + G ^a
353.07	10.910	I + G \leftrightarrow I ^a	331.02	9.155	I + N + G ^a
358.01	10.815	I + G \leftrightarrow I ^a	332.44	7.555	I + N + G ^a
363.01	10.736	I + G \leftrightarrow I ^a	333.90	6.054	I + N + G ^a
			335.48	4.553	I + N + G ^a

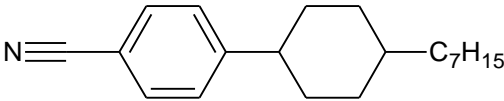
N = nematic, I = isotropic and G = gas.
^a: $u(P) = 0.005$ MPa, $u(T) = 0.01$ K, $u(x) = 0.001$
^b: $u(P) = 0.005$ MPa, $u(T) = 0.02$ K, $u(x) = 0.001$

Appendix F. Overview of the LCs used

Table F.1. Abbreviation and chemical structure of the liquid crystals used in this study.

Name	Abbr.	Chemical structure
4'-pentyloxy-4-cyanobiphenyl	5OCB	
4'-pentyl-4-cyanobiphenyl	5CB	
4-ethyl-4'-propyl-bicyclohexyl	2,3-BCH	
4-propyl-4'-butyl-bicyclohexyl	3,4-BCH	
4'-octyloxy-4-cyanobiphenyl	8OCB	
4'-heptyloxy-4-cyanobiphenyl	7OCB	
4,4'-hexyloxy benzyldene aminobenzonitrile	-	
4'-propylcyclohexyl-4-benzonitrile	PCH3	

Table F.1. Continued.

4'-heptylcyclohexyl- 4-benzonitrile	PCH7	
4'-pentylcyclohexyl -4- benzonitrile	PCH5	